Proximal and distal spinal neurons innervating multiple synergist and antagonist motor pools

Remi Ronzano*[,1,2,3], Camille Lancelin*[,1], Gardave S. Bhumbra[2], Robert M. Brownstone[§,1], Marco Beato[§,2]

1 Department of Neuromuscular Diseases, UCL Queen Square Institute of Neurology, University College London, London WC1N 3BG, UK

2 Department of Neuroscience Physiology and Pharmacology (NPP), Gower Street, University College London, WC1E 6BT, UK

3 Université Paris-Saclay, ENS Paris-Saclay, CNRS, Department of Biology, 91190, Gif-sur-Yvette, France

* equal contribution

§ co-senior authors

Abstract

Motoneurons control muscle contractions, and their recruitment by premotor circuits is tuned to produce accurate motor behaviours. To understand how these circuits coordinate movement across and between joints, it is necessary to understand whether spinal neurons pre-synaptic to motor pools have divergent projections to more than one motoneuron population. Here, we used modified rabies virus tracing in mice to investigate premotor INs projecting to synergist flexor or extensor motoneurons, as well as those projecting to antagonist pairs of muscles controlling the ankle joint. We show that similar proportions of premotor neurons diverge to synergist and antagonist motor pools. Divergent premotor neurons were seen throughout the spinal cord, with decreasing numbers but increasing proportion with distance from the hindlimb enlargement. In the cervical cord, divergent long descending propriospinal neurons were found in contralateral lamina VIII, had large somata, were neither glycinergic, nor cholinergic, and projected to both lumbar and cervical motoneurons. We conclude that distributed spinal premotor neurons coordinate activity across multiple motor pools and that there are spinal neurons mediating co-contraction of antagonist muscles.

Introduction

The spinal cord is ultimately responsible for organising movement by controlling the activation pattern of motoneurons (MNs), which in turn produce appropriate patterns of muscle contractions to produce limb movement. Across any single limb joint, there are fundamentally 3 types of control – or 3 “syllables of movement” – possible. The 3 basic syllables are: (1) changing a joint angle, (2) stiffening a joint, and (3) relaxing a joint. The concatenation of these syllables across joints within and between limbs ultimately produces behaviour (Brownstone, 2020; Wiltschko et al., 2015).

To change a joint angle, MNs innervating synergist muscle fibres are activated whilst those that innervate antagonist muscle fibres are inhibited. This “reciprocal inhibition” (Eccles, 1969; Eccles et al., 1956), is mediated locally by spinal interneurons (INs) throughout the spinal cord; this syllable has been fairly well characterised, with responsible neurons identified and classified (Alvarez et al., 2005; Benito-Gonzalez and Alvarez, 2012; Sapir et al., 2004; Zhang et al., 2014).

The other 2 syllables are less well studied, but it is clear that behavioural joint stiffening requires co-activation of MNs innervating antagonist muscle groups, while joint relaxation would require co-inhibition of these MNs. Co-contraction has largely been thought to result from brain activity (Humphrey and Reed, 1983), whereas circuits mediating co-inhibition remain elusive. Since the spinal cord controls movement not only across single joints but throughout the body, it is natural to consider whether it contains the circuits necessary to produce these different syllables.

To identify whether these syllables are produced by spinal circuits, several questions can be asked: Does the spinal cord contain circuits that lead to co-activation or co-inhibition of different pools of MNs – either synergists or antagonists? Does each motor pool have its own dedicated population of premotor INs, and are these INs interconnected in such a way that they can produce contraction of different muscle groups? Or are there populations of INs that project to multiple motor pools in order to effect contraction (or relaxation) of multiple muscles? Indeed, INs that have activity in keeping with innervation of multiple synergists, leading to motor “primitives” or synergies (Bizzi and Cheung, 2013; Giszter, 2015; Hart and Giszter, 2010; Takei et al., 2017; Tresch and Jarc, 2009) have been identified, but knowledge of their locations and identities remains scant.

Normal behaviours in quadrupeds as well as bipeds require coordination of syllables across joints between forelimbs and hindlimbs. This coordination relies on populations of propriospinal neurons projecting in either direction between the lumbar and cervical enlargements (Eidelberg et al., 1980; Giovanelli Barilari and Kuypers, 1969; Miller and van der Meché, 1976; Ruder et al., 2016). Long descending propriospinal neurons (LDPNs) were first proposed in cats and dogs more than a century ago (Sherrington and Laslett, 1903), and their existence has been confirmed in several other species including humans (Alstermark et al., 1987a, 1987b; Ballion et al., 2001; Brockett et al., 2013; Flynn et al., 2017; Giovanelli Barilari and Kuypers, 1969; Jankowska et al., 1974; Mitchell et al., 2016; Nathan et al., 1996; Ni et al., 2014; Reed et al., 2009; Ruder et al., 2016; Skinner et al., 1979). While LDPNs that establish disynaptic connections to lumbar MNs have been identified, it was initially suggested that at least some cervical LDPNs could establish monosynaptic inputs to lumbar MNs (Jankowska et al., 1974). This connectivity was later confirmed using monosynaptic modified rabies virus (RabV) tracing (Ni et al., 2014). More recently, descending and ascending spinal neurons and their involvement in the control of stability and interlimb coordination have been characterized, but these studies did not directly focus on monosynaptic premotor circuits (Pocratsky et al., 2017; Ruder et al., 2016). It is likely that LDPNs function to ensure coordination between fore and hindlimbs, and they could be an important source of premotor input to MNs, providing a substrate for coordination between distant joints.

In the present study, we examine circuits underlying co-activation and co-inhibition in the spinal cord by assessing premotor neurons through the use of RabV tracing techniques (Ronzano et al., 2021; Ugolini, 1995; Wickersham et al., 2007). We used glycoprotein (G)-deleted RabV (ΔG-Rab), and supplied G to MNs through crossing ChAT-Cre mice with RΦGT mice (Ronzano et al., 2021; Takatoh et al., 2013). We injected ΔG-RabV tagged with two different fluorescent proteins into hindlimb muscle pairs of ChAT-Cre mice to retrogradely trace premotor circuits throughout the spinal cord. At the lumbar level, this method revealed apparent low rates of INs projecting to both MN pools targeted. As the distance from targeted MN pool to premotor INs increased, the density of infected premotor INs decreased. But the apparent rate of divergence to multiple pools was higher in thoracic and cervical regions than in the lumbar spinal cord. Interestingly, the extent of divergence throughout the spinal cord was similar whether injections were performed in flexor or extensor pairs, or in synergist or antagonist pairs of muscles. In addition, a population of premotor LDPNs was identified in the cervical spinal cord. These neurons had a high rate of divergence and large somata, projected contralaterally, were neither glycinergic nor cholinergic, located in lamina VIII, and projected to cervical MNs as well as lumbar MNs. Together, these data show that the spinal cord contains

premotor INs that project to multiple motor pools (including antagonists), and could thus form substrates for the fundamental syllables of movement.

Results

Lumbar premotor INs reveal similar divergence patterns to synergist and antagonist motor pools

Given evidence that INs are involved in motor synergies (Hart and Giszter, 2010; Levine et al., 2014; Takei et al., 2017; Takei and Seki, 2010), we would expect that there would be INs in the lumbar spinal cord that project to synergist motor pools. We thus first investigated whether such premotor INs could be infected with two RabVs expressing two different fluorescent proteins injected in pairs of muscles. We injected ΔG-Rab expressing eGFP or mCherry into synergist ankle extensors (LG and MG) or synergist ankle flexors (TA and PL) in ChAT-Cre;RΦGT P1-P3 mice (Ronzano et al., 2021). These mice selectively express rabies G in cholinergic neurons (including MNs), providing the necessary glycoprotein for retrograde trans-synaptic transfer from infected MNs to premotor INs (Figure 1A). After 9 days, we visualized the distribution of premotor INs that expressed one or both fluorescent proteins, specifying the premotor INs that make synaptic contact with two motor pools as “divergent” premotor INs (Figure 1-figure supplement 1A-B, Figure 1-figure supplement 2A-B). We found divergent premotor INs distributed across the lumbar spinal cord (Figure 1-figure supplement 4A-B) bilaterally in the ventral quadrants and ipsilaterally in the dorsal quadrant of the spinal cord (Figure 1C-D), consistently across experiments (Figure 1-figure supplement 5A, Supplementary file 1). Across the lumbar spinal cord, we quantified infected MNs and found that 380 MNs were labelled from synergist injections (n=4, 2 extensor and 2 flexor pairs). Notably, 5 MNs were double labelled, most likely due to secondary infection of synaptically connected MNs (Supplementary file 1, (Bhumbra and Beato, 2018)). We then quantified premotor INs on one of every three sections and found that 4.0 ± 0.3 % (276/7043, n=4, 2 extensor and 2 flexor pairs, Figure 1-figure supplement 1C-D, and figure supplement 2C-D) of labelled premotor INs were double-labelled, confirming that INs can be infected by more than one RabV. We would expect this to be an underestimate of the number of INs that have divergent projections since RabV is not expected to label 100% of presynaptic neurons and as there is a reduced efficiency of double infections compared to single infections (Ohara et al., 2009) (see Discussion).

We next sought to determine whether this divergence was restricted to synergist motor pools or whether there are also premotor INs that diverge to antagonist pools and could thus be involved in co-contraction or joint stiffening. Following injections into flexor (TA) and extensor (LG) muscles, 260 MNs were labelled (n=3 antagonist pairs), 1 of them being double labelled (Supplementary file 1). Following these injections, we also found divergent INs (Figure 1B, Figure 1-figure supplement 3A-B). We found a similar rate of divergence to antagonist

pools as to synergist muscles, with 4.7 ± 0.5 % (206/4341, n=3 antagonist pairs, Figure 1E, Figure 1-figure supplement 3C-E) double-labelled. The mapping of all divergent INs in every section revealed that, whether injections were in synergist (n=4, 2 extensor and 2 flexor synergist pairs) or antagonist (n=3 pairs) pairs of muscles, double-labelled premotor INs were distributed similarly (Figure 1F-G, Figure 1-figure supplement 4, Figure 1- figure supplement 5, and Supplementary file 1 for summary of individual experiments). The proportion of divergent cells was calculated from the ratio of double and single infected cells in 1/3 sections, in order to avoid double counting cells present in consecutive sections (see Methods). Equal proportions of divergent premotor INs were found in the ventral ipsilateral quadrant (synergists: 74/1913 (3.9%) vs antagonists: (46/1046 (4.4%)), ventral contralateral quadrant (46/1020 (3.8%) vs 21/502 (4.2%)), and dorsal ipsilateral quadrant (153/3874 (3.9%) vs 134/2651 (5.1%)). There were few labelled neurons in the dorsal contralateral quadrant following either synergist or antagonist injections and a similarly low proportion were double labelled (in 1/3 sections: 3/236 (1.3%) and 5/142 (3.5%), respectively). Divergence in premotor circuits is thus common, with at least 1/25 (see Discussion) premotor INs diverging to 2 MN pools, whether synergists or antagonists.

Since motor synergies can span across more than a single joint, it is possible that divergent premotor INs could project to motor pools other than those injected. Indeed, following injection of ΔG-Rab-mCherry into the TA muscle, we could visualize mCherry positive excitatory (vGluT2+) boutons in apposition to L1 (Figure 1-figure supplement 6A, D-E), as well as to thoracic (as rostral as at least T10) MNs (Figure 1-figure supplement 6B-C), i.e., 3-7 segments rostral to the infected motor pool. mCherry positive excitatory boutons on MNs were consistently observed in all upper lumbar and thoracic sections taken from 3 injected mice (3-4 sections in each region). This observation, in agreement with a previous study that described premotor INs coordinating the activity of multiple lumbar motor groups from L2 to L5 (Levine et al., 2014), supports the possibility that thoraco-lumbar premotor circuits comprise a substrate for multi-joint synergies.

Thoracic premotor neurons project to multiple lumbar motor pools

In order to maintain posture and stability, trunk muscles are coordinated with hindlimb movements. Neurons in the thoracic cord that are premotor to lumbar MNs have previously been described (Ni et al., 2014); we thus next examined the projections of thoracic premotor neurons to lumbar motor pools. These premotor neurons were found with decreasing density from T11 through T3 whether the injections were in extensor (LG and MG; Figure 2A, Figure 2-figure supplement 1A-B) or flexor (TA and PL, Figure 2-figure supplement 2A-B) pairs of muscles (Figure 2-figure supplement 4A-B). The distributions of single labelled as well as

divergent premotor neurons were similar whether injections were performed in flexor, extensor, or antagonist pairs of muscles (Figure 2 B-H, Figure 2-figure supplement 4A-C). Divergence rates calculated from the whole thoracic spinal cords were similar between synergist and antagonist injections with 16.2 ± 5.7% (77/497, n=4, 2 extensor and 2 flexor pairs, Figure 2B-C, Figure 2-figure supplement 1C-D, Figure 2-figure supplement 2C-D) and 9.0 ± 0.7% (59/401, n=3 antagonist pairs, Figure 2D, Figure 2-figure supplement 3C-E), respectively. In all animals (7/7), the overall proportion of double-labelled neurons in the thoracic spinal cord was higher than in the lumbar cord (13.1 ± 5.6%, Figure 7B).

In all animals (7/7), most divergent premotor neurons in the thoracic cord were located in the ipsilateral dorsal quadrant (46/77, n=4 synergist and 42/59, n=3 antagonist pairs, Figure 2 E-H), and within this quadrant 22.1 ± 8.6% (46/188 synergists and 42/211 antagonists, Figure 2E-F) of premotor neurons were double labelled. The divergence rates in the two ventral quadrants were lower: in the ventral cord, double-labelled neurons were observed in 5/7 animals (3/4 synergist; 2/3 antagonist in both quadrants) ipsilaterally (6.7 ± 4.8%; 10/118 synergist and 5/70 antagonist pairs), as well as contralaterally (11.1 ± 10.7%; 21/167 synergist and 12/104 antagonist pairs) to the injection (Figure 2E-F). Thus, there are premotor neurons throughout the thoracic cord that project directly to more than one motor pool, including antagonist pairs, in the lumbar spinal cord, with most of these located in the ipsilateral dorsal quadrant.

Cervical premotor long propriospinal descending neurons diverge and share a typical location and morphology

Cervical long descending propriospinal neurons (LDPNs) have been shown to modulate interlimb coordination to provide stability (Eidelberg et al., 1980; Miller and van der Meché, 1976; Pocratsky et al., 2017; Ruder et al., 2016). Given that cervical premotor LDPNs projecting to TA MNs have previously been demonstrated (Ni et al., 2014), we asked whether these neurons could be premotor to hindlimb and/or hindlimb-forelimbs MN pairs.

We found that premotor LDPNs projecting to flexor (TA and PL) and extensor (LG and MG) MNs were localised throughout the rostrocaudal extent of the ventral cervical cord with an enrichment between C6 and T1 (Figure 3-figure supplement 4). Of 92 premotor LDPNs, 88 were localized in the ventral quadrants, 68 of which were in contralateral lamina VIII (n=7, 4 synergist and 3 antagonist pairs, Figure 3A-F, Figure 3-figure supplement 4). A substantial proportion of premotor LDPNs was double-labelled, with the proportion and location of double-labelling similar across experiments (Figure 1-figure supplement 5C and Supplementary file 1) whether injections were into synergist or antagonist pairs (42.4 ± 22.1 % per animal, total of

19/55 neurons, n=4 synergist pairs and 47.9 ± 7.1 % per animal, total of 19/37 neurons, n=3 antagonist pairs, Figure 3E-F, Figure 3-figure supplement 1, Figure 3-figure supplement 2, Figure 3-figure supplement 3). This apparent divergence rate of LDPNs in the cervical cord was higher than in the lumbar and thoracic cords in all animals (7/7, Figure 7B). These divergent premotor LDPNs exhibited a stereotypical morphology with an unusually large soma (774 ± 231 μm^2, n=38 premotor LDPNs) compared to the double-labelled premotor neurons in the thoracic and lumbar cords (respectively 359 ± 144 μm^2 and 320 ± 114 μm^2, n=135 premotor neurons (thoracic), n=61 premotor INs (lumbar), $p<0.0001$ Kruskal-Wallis test, $p<0.0001$ (lumbar vs cervical) and $p<0.0001$ (thoracic vs cervical), Dunn's multiple comparisons test). On average, the cross-sectional area of divergent cervical LDPNs was comparable to that of cervical MNs (661 ± 86 μm^2, n=17 MNs, Figure 3H). Their location and size suggests that these divergent, commissural cervical premotor LDPNs may constitute a somewhat homogeneous population.

Cervical premotor LDPNs are neither glycinergic nor cholinergic

To determine the neurotransmitter phenotype of the premotor LDPNs, we used single ΔG-Rab-mCherry injections in ChAT-Cre;RΦGT mice crossed with mice expressing eGFP under the control of the promoter for the neuronal glycine transporter GlyT2 (Zeilhofer et al., 2005), Figure 4A). GlyT2 is expressed in the vast majority of spinal inhibitory INs (Todd et al., 1996; Todd and Sullivan, 1990), making GlyT2-eGFP mice a suitable tool to determine whether premotor LDPNs are inhibitory. Given that at least 40% of the labelled INs in the cervical region are divergent (see above), many of the neurons labelled following even single RabV injections would be expected to be divergent. Following injection into LG (Figure 4A), we found that only 1/21 infected cervical commissural premotor LDPNs was eGFP positive (n=3 LG injections, Figure 4B, C, F). Since none of the labelled neurons expressed ChAT, the majority of cervical premotor LDPNs are likely to be glutamatergic by exclusion. However, in agreement with previous results from TA injections (Ni et al., 2014), single-labelled thoracic premotor neurons comprised a mixed population of inhibitory and non-inhibitory neurons (34.4 ± 5.9%, 96/273, mCherry+ eGFP+ premotor neurons, n=3 LG injections, Figure 4D-F).We cannot determine whether the thoracic or lumbar GFP+ or GFP- premotor INs are divergent, as these data were obtained following single injections. However, in the lumbar cord, as expected, we observed that some divergent interneurons were cholinergic (Figure 4-figure supplement 1).

A subset of cervical premotor LDPNs arise from the V0 or dI2 domain

We next sought to determine the genetic provenance of divergent cervical LDPNs. Among the classes of ventral interneurons defined by the early expression of transcription factors (Lee

and Pfaff, 2001), the V0 and V3 cardinal classes are known to project to contralateral MNs. These classes can be further subdivided, with all V3 subclasses being glutamatergic (Zhang et al., 2008), and V0 INs being neuromodulatory ($V0_C$, cholinergic, (Miles et al., 2007), inhibitory ($V0_D$, dorsal, Talpalar et al., 2013), or excitatory ($V0_V$, ventral, (Talpalar et al., 2013), or $V0_G$, medial glutamatergic neurons that project to dorsal and intermediate lamina but not to MNs, (Zagoraiou et al., 2009)). Since previous studies showed that none of the LDPNs with soma in the cervical cord belong to the V3 population (Flynn et al., 2017), we sought to determine whether these LDPNs were of the V0 class.

V0 INs are defined by their embryonic expression of the transcription factor Dbx1 (Pierani et al., 2001) and Evx1 (Moran-Rivard et al., 2001). However, neither of these two transcription factors can reliably be detected at the postnatal ages of our mice. On the other hand, Lhx1 is expressed throughout the V0 and V1 populations (as well as dI2, dI4, and dIL_A populations) and may be detectable at this early postnatal stage (Skarlatou et al, 2020). However, V1 and $V0_D$ INs are glycinergic (Alvarez et al, 2013; Talpalar et al, 2013), $V0_C$ are cholinergic (Miles et al, 2007). Since we have shown that LDPNs are negative for GlyT2 and ChAT and dI4 and dIL_A INs are dorsal neurons (Glasgow et al., 2005; Pillai et al., 2007) expression of Lhx1 would point to cervical LDPNs belonging to either the $V0_V$ or dI2 class. In fact, it has very recently been shown that dorsally derived excitatory dI2 INs migrate to this region in the chick spinal cord and have divergent axons along the length of the cord and to the cerebellum (Haimson et al., 2021). While these neurons are not premotor in the chick (Haimson et al., 2021), it is possible that they are in the mouse.

Following injection of gastrocnemius (GS, n=4, Figure 5A), we detected 33 premotor LDPNs. Of these infected cervical premotor LDPNs, 8 (~24%) were clearly Lhx1 positive (Figure 5B, 5C). Given that there is a decrease of Lhx1 expression along the course of postnatal development (Figure 5-figure supplement 1), it is possible that the proportion of premotor LDPNs that were positive for Lhx1 was underestimated. Nevertheless, although we cannot conclude that the identified LDPNs arise from a homogenous population, it is likely that at least a portion of them arise from $V0_v$ neurons and/or dI2 neurons.

Cervical premotor LDPNs also project to local cervical MNs

Given that propriospinal neurons are involved in interlimb coordination, we next sought to determine whether the divergent cervical premotor LDPNs also project to cervical MNs. We therefore performed a series of experiments in which we injected forearm muscles (FMs; Supplementary file 2) with ΔG-Rab-mCherry, and extensor hindlimb GS with ΔG-Rab-eGFP.

Since it has been suggested that LDPNs participate in ipsilateral control of fore- and hindlimb (Miller and van der Meché, 1976), we sought to determine if premotor LDPNs project to homolateral lumbar and cervical motor pools (Figure 6A). When homolateral limbs were targeted, we found that some premotor LDPNs infected from ankle extensor injections were also infected from homolateral FMs injection (in 5/6 animals, 16/80 premotor LDPNs were also infected from FMs injection 18.7 ± 12.9%, Figure 6B-D). These divergent premotor LDPNs that projected to lumbar and cervical MNs were all located in the ventral quadrants with 11/16 located in contralateral lamina VIII, and were distributed throughout the rostrocaudal extent of the cervical cord, including segments rostral (C4) to the MN pools innervating the injected forelimb muscles. Furthermore, they had a soma size similar to the premotor LDPNs double labelled by dual hindlimb injections (632 ± 236 μm^2, p=0.056, n_1=16 premotor LDPNs infected from both homolateral fore and hindlimb injections vs n_2=38 divergent premotor LDPNs infected from dual hindlimb injections (see above), Mann-Whitney test; Figure 6E).

Given the involvement of LPDNs in the diagonal synchronisation of fore and hindlimb during locomotion (Bellardita and Kiehn, 2015; Ruder et al., 2016; Sherrington et al., 1906), we also injected contralateral FMs and GS (Figure 6-figure supplement 1A). We found that 2/26 cervical premotor LDPNs were also infected from the FMs injection with 1 divergent LDPNs in the lamina VIII contralateral to the hindlimb injection in each of 2 of the 3 injected animals (Figure 6-figure supplement 1B). Thus, at least a few cervical premotor LDPNs monosynaptically project to diagonal lumbar and cervical MNs. However, given the paucity of these cervical premotor LDPNs projecting to local cervical MNs, we could not reliably determine whether this subpopulation shared the same morphology as described above.

While sharing similar features with the LDPNs infected from dual hindlimb injections, it remains to be determined whether these INs premotor to hindlimb and forelimb muscles form a homogenous population with the divergent LDPNs.

Distribution of premotor long ascending propriospinal neurons differs from that of LDPNs

Having identified a population of divergent premotor long descending propriospinal neurons with projections from the cervical to the lumbar region, we next investigated whether ascending propriospinal neurons projecting from the lumbar or thoracic segments to cervical MNs could be identified. Following FMs injections, ascending premotor INs were observed throughout the cord (thoracic to sacral). There were very few (<1%) bifurcating (ascending/descending) premotor neurons in the thoracic cord after injections in homolateral GS and FMs (4/523

double labelled premotor neurons between T2 and T11, n=3, Figure 6-figure supplement 2A-B).

We identified premotor long ascending propriospinal neurons (LAPNs) in the lumbar cord, about half of which were localised in the dorsal ipsilateral quadrant (56/117, n=6 fore-hindlimb injections). This distribution of lumbar premotor LAPNs is different from that of cervical premotor LDPNs, which were almost exclusively ventral (164/172, n=13 pair of injections, see above). Of the 117 lumbar premotor LAPNs identified, 10 were also labelled from GS injections, indicating that some neurons projected both to local lumbar MNs as well as to cervical MNs (n=6 ipsilateral fore-hindlimb injections, Figure 6-figure supplement 2C-D). However, the position of these particular divergent premotor LAPNs was different from that of the premotor LDPNs, in that they were not localized within one quadrant of the cord (Figure 6-figure supplement 2D).

Finally, we turned our attention to the sacral spinal cord, where we found few premotor LAPNs (12 neurons in 4 of 6 mice). Of these, however, 10/12 were in the ventral contralateral quadrant (n=6 ipsilateral fore-hindlimb injections, Figure 6-figure supplement 2E-F), similar to the location of the cervical premotor LDPNs. Like these cervical neurons, the sacral LAPNs had strikingly large somata (710 ± 310 μm^2, n=11 premotor LAPNs, Figure 6- figure supplement 2G). Of 12 labelled neurons, 3 were also infected from the hindlimb (LG) injections (Figure 6-figure supplement 2E-G). Given that the size and location of these sacral premotor LAPNs were similar to the population of cervical divergent premotor LDPNs, they may represent a “reverse counterpart” of this descending system.

Discussion

Animals perform rich repertoires of movements through controlling muscle contractions around joints to produce the fundamental syllables of movement (Brownstone, 2020). To understand how behavioural repertoires are formed, it is important to understand the organization of the neural circuits underlying the production of each syllable. By using monosynaptic restricted RabV tracing techniques, we investigated the presence of spinal premotor interneurons that project to multiple motor pools and could thus potentially comprise circuits underlying co-activation (joint stiffening) or co-inhibition (joint relaxation) of motor pools across joints and between limbs. We found that at least 1/25 local lumbar premotor INs projects to multiple motor pools, in similar proportions whether these pools were synergist or antagonist pairs. Furthermore, we found that whereas the density of premotor neurons decreases with distance rostral to the motor pool targeted, a high proportion of labelled cervical LDPNs projects to multiple motor pools. These premotor LDPNs are in contralateral lamina VIII, have large somata, are neither glycinergic nor cholinergic, and project to multiple motor pools including those in the lumbar and cervical enlargements. These divergent neurons could thus form a substrate for joint and multi-joint stiffening that contributes to the production of a fundamental syllable of movement.

Estimating proportions of divergent premotor interneurons

The control of MNs across motor pools through spinal premotor circuits is required for the performance of all motor tasks involving limb movements. Previous studies showed the importance of motor synergies in the production of complex movements (Giszter, 2015; Takei et al., 2017), with the spinal cord identified as a potential site for muscle synergy organisation (Bizzi and Cheung, 2013; Levine et al., 2014). In this regard, it might be expected that a significant proportion of local spinal premotor INs innervate multiple motor pools, in particular those corresponding to synergist muscles. Perhaps surprisingly, we found similar rate of divergence throughout the spinal cord be the targeted MN pools synergist or antagonist. In the lumbar region, at least 4% of the local premotor INs project to two motor pools. More remotely, in thoracic as well as cervical premotor circuits, the apparent rate of divergence was higher but with a decreased density of labelled premotor neurons. Regardless of the proportion of divergent premotor neurons amongst the total premotor population, it is possible that these neurons effectively modulate the synchrony of MN activation and participate in co-activation or co-inhibition of different MN populations.

What proportion of premotor neurons project to more than one motor pool? To investigate the presence of premotor neurons projecting to multiple motor pools in the spinal cord, we used

RabV tracing, injecting ΔG-RabV expressing eGFP or mCherry into different pairs of muscles. Although this technique allowed for visualization of divergent premotor neurons throughout the spinal cord, the proportion of divergent premotor neurons has undoubtedly been underestimated. A divergent neuron will be double labelled only if each virus has been efficiently transmitted across its synapses with motoneurons from both motor pools. Therefore, due to the stochastic nature of the process of crossing a synapse, any given transfer efficiency lower than 100% will inevitably give rise to an underestimate of the real number of divergent neurons. The efficiency of trans-synaptic jumps for the SADB19 rabies virus that we used is unknown, and may depend in part on the type of synapse, with stronger connections facilitating transmission of the virus (Ugolini, 2011). The only indirect indication of efficiency comes from the direct comparison of the SADB19 and the more efficient CVS-N2c strains, for which there was at least a 4-fold increase in the ratio of local secondary to primary infected premotor interneurons (Reardon et al., 2016). This result suggests that the trans-synaptic efficiency of SADB19 is no higher than 25%. While there is no evidence for a bias towards stronger or weaker synapses (i.e., the actual number of physical contacts) between proximal and distal premotor interneurons, such a bias could affect efficiency of viral transmission, and could thus also have potentially skewed our relative estimate of divergence. With the simplifying assumption that the efficiencies of viral transfer are equal and independent from each other across spinal cord regions, we simulated a double injection experiment, extracting a binomial distribution, and calculated the relation between the observed and true rate of divergence. With a jump efficiency of 25%, the 4% divergence rate we observed in the lumbar spinal cord would correspond to an actual rate of divergence of 18% (Figure 8). And this calculated rate is almost certainly an underestimate because of the phenomenon of viral interference, whereby there is a reduced probability of subsequent infection with a second RabV after a window of a few hours after the first infection (Ohara et al., 2009). It is therefore likely that the actual rate of divergence of premotor circuit throughout the cord is substantially higher than we observed. Specifically, it is possible that the vast majority of, if not all, premotor LDPNs innervate more than one motor pool.

Mapping premotor circuits using the ChAT-Cre;RΦGT mouse

In our experimental model, the rabies glycoprotein is expressed only in neurons expressing ChAT, such as MNs. By restricting primary infection to specific MNs via intramuscular injection of RabV, trans-synaptic viral spread was thus restricted to neurons pre-synaptic to the infected MN population. It is therefore theoretically possible that there might be double jumps via other presynaptic cholinergic neurons such as medial partition neurons ($V0_C$ neurons; (Zagoraiou et al., 2009). Motoneurons also form synapses with other MNs (Bhumbra and Beato, 2018), so it

could also be possible that specificity is lost due to second order jumps via these cells. We consider double jumps unlikely for two main reasons: 1) following muscle injections, the first transsynaptic labelling occurs after 5-6 days. Since the tissue was fixed 9 days after injections, it is unlikely that many secondary jumps could have occurred in such a brief time window. And 2) most pre-synaptic partners of $V0_C$ INs are located in the superficial dorsal laminae (Zampieri et al., 2014), a region in which we did not observe any labelled INs. We are thus confident that the labelled neurons are premotor. We also acknowledge the possibility that some of the labelled premotor cells might originate from tertiary infection originating from secondary infection of synaptically connected MNs (Bhumbra and Beato, 2018). Such events might be rare (Ronzano et al., 2021) and would not alter our findings on the organization of divergent premotor neurons, since we have shown that their distributions are similar, regardless of the particular pair of injected muscles.

Premotor interneurons innervating antagonist motor pools: implications for movement

The similar rate of divergence between synergist and antagonist pairs might be surprising. But divergence to agonist and antagonist motor pools has been shown in adult mice (Gu et al., 2017), indicating that these circuits are not limited to an early developmental stage. Apart from the cervical divergent premotor LDPNs that are likely to represent a rather homogenous group of excitatory neurons, the divergent premotor neurons in the thoracic and lumbar regions could be comprised of different neural populations, with a mixed population of excitatory, inhibitory, and, in lower proportion, cholinergic neurons (Figure 1-figure supplement 6 and Figure 4-figure supplement 1). These INs that project to antagonist motor pools could thus be involved in modulating either joint stiffening (excitatory) or relaxation (inhibitory). For example, during postural adjustment and skilled movements, divergent excitatory premotor INs would lead to co-contraction of antagonist muscles to facilitate an increase in joint stiffness and to promote stability (Hansen et al., 2002; Nielsen and Kagamihara, 1993, 1992). In invertebrates, co-contraction of antagonist muscles has also been described preceding jumping (Pearson and Robertson, 1981): co-contraction could thus also be important for the initiation of movement.

On the other hand, divergent inhibitory premotor neurons would lead to joint relaxation. This phenomenon is less well studied (Leis et al., 2000; Manconi et al., 1998). One example could be their involvement in the loss of muscle tone that accompanies rapid eye movement sleep (Uchida et al., 2021; Valencia Garcia et al., 2018).

Projections of long descending propriospinal neurons to multiple motor pools

In the cat, long descending fibres originating in the cervical cord have been shown to innervate lumbar MNs (Giovanelli Barilari and Kuypers, 1969) and trigger monosynaptic

potentials (Jankowska et al., 1974). The existence of LDPNs has been confirmed anatomically in neonatal mice (Ni et al., 2014) and functionally in adult cats (Alstermark et al., 1987a, 1987b), where they are thought to play a role in posture and stability. Our study confirms the existence of premotor LDPNs, and also indicates that they have a high rate of divergence (up to ~40% compared to ~13% for thoracic neurons). Most cervical LDPNs are clustered in contralateral lamina VIII, are virtually all excitatory, and have a distinct morphology with somal size ~2-fold larger than other local cells (and similar to MNs). These findings contrast with the divergent premotor neurons found in the thoracic spinal cord: these are distributed in ipsilateral lamina VI and VII as well as in contralateral lamina VIII and thus clearly comprise multiple neuronal populations. In contrast to thoracic divergent premotor neurons, cervical LDPNs may thus have a more unifying function. Given their apparent widespread divergence, it is possible that these LDPNs are involved in producing widespread increases in muscle tone.

One step towards being able to further assess the function of this population of interneurons would be through understanding their lineage. Given the poor detection of the Lhx1 transcription factor in postnatal mice (Figure 5-figure supplement 1), we could not conclude that the labelled cervical LDPNs are a population that derive from the $V0_V$ or dI2 class. Although in the chick, dI2 INs do not project to MNs (Haimson et al., 2021), it is possible that they could in the mouse: these are large neurons located in the ventromedial spinal cord (Haimson et al., 2021), and express Lhx1(Avraham et al., 2009). Further experiments using a Dbx1-IRES-GFP mouse line (Bouvier et al., 2010), for example, could help to determine the identity of these divergent cervical LDPNs. Genetic access to this particular set of INs would also allow the design of experiments aimed at acute and specific activation or inactivation of divergent LDPNs, and could unravel their anatomy and function in behaviour.

Concluding remarks

The completion of movements requires well controlled muscle contractions across multiple joints within and between limbs. The control of any one joint is analogous to the production of syllables of speech, with the three most fundamental syllables of movement being a change in joint angle (requiring reciprocal inhibition of flexors and extensor MNs), a stiffening of a joint (requiring co-activation of flexors and extensor MNs), and a relaxation of a joint (requiring co-inhibition of flexor and extensor MNs). While neural circuits for reciprocal inhibition have been well studied over many decades (Eccles, 1969; Eccles et al., 1956), circuits for stiffening or relaxation have not been. Our anatomical data identify neurons that could be potentially implicated in these circuits and show that they are present within and distributed throughout the spinal cord. Thus, the mechanisms that lead to the production of the fundamental syllables of movement could be contained within the spinal cord itself.

Materials and Methods

Key resources table

Reagent type (species) or resource	Designation	Source or reference	Identifiers	Additional information
strain, strain background (Rabies virus)	ΔG-Rab-eGFP	Gift from M. Tripodi lab, LMCB Cambridge		G-deleted Rabies virus
strain, strain background (Rabies virus)	ΔG-Rab-mCherry	Gift from M. Tripodi lab, LMCB Cambridge		G-deleted Rabies virus
strain, strain background (*Mus musculus*)	ChAT-IRES-Cre	Jackson laboratory	IMSR Cat# JAX:006410; RRID:IMSR_JAX:006410	allele symbol: $Chat^{tm2(cre)Lowl}$; maintained on a C57BL6/J background
strain, strain background (*Mus musculus*)	RΦGT	Jackson laboratory	IMSR Cat# JAX:024708; RRID:IMSR_JAX:024708	allele symbol: Gt(ROSA)26Sortm1(CAG-RABVgp4,-TVA)Arenk; maintained on a C57BL6/J background
strain, strain backgroun	GlyT2-eGFP	Gift from H. Zeilhofer lab,	IMSR Cat# RBRC04708; RRID:IMSR_RBRC04708	allele symbol: Tg(Slc6a5-

d (*Mus musculus*)		University of Zurich		EGFP)1Uze; maintained on a C57BL6/J background
cell line (*Homo-sapiens*, female)	HEK293t/17	Gift from M. Tripodi lab, LMCB Cambridge	RRID:CVCL_1926	ATCC, cat. no. CRL-1126
cell line (*Mesocricetus auratus*, male)	BHK-21	Gift from M. Tripodi lab, LMCB Cambridge	RRID: CVCL_1915	ATCC # CCL-10
cell line (*Mesocricetus auratus*, male)	BHK-G	Gift from M. Tripodi lab, LMCB Cambridge	RRID: CVCL_1915	Modified from ATCC Cat# CCL-10; RRID: CVCL_1915 to express the rabies glycoprotein
antibody	anti-ChAT (Goat polyclonal)	Millipore	Cat# AB144P; RRID:AB_2079751	IF (1:100)
antibody	anti-mCherry (Chicken polyclonal)	Abcam	Cat# ab205402; RRID:AB_2722769	IF (1:2500)
antibody	anti-GFP (Rabbit polyclonal)	Abcam	Cat# ab290; RRID:AB_303395	IF (1:2500)
antibody	anti-vGluT2 (Guinea pig polyclonal)	Millipore	Cat# AB2251-I; RRID:AB_2665454	IF (1:2500)

antibody	anti-Lhx1 (Rabbit polyclonal)	Gift from T. Jessell lab, Columbia University, New York		IF (1:5000)
antibody	anti-Rabbit IgG H&L Alexa Fluor® 647 (Donkey polyclonal)	Abcam	Cat# ab150079; RRID:AB_2722623	IF (1:1000)
antibody	anti-Goat IgG H&L Alexa Fluor® 405 (Donkey polyclonal preadsorbed)	Abcam	Abcam Cat# AB175665; RRID:AB_2636888	IF (1:200)
antibody	anti-Rabbit IgG H&L Alexa Fluor®488 (Donkey polyclonal Highly Cross-Adsorbed)	Thermo Fisher Scientific	Cat# A-21206; RRID:AB_2535792	IF (1:1000)
antibody	anti-Chicken IgY (IgG) H&L Cy3-AffiniPure (Donkey polyclonal)	Jackson Immuno Research Labs	Cat# 703-165-155; RRID:AB_2340363	IF (1:1000)
chemical compound, drug	Mowiol® 4-88	Sigma Aldrich	Cat# 81381-250G	
software, algorithm	ZEN Digital Imaging for Light Microscopy: Zen Blue 2.3	Carl Zeiss light microscopy imaging systems	RRID:SCR_013672	
software, algorithm	Imaris 9.1	Bitplane	RRID:SCR_007370	

software, algorithm	R 3.6.2	R Project for Statistical Computing	RRID:SCR_001905	
software, algorithm	Prism 7.0	GraphPad	RRID:SCR_002798	
software, algorithm	Adobe illustrator version CC 2019	Adobe	RRID:SCR_010279	

466

467 **Mouse strains**

468 All experiments (n=27) were performed according to the Animals (Scientific Procedures) Act
469 UK (1986) and certified by the UCL AWERB committee, under project licence number 70/7621.
470 Homozygous ChAT-IRES-Cre mice (which have an IRES-Cre sequence downstream of the
471 ChAT stop codon, such that Cre expression is controlled by the endogenous ChAT gene
472 promoter without affecting ChAT expression; Rossi et al., 2011, Jackson lab, stock #006410)
473 crossed with homozygous RΦGT mice (Takatoh et al., 2013), Jackson lab, stock #024708, that
474 have Cre dependent expression of the rabies glycoprotein and the avian viral receptor TVA,
475 whose expression is not employed in this study) were used for double injections (see
476 Supplementary file 3 the detail of animal use for each type of injection). For single injections,
477 homozygous ChAT-IRES-Cre mice (termed ChAT-Cre here) were crossed with hemizygous
478 GlyT2-eGFP mice (BAC transgene insertion in exon 2 of *Slc6a5* gene allowing specific eGFP
479 expression in GlyT2 positive cells, MGI:3835459, Zeilhofer et al., 2005) and their eGFP
480 positive offspring was mated with homozygous RΦGT (see Supplementary file 3).

481 **Virus production, collection, and titration**

482 We used the glycoprotein G-deleted variant of the SAD-B19 vaccine strain rabies virus (a
483 kind gift from Dr M. Tripodi). Modified rabies virus (ΔG-Rab) with the glycoprotein G sequence
484 replaced by mCherry or eGFP (ΔG-Rab-eGFP/mCherry) was produced at a high concentration
485 with minor modifications to the original protocol (Osakada et al., 2011). BHK cells expressing
486 the rabies glycoprotein G (BHK-G cells) were plated in standard Dulbecco modified medium
487 with 10% fetal bovine serum (FBS) and split after 6-7 hours incubating at 37°C and 5% CO_2.
488 They were inoculated at a multiplicity of infection of 0.2-0.3 with either ΔG-Rab-eGFP or
489 mCherry virus in 2% FBS, and incubated at 35°C and 3% CO_2. Plates were then split in 10%

FBS at 37°C and 5% CO_2. After 24h the medium was replaced by 2% FBS medium and incubated at 35°C and 3% CO_2 for 3 days (virus production). The supernatant was collected and medium was added for another cycle (3 cycles maximum), after which the supernatant was filtered (0.45 µm filter) and centrifuged 2h at 19,400 rpm (SW28 Beckman rotor). The pellets were re-suspended in phosphate buffered saline (PBS) and centrifuged together at 21,000 rpm, 4°C, 4 hours in a 20% sucrose gradient. Pellets of each collection were then re-suspended and stored in 5-10 µl aliquots at -80°C.

Virus titration was performed on BHK cells plated in 10% FBS medium at 1.5 x 10^5 cells/ml and incubated overnight at 37°C and 10% CO_2 (growth). The virus was prepared for 2 serial dilutions with 2 different aliquots and added in the well after an equal volume of medium had been removed (serial dilution from 10^{-3} to 10^{-10}) and incubated 48h at 35°C and 3% CO_2. The titre was determined from the count of cells in the higher dilution well and was between 10^9 and 10^{10} infectious units (IU)/ml.

Intramuscular injections

A subcutaneous injection of analgesic (carprofen, 1 µl, 10% w/v) was given to the neonatal pups (P1-P3) prior to surgery and all procedures were carried out under general isoflurane anaesthesia. After a skin incision to expose the targeted muscle, the virus (1µl) was injected intramuscularly using a Hamilton injector (model 7652-01) mounted with a bevelled glass pipette (inner diameter 50-70 µm). The mice were injected in tibialis anterior (TA) and peroneus longus (PL) (ankle flexor pair), lateral and medial gastrocnemius (LG and MG) (ankle extensor pair) for synergist pairs and TA and LG for antagonist pairs. In hindlimb/forelimb double injections, the LG and MG were both injected with 1 µl of one RabV to increase the number of long projecting cells infected. In addition, 1 µl of the second RabV was injected in forearm muscles (FMs, see Supplementary file 2) without selecting a specific muscle. The injected viruses were used at a titre between 10^9 and 10^{10} IU/ml. The incisions were closed with vicryl suture, and the mice were closely monitored for 24 hours post-surgery. Mice were perfused 9 days after the injections. Due to the proximity of synergist pairs of muscles, prior to spinal tissue processing, we dissected the injected leg and confirmed that there was no contamination of virus across the injected muscles or in adjacent muscles below or above the knee. When injecting forearm muscles, we could not target a single muscle. To visualize which muscles had been infected, we carefully dissected each forearm muscles and assess for the presence of fluorescent signal (see Supplementary file 2). Three heterozygous RΦGT mice were also injected (LG muscle) with an EnvA pseudotyped rabies virus in order to test simultaneously for ectopic expression of G or of the TVA receptors. In three control animals

we observed 1-3 labelled motoneurons, but no interneuron labelling. This indicates the presence of minimal ectopic TVA expression, but not of G (Ronzano et al., 2021).

Tissue collection and immunohistochemistry

The mice were perfused with phosphate buffer solution (PBS, 0.1 M) followed by PBS 4% paraformaldehyde under terminal ketamine/xylazine anaesthesia (i.p. 80 mg/kg and 10 mg/kg respectively). The spinal cords were then collected through a ventral laminectomy and post-fixed for 2 hours. The cords were divided into the different parts of the spinal cord (cervical (C1-T1), thoracic (T2-T11), lumbar (L1-L6) and sacral (S1-S4)), cryoprotected overnight in 30% sucrose PBS, embedded in optimal cutting temperature compound (Tissue-Tek) and sliced transversally (30 µm thickness) with a cryostat (Bright instruments, UK). Sections were incubated with primary antibodies for 36h at 4°C and with secondary antibodies overnight at 4°C in PBS double salt, 0.2% Triton 100-X (Sigma), 7% donkey normal serum (Sigma). The primary antibodies used were: goat anti-choline acetyltransferase (ChAT, 1:100, Millipore, AB144P), chicken anti-mCherry (1:2500, Abcam, Ab205402), rabbit anti-GFP (1:2500, Abcam, Ab290), guinea pig anti-vGluT2 (1:2500, Millipore, AB2251-I), and rabbit anti-Lhx1 (1:5000, from Dr. T Jessell, Columbia University, New York); and the secondary antibodies: donkey anti-rabbit Alexa 647 (1:1000, Abcam, Ab150079), donkey anti-goat preadsorbed Alexa 405 (1:200, Abcam, Ab175665), donkey anti-rabbit Alexa 488 (1:1000, Thermofisher, A21206), and donkey anti-chicken Cy3 (1:1000, Jackson ImmunoResearch, #703-165-155). The slides were mounted in Mowiol (Sigma, 81381-250G) and coverslipped (VWR, #631-0147) for imaging.

Confocal imaging and analysis

Images of the entire sections were obtained using a Zeiss LSM800 confocal microscope with a 20x air objective (0.8 NA) and tile advanced set up function (ZEN Blue 2.3 software). A 63x oil objective was used for Airy scan imaging of somata and excitatory boutons. Tiles were stitched using Zen Blue and analyses were performed using Zen Blue and Imaris (Bitplane, version 9.1) software packages. Location maps were plotted setting the central canal as (0,0) in the (x,y) Cartesian system and using the “Spots" function of Imaris. The y-axis was set to the dorso-ventral axis. Positive values were assigned for dorsal neurons in the y-axis and ipsilateral (to the hindlimb injection) neurons in the x-axis. Coordinates were collected on every section and normalized through the cervical, thoracic, lumbar and sacral parts separately using grey matter borders and fixing the width and the height of the transverse hemisections. To calculate divergence rates, given the high density of premotor INs infected in the lumbar cord all infected premotor INs (eGFP+, mCherry+ and eGFP+mCherry+) were quantified in 1 of

every 3 sections which further allowed to avoid counting the same cells twice on consecutive sections. In the cervical, thoracic and sacral regions, all cells were quantified, as their low density allowed for manually excluding premotor INs found in consecutive sections. Since MNs are big cells localised as a restricted column of the ventral spinal cord, we quantified them on every other sections, to avoid counting the same cell twice on consecutive sections.

Statistics

All statistical analyses and plots were made using R (R foundation for statistical computing, Vienna, Austria, 2005, http://www.r-project.org, version 3.6.2) and GraphPad PRISM (version 7.0). To compare cell sectional areas, non-parametric rank tests were used as specified in each related result. The numbers of animals/cells in each experiment and statistical tests used are reported in the figure legends or directly in the text. Results and graphs illustrate the mean ± standard deviation. Statistical significance levels are represented as follows: * $p < 0.05$, ** $p < 0.01$, *** $p < 0.001$, **** $p < 0.0001$ and ns: not significant.

Acknowledgments

We are grateful to Dr N. Zampieri and all the members of Brownstone and Beato labs for insightful comments on the manuscript. We want to thank S. Morton for providing Lhx1 antibodies, Prof L. Greensmith for access to her lab facilities and Dr M.G. Özyurt for helping with immunostaining. This work was supported by a Leverhulme Trust grant (grant number RPG-2013-176) and a BBSRC grant (BB/L001454) to MB and a Wellcome Trust Investigator Award to RMB (110193). RMB is supported by Brain Research UK.

Declaration of interests

The authors declare no conflict of interest.

582 # References

583 Alstermark B, Lundberg A, Pinter M, Sasaki S. 1987a. Subpopulations and functions of long
584 C3-C5 propriospinal neurones. *Brain Res*. doi:10.1016/0006-8993(87)91402-8

585 Alstermark B, Lundberg A, Pinter M, Sasaki S. 1987b. Long C3-C5 propriospinal neurones in
586 the cat. *Brain Res* **404**:382–388. doi:10.1016/0006-8993(87)91400-4

587 Alvarez FJ, Jonas PC, Sapir T, Hartley R, Berrocal MC, Geiman EJ, Todd AJ, Goulding M.
588 2005. Postnatal phenotype and localization of spinal cord V1 derived interneurons. *J*
589 *Comp Neurol* **493**:177–192. doi:10.1002/cne.20711

590 Avraham O, Hadas Y, Vald L, Zisman S, Schejter A, Visel A, Klar A. 2009. Transcriptional
591 control of axonal guidance and sorting in dorsal interneurons by the Lim-HD proteins
592 Lhx9 and Lhx1. *Neural Dev* **4**:21. doi:10.1186/1749-8104-4-21

593 Ballion B, Morin D, Viala D. 2001. Forelimb locomotor generators and quadrupedal
594 locomotion in the neonatal rat. *Eur J Neurosci* **14**:1727–1738. doi:10.1046/j.0953-
595 816x.2001.01794.x

596 Bellardita C, Kiehn O. 2015. Phenotypic characterization of speed-associated gait changes in
597 mice reveals modular organization of locomotor networks. *Curr Biol* **25**:1426–1436.
598 doi:10.1016/j.cub.2015.04.005

599 Benito-Gonzalez A, Alvarez FJ. 2012. Renshaw Cells and Ia Inhibitory Interneurons Are
600 Generated at Different Times from p1 Progenitors and Differentiate Shortly after Exiting
601 the Cell Cycle. *J Neurosci* **32**:1156–1170. doi:10.1523/JNEUROSCI.3630-12.2012

602 Bhumbra GS, Beato M. 2018. Recurrent excitation between motoneurones propagates
603 across segments and is purely glutamatergic. *PLoS Biol* **16**:e2003586.
604 doi:10.1371/journal.pbio.2003586

605 Bizzi E, Cheung VCK. 2013. The neural origin of muscle synergies. *Front Comput Neurosci*
606 **7**:1–6. doi:10.3389/fncom.2013.00051

607 Bouvier J, Thoby-Brisson M, Renier N, Dubreuil V, Ericson J, Champagnat J, Pierani A,
608 Chédotal A, Fortin G. 2010. Hindbrain interneurons and axon guidance signaling critical
609 for breathing. *Nat Neurosci* **13**:1066–1074. doi:10.1038/nn.2622

610 Brockett EG, Seenan PG, Bannatyne BA, Maxwell DJ. 2013. Ascending and descending
611 propriospinal pathways between lumbar and cervical segments in the rat: Evidence for a

substantial ascending excitatory pathway. *Neuroscience* **240**:83–97. doi:10.1016/j.neuroscience.2013.02.039

Brownstone RM. 2020. Key Steps in the Evolution of Mammalian Movement: A Prolegomenal Essay. *Neuroscience* **450**:135–141. doi:10.1016/j.neuroscience.2020.05.020

Eccles JC. 1969. The Inhibitory Pathways of the Central Nervous System., Springfield: Charles C. Thomas.

Eccles JC, Fatt P, Landgren S. 1956. CENTRAL PATHWAY FOR DIRECT INHIBITORY ACTION OF IMPULSES IN LARGEST AFFERENT NERVE FIBRES TO MUSCLE. *J Neurophysiol* **19**:75–98. doi:10.1152/jn.1956.19.1.75

Eidelberg E, Story JL, Meyer BL, Nystel J. 1980. Stepping by chronic spinal cats. *Exp Brain Res*. doi:10.1007/BF00237787

Flynn JR, Conn VL, Boyle KA, Hughes DI, Watanabe M, Velasquez T, Goulding MD, Callister RJ, Graham BA. 2017. Anatomical and molecular properties of long descending propriospinal neurons in mice. *Front Neuroanat* **11**:1–13. doi:10.3389/fnana.2017.00005

Giovanelli Barilari M, Kuypers HGJM. 1969. Propriospinal fibers interconnecting the spinal enlargements in the cat. *Brain Res* **14**:321–330. doi:10.1016/0006-8993(69)90113-9

Giszter SF. 2015. Motor primitives-new data and future questions. *Curr Opin Neurobiol* **33**:156–165. doi:10.1016/j.conb.2015.04.004

Glasgow SM, Henke RM, MacDonald RJ, Wright CVE, Johnson JE. 2005. Ptf1a determines GABAergic over glutamatergic neuronal cell fate in the spinal cord dorsal horn. *Development* **132**:5461–5469. doi:10.1242/dev.02167

Gu Z, Serradj N, Ueno M, Liang M, Li J, Baccei ML, Martin JH, Yoshida Y. 2017. Skilled Movements Require Non-apoptotic Bax/Bak Pathway-Mediated Corticospinal Circuit Reorganization. *Neuron*. doi:10.1016/j.neuron.2017.04.019

Haimson B, Hadas Y, Bernat N, Kania A, Daley MA, Cinnamon Y, Lev-Tov A, Klar A. 2021. Spinal lumbar dI2 interneurons contribute to stability of bipedal stepping. *Elife* **10**. doi:10.7554/eLife.62001

Hansen S, Hansen NL, Christensen LOD, Petersen NT, Nielsen JB. 2002. Coupling of antagonistic ankle muscles during co-contraction in humans. *Exp Brain Res*. doi:10.1007/s00221-002-1152-3

642 Hart CB, Giszter SF. 2010. A neural basis for motor primitives in the spinal cord. *J Neurosci*
643 **30**:1322–1326. doi:10.1523/JNEUROSCI.5894-08.2010

644 Humphrey DR, Reed DJ. 1983. Separate cortical systems for control of joint movement and
645 joint stiffness: reciprocal activation and coactivation of antagonist muscles. *Adv Neurol*
646 **39**:347–372.

647 Jankowska E, Lundberg A, Roberts WJ, Stuart D. 1974. A long propriospinal system with
648 direct effect on motoneurones and on interneurones in the cat lumbosacral cord. *Exp*
649 *Brain Res* **21**:169–194. doi:10.1007/BF00234388

650 Lee SK, Pfaff SL. 2001. Transcriptional networks regulating neuronal identity in the
651 developing spinal cord. *Nat Neurosci* **4 Suppl**:1183–1191. doi:10.1038/nn750
652 [doi];nn750 [pii]

653 Leis AA, Stokic DS, Fuhr P, Kofler M, Kronenberg MF, Wissel J, Glocker FX, Seifert C,
654 Stetkarova I. 2000. Nociceptive fingertip stimulation inhibits synergistic motoneuron
655 pools in the human upper limb. *Neurology* **55**:1305–1309. doi:10.1212/WNL.55.9.1305

656 Levine AJ, Hinckley CA, Hilde KL, Driscoll SP, Poon TH, Montgomery JM, Pfaff SL. 2014.
657 Identification of a cellular node for motor control pathways. *Nat Neurosci* **17**:586–593.
658 doi:10.1038/nn.3675

659 Manconi FM, Syed NA, Floeter MK. 1998. Mechanisms underlying spinal motor neuron
660 excitability during the cutaneous silent period in humans. *Muscle Nerve* **21**:1256–1264.
661 doi:10.1002/(SICI)1097-4598(199810)21:10<1256::AID-MUS3>3.0.CO;2-A

662 Miles GB, Hartley R, Todd AJ, Brownstone RM. 2007. Spinal cholinergic interneurons
663 regulate the excitability of motoneurons during locomotion. *Proc Natl Acad Sci U S A*
664 **104**:2448–2453. doi:10.1073/pnas.0611134104

665 Miller S, van der Meché FGA. 1976. Coordinated stepping of all four limbs in the high spinal
666 cat. *Brain Res* **109**:395–398. doi:10.1016/0006-8993(76)90541-2

667 Mitchell EJ, McCallum S, Dewar D, Maxwell DJ. 2016. Corticospinal and reticulospinal
668 contacts on cervical commissural and long descending propriospinal neurons in the
669 adult rat spinal cord; evidence for powerful reticulospinal connections. *PLoS One* **11**:1–
670 19. doi:10.1371/journal.pone.0152094

671 Moran-Rivard L, Kagawa T, Saueressig H, Gross MK, Burrill J, Goulding M. 2001. Evx1 Is a

672 Postmitotic Determinant of V0 Interneuron Identity in the Spinal Cord. *Neuron* **29**:385–
673 399. doi:10.1016/S0896-6273(01)00213-6

674 Nathan PW, Smith M, Deacon P. 1996. Vestibulospinal, reticulospinal and descending
675 propriospinal nerve fibres in man. *Brain* **119**:1809–1833. doi:10.1093/brain/119.6.1809

676 Ni Y, Nawabi H, Liu X, Yang L, Miyamichi K, Tedeschi A, Xu B, Wall NR, Callaway EM, He Z.
677 2014. Characterization of Long Descending Premotor Propriospinal Neurons in the
678 Spinal Cord. *J Neurosci* **34**:9404–9417. doi:10.1523/JNEUROSCI.1771-14.2014

679 Nielsen J, Kagamihara Y. 1993. The regulation of presynaptic inhibition during co-contraction
680 of antagonistic muscles in man. *J Physiol*. doi:10.1113/jphysiol.1993.sp019652

681 Nielsen J, Kagamihara Y. 1992. The regulation of disynaptic reciprocal Ia inhibition during co-
682 contraction of antagonistic muscles in man. *J Physiol*.
683 doi:10.1113/jphysiol.1992.sp019341

684 Ohara S, Inoue KI, Witter MP, Iijima T. 2009. Untangling neural networks with dual retrograde
685 transsynaptic viral infection. *Front Neurosci* **3**:344–349. doi:10.3389/neuro.01.032.2009

686 Osakada F, Mori T, Cetin AH, Marshel JH, Virgen B, Callaway EM. 2011. New Rabies Virus
687 Variants for Monitoring and Manipulating Activity and Gene Expression in Defined
688 Neural Circuits. *Neuron* **71**:617–631. doi:10.1016/j.neuron.2011.07.005

689 Pearson KG, Robertson RM. 1981. Interneurons coactivating hindleg flexor and extensor
690 motoneurons in the locust. *J Comp Physiol ??? A*. doi:10.1007/BF00612571

691 Pierani A, Moran-Rivard L, Sunshine MJ, Littman DR, Goulding M, Jessell TM. 2001. Control
692 of interneuron fate in the developing spinal cord by the progenitor homeodomain protein
693 Dbx1. *Neuron* **29**:367–384. doi:10.1016/S0896-6273(01)00212-4

694 Pillai A, Mansouri A, Behringer R, Westphal H, Goulding M. 2007. Lhx1 and Lhx5 maintain
695 the inhibitory-neurotransmitter status of interneurons in the dorsal spinal cord.
696 *Development* **134**:357–366. doi:10.1242/dev.02717

697 Pocratsky AM, Burke DA, Morehouse JR, Beare JE, Riegler AS, Tsoulfas P, States GJR,
698 Whittemore SR, Magnuson DSK. 2017. Reversible silencing of lumbar spinal
699 interneurons unmasks a task-specific network for securing hindlimb alternation. *Nat*
700 *Commun* **8**:1963. doi:10.1038/s41467-017-02033-x

701 Reardon TR, Murray AJ, Turi GF, Wirblich C, Croce KR, Schnell MJ, Jessell TM, Losonczy A.

2016. Rabies Virus CVS-N2c Strain Enhances Retrograde Synaptic Transfer and Neuronal Viability. *Neuron*. doi:S0896-6273(16)00005-2 [pii];10.1016/j.neuron.2016.01.004 [doi]

Reed WR, Shum-Siu A, Whelan A, Onifer SM, Magnuson DSK. 2009. Anterograde labeling of ventrolateral funiculus pathways with spinal enlargement connections in the adult rat spinal cord. *Brain Res* **1302**:76–84. doi:10.1016/j.brainres.2009.09.049

Ronzano R, Skarlatou S, Bannatyne BA, Bhumbra GS, Foster JD, Lancelin C, Pocratsky A, Özyurt MG, Smith CC, Todd AJ, Maxwell DJ, Murray AJ, Brownstone RM, Zampieri N, Beato M. 2021. On the distribution of spinal premotor interneurons. *bioRxiv*. doi:https://doi.org/10.1101/2021.02.10.430608

Rossi J, Balthasar N, Olson D, Scott M, Berglund E, Lee CE, Choi MJ, Lauzon D, Lowell BB, Elmquist JK. 2011. Melanocortin-4 Receptors Expressed by Cholinergic Neurons Regulate Energy Balance and Glucose Homeostasis. *Cell Metab* **13**:195–204. doi:10.1016/j.cmet.2011.01.010

Ruder L, Takeoka A, Arber S. 2016. Long-Distance Descending Spinal Neurons Ensure Quadrupedal Locomotor Stability. *Neuron* **92**:1063–1078. doi:10.1016/j.neuron.2016.10.032

Sapir T, Geiman EJ, Wang Z, Velasquez T, Mitsui S, Yoshihara Y, Frank E, Alvarez FJ, Goulding M. 2004. Pax6 and Engrailed 1 Regulate Two Distinct Aspects of Renshaw Cell Development. *J Neurosci* **24**:1255–1264. doi:10.1523/JNEUROSCI.3187-03.2004

Sherrington CS, Laslett EE. 1903. Observations on some spinal reflexes and the interconnection of spinal segments. *J Physiol* **29**:58–96. doi:10.1113/jphysiol.1903.sp000946

Sherrington, CS, New Haven C, Press YU. 1906. The integrative action of the nervous system, New Haven,. ed.

Skinner RD, Coulter JD, Adams RJ, Remmel RS. 1979. Cells of origin of long descending propriospinal fibers connecting the spinal enlargements in cat and monkey determined by horseradish peroxidase and electrophysiological techniques. *J Comp Neurol* **188**:443–454. doi:10.1002/cne.901880307

Takatoh J, Nelson A, Zhou X, Bolton MML, Ehlers MD, Arenkiel BR, Mooney R, Wang F. 2013. New Modules Are Added to Vibrissal Premotor Circuitry with the Emergence of

Exploratory Whisking. *Neuron* **77**:346–360. doi:10.1016/j.neuron.2012.11.010

Takei T, Confais J, Tomatsu S, Oya T, Seki K. 2017. Neural basis for hand muscle synergies in the primate spinal cord. *Proc Natl Acad Sci U S A* **114**:8643–8648. doi:10.1073/pnas.1704328114

Takei T, Seki K. 2010. Spinal interneurons facilitate coactivation of hand muscles during a precision grip task in monkeys. *J Neurosci* **30**:17041–17050. doi:10.1523/JNEUROSCI.4297-10.2010

Talpalar AE, Bouvier J, Borgius L, Fortin G, Pierani A, Kiehn O. 2013. Dual-mode operation of neuronal networks involved in left-right alternation. *Nature* **500**:85–88. doi:10.1038/nature12286

Todd A, Watt C, Spike R, Sieghart W. 1996. Colocalization of GABA, glycine, and their receptors at synapses in the rat spinal cord. *J Neurosci* **16**:974–982. doi:10.1523/JNEUROSCI.16-03-00974.1996

Todd AJ, Sullivan AC. 1990. Light microscope study of the coexistence of GABA-like and glycine-like immunoreactivities in the spinal cord of the rat. *J Comp Neurol* **296**:496–505. doi:10.1002/cne.902960312

Tresch MC, Jarc A. 2009. The case for and against muscle synergies. *Curr Opin Neurobiol* **19**:601–607. doi:10.1016/j.conb.2009.09.002

Uchida S, Soya S, Saito YC, Hirano A, Koga K, Tsuda M, Abe M, Sakimura K, Sakurai T. 2021. A Discrete Glycinergic Neuronal Population in the Ventromedial Medulla That Induces Muscle Atonia during REM Sleep and Cataplexy in Mice. *J Neurosci* **41**:1582–1596. doi:10.1523/JNEUROSCI.0688-20.2020

Ugolini G. 2011. Rabies Virus as a Transneuronal Tracer of Neuronal Connections, Advances in Virus Research. doi:10.1016/B978-0-12-387040-7.00010-X

Ugolini G. 1995. Specificity of rabies virus as a transneuronal tracer of motor networks: Transfer from hypoglossal motoneurons to connected second-order and higher order central nervous system cell groups. *J Comp Neurol* **356**:457–480. doi:10.1002/cne.903560312

Valencia Garcia S, Brischoux F, Clément O, Libourel PA, Arthaud S, Lazarus M, Luppi PH, Fort P. 2018. Ventromedial medulla inhibitory neuron inactivation induces REM sleep

without atonia and REM sleep behavior disorder. *Nat Commun* **9**:1–11. doi:10.1038/s41467-017-02761-0

Wickersham IR, Lyon DC, Barnard RJO, Mori T, Finke S, Conzelmann KK, Young JAT, Callaway EM. 2007. Monosynaptic Restriction of Transsynaptic Tracing from Single, Genetically Targeted Neurons. *Neuron* **53**:639–647. doi:10.1016/j.neuron.2007.01.033

Wiltschko AB, Johnson MJ, Iurilli G, Peterson RE, Katon JM, Pashkovski SL, Abraira VE, Adams RP, Datta SR. 2015. Mapping Sub-Second Structure in Mouse Behavior. *Neuron* **88**:1121–1135. doi:10.1016/j.neuron.2015.11.031

Zagoraiou L, Akay T, Martin JF, Brownstone RM, Jessell TM, Miles GB. 2009. A Cluster of Cholinergic Premotor Interneurons Modulates Mouse Locomotor Activity. *Neuron* **64**:645–662. doi:10.1016/j.neuron.2009.10.017

Zampieri N, Jessell TM, Murray AJ. 2014. Mapping sensory circuits by anterograde transsynaptic transfer of recombinant rabies virus. *Neuron* **81**:766–778. doi:10.1016/j.neuron.2013.12.033

Zeilhofer HU, Studler B, Arabadzisz D, Schweizer C, Ahmadi S, Layh B, Bosl MR, Fritschy JM. 2005. Glycinergic neurons expressing enhanced green fluorescent protein in bacterial artificial chromosome transgenic mice. *J Comp Neurol* **482**:123–141.

Zhang J, Lanuza GM, Britz O, Wang Z, Siembab VC, Zhang Y, Velasquez T, Alvarez FJ, Frank E, Goulding M. 2014. V1 and V2b interneurons secure the alternating flexor-extensor motor activity mice require for limbed locomotion. *Neuron* **82**:138–150. doi:10.1016/j.neuron.2014.02.013

Zhang Y, Narayan S, Geiman E, Lanuza GM, Velasquez T, Shanks B, Akay T, Dyck J, Pearson K, Gosgnach S, Fan CM, Goulding M. 2008. V3 Spinal Neurons Establish a Robust and Balanced Locomotor Rhythm during Walking. *Neuron* **60**:84–96. doi:10.1016/j.neuron.2008.09.027

Figure 1: Organisation of divergent premotor INs in the lumbar spinal cord.

(A) Experimental strategy to describe divergent premotor INs that project to 2 motor pools of synergist (injection in TA and PL or LG and MG) or antagonist (TA and LG) pair of muscles. **(Bi)** Representative example of a lumbar transverse section following an injection in the TA (ΔG-Rab-mCherry) and LG (ΔG-Rab-eGFP), showing ChAT (grey blue), GFP (green) and mCherry (pink). A divergent premotor IN is highlighted in the dashed box. Filled arrowheads show divergent premotor INs and contour arrowheads show infected MNs. The dashed line drawn outlines the grey matter contour. **(ii-iv)** Higher magnification of a divergent premotor IN that has been infected by the ΔG-Rab-eGFP and ΔG-Rab-mCherry, showing (ii) eGFP, (iii) mCherry and (iv) the overlay. More representative examples of lumbar sections following injections in LG and MG, TA and PL, LG and TA are shown on Figure 1-figure supplement 1, 2 and 3 respectively. **(C-E)** Distribution of the lumbar divergent premotor INs following injections in (C) LG and MG (n=2), (D) PL and TA (n=2), (E) LG and TA (n=3). (**F**) Asymmetric violin plots showing the medio-lateral and dorso-ventral distributions of divergent premotor INs. The halves correspond respectively to the dorsal (top) and ventral (bottom) distributions and to the ipsilateral (right) and contralateral (left) distributions of divergent premotor INs in the lumbar cord. Violin areas were normalized on the number of divergent INs. **(G)** Distribution of the premotor INs within each quadrant of the lumbar cord, with pie sizes proportional to the percentage of premotor INs in each quadrant of the lumbar cord. Numbers along the axis indicate distances (in μm). Scale bars: (Bi) 200 μm; (Biv) 10 μm. Raw number of eGFP, mCherry and double labelled premotor neurons per samples per muscle pair injected, are shown on the Figures 1-figure supplement 1, 2 and 3.

Figure 1-source data 1

Source data for Figure 1C,D,E,G

Figure 1-figure supplement 1: Divergent premotor INs in the lumbar spinal cord following injections in synergists LG and MG.

(A-B) Representative examples of lumbar transverse sections following injections in the LG (ΔG-Rab-eGFP) and MG (ΔG-Rab-mCherry) showing GFP (green) and mCherry (pink). A divergent premotor IN is highlighted in the dashed box. Filled arrowheads show divergent premotor INs and contour arrowheads show infected MNs. The dashed lines drawn outline the grey matter. **(ii-iv)** Higher magnification of a divergent premotor IN that has been infected by the ΔG-Rab-eGFP and ΔG-Rab-mCherry, showing (ii) mCherry, (iii) eGFP and (iv) the overlay. **(C-D)** Venn diagrams showing the distributions of lumbar infected premotor INs in the two samples injected in LG and MG. Scale bars: (Ai, Bi) 200 μm; (Aiv, Biv) 20 μm.

Figure 1-figure supplement 2: Divergent premotor INs in the lumbar spinal cord following injections in synergists PL and TA.

(A-B) Representative examples of lumbar transverse sections following injections in the PL (ΔG-Rab-eGFP) and TA (ΔG-Rab-mCherry) showing GFP (green) and mCherry (pink). A divergent premotor IN is highlighted in the dashed box. Filled arrowheads show divergent premotor INs. The dashed lines drawn outline the grey matter contour. **(ii-iv)** Higher magnification of a divergent premotor IN that has been infected by the ΔG-Rab-eGFP and ΔG-Rab-mCherry, showing (ii) mCherry, (iii) eGFP and (iv) the overlay. **(C-D)** Venn diagrams showing the distributions of lumbar infected premotor INs in the two samples injected in PL and TA. Scale bars: (Ai, Bi) 200 μm; (Aiv, Biv) 20 μm.

Figure 1-figure supplement 3: Divergent premotor INs in the lumbar spinal cord following injections in antagonists LG and TA.

(A-B) Representative examples of lumbar transverse sections following injections in the LG (ΔG-Rab-eGFP) and TA (ΔG-Rab-mCherry) showing GFP (green) and mCherry (pink). A divergent premotor IN is highlighted in the dashed box. Filled arrowheads show divergent premotor INs and contour arrowheads show infected MNs. The dashed lines drawn outlines the grey matter. **(ii-iv)** Higher magnification of a divergent premotor IN that has been infected by the ΔG-Rab-eGFP and ΔG-Rab-mCherry, showing (ii) mCherry, (iii) eGFP and (iv) the overlay. **(C-E)** Venn diagrams showing the distributions of lumbar infected premotor INs in the three samples injected in LG and TA. Scale bars: (Ai, Bi) 200 μm; (Aiv, Biv) 20 μm.

Figure 1-figure supplement 4: Rostro-caudal distributions of divergent lumbar premotor INs.

(A-C) Rostro-caudal distributions of divergent premtor INs along the sagittal and coronal axis of the lumbar cord following injections in (A) LG and MG (n=2), (B) PL and TA (n=2), (C) LG and TA (n=3). Numbers along the axis indicate distances (in μm).

Figure 1-source data 2-figure supplement 4

Source data for Figure 1-figure supplement 4A,B,C

Figure 1-figure supplement 5: Medio-lateral and dorso-ventral distributions of divergent premotor neurons across individual experiments.

Boxplo showing the medio-lateral and the dorso-ventral distributions of divergent premotor neurons in the (A) lumbar, (B) thoracic and (C) cervical regions across individual experiments.

The distributions are consistent across experiment and pairs of muscles injected. Numbers along the axis indicate the sample codes and distances (in μm).

Figure 1-figure supplement 6: Excitatory boutons from infected premotor neurons and apposed to MNs reveal divergence through different segments and regions of the spinal cord.

(A) Schematic showing experimental design to visualise projections of excitatory boutons to MNs. **(B, D)** Representative images of transverse sections in the (B) thoracic region and (D) L1 (upper lumbar) segment, following an injection of ΔG-Rab-mCherry in the TA, showing ChAT (blue grey) and mCherry (pink). MNs with vGluT2+ (yellow); mCherry+ boutons in apposition are highlighted in the dashed boxes. The dashed lines drawn outlines the grey matter. **(C, E)** Dashed boxes from B and D at higher magnification. Dashed boxes (enlarged in panels ii, iii, and iv) indicate a ChAT-; vGluT2+; mCherry+ bouton and arrowheads (enlarged in v, vi, and vii) show ChAT-; vGluT2-; mCherry+ boutons in apposition to (C) L1 and (E) thoracic MNs. Scale bars: (B, D) 100 μm; (Ci,Ei) 10 μm; (Civ-vii, Eiv-vii) 0.5 μm.

Figure 2: Organisation of divergent premotor neurons in the thoracic segments.

(Ai) Representative example of a thoracic transverse section following an injection in the PL (ΔG-Rab-eGFP) and TA (ΔG-Rab-mCherry), showing ChAT (grey blue), GFP (green) and mCherry (pink). A divergent premotor neuron is highlighted in the dashed box. The dashed line drawn outlines the grey matter contour. **(ii-iv)** Higher magnification of a divergent premotor neuron that has been infected by both ΔG-Rab-eGFP and ΔG-Rab-mCherry, showing (ii) eGFP, (iii) mCherry and (iv) the overlay. More representative examples of thoracic sections following injections in LG and MG, TA and PL, LG and TA are shown on Figure 2-figure supplement 1, 2 and 3 respectively. **(B-D)** Distribution of the thoracic premotor neurons infected following injections in (B) LG and MG (n=2), (C) PL and TA (n=2) and (D) LG and TA (n=3). Divergent premotor neurons infected from both injections are labelled in black. The violin plots show the dorso-ventral and medio-lateral distributions of divergent (black), GFP positive (green) and mCherry positive (pink) premotor neurons along the medio-lateral and dorso-ventral axis. Each violin area is normalised to 1. **(E)** Pies showing the distribution of infected premotor neurons in each quadrant; the size of the pies is proportional to the number of infected neurons. **(F)** Plot showing the divergence rate in each quadrant of the thoracic cord. DI: dorsal ipsilateral; VC: ventral contralateral; VI: ventral ipsilateral. **(G)** Overlap of distributions of divergent thoracic premotor neurons followings each pair of muscles injected. (**H**) Asymmetric violin plots showing the medio-lateral and dorso-ventral distributions of divergent premotor neurons. The halves correspond respectively to the dorsal (top) and ventral (bottom) distributions and to the ipsilateral (right) and contralateral (left) distributions of

divergent premotor neurons in the thoracic cord. Violin areas were normalized on the number of divergent neurons. When not specified numbers along the axis indicate distances (in µm). Scale bars: (Ai) 100 µm, (Aiv) 10 µm. Raw number of eGFP, mCherry and double labelled premotor neurons per samples per muscle pair injected, are shown on the Figures 2-figure supplement 1, 2 and 3.

Figure 2-source data 1

Source data for Figure 2B-G

Figure 2-figure supplement 1: Divergent premotor INs in the thoracic spinal cord following injections in synergists LG and MG.

(A-B) Representative examples of thoracic transverse sections following injections in the LG (ΔG-Rab-eGFP) and MG (ΔG-Rab-mCherry) showing GFP (green) and mCherry (pink). A divergent premotor IN is highlighted in the dashed box. The filled arrowhead shows an additional divergent premotor IN. The dashed lines drawn outline the grey matter. **(ii-iv)** Higher magnification of a divergent premotor IN that has been infected by the ΔG-Rab-eGFP and ΔG-Rab-mCherry, showing (ii) mCherry, (iii) eGFP and (iv) the overlay. **(C-D)** Venn diagrams showing the distributions of thoracic infected premotor INs in the two samples injected in LG and MG. Scale bars: (Ai, Bi) 100 µm; (Aiv, Biv) 20 µm.

Figure 2-figure supplement 2: Divergent premotor INs in the thoracic spinal cord following injections in synergists PL and TA.

(A-B) Representative examples of thoracic transverse sections following injections in the PL (ΔG-Rab-eGFP) and TA (ΔG-Rab-mCherry) showing GFP (green) and mCherry (pink). A divergent premotor IN is highlighted in the dashed box. The filled arrowhead shows an additional divergent premotor IN. The dashed lines drawn outline the grey matter contour. **(ii-iv)** Higher magnification of a divergent premotor IN that has been infected by the ΔG-Rab-eGFP and ΔG-Rab-mCherry, showing (ii) mCherry, (iii) eGFP and (iv) the overlay. **(C-D)** Venn diagrams showing the distributions of thoracic infected premotor INs in the two samples injected in PL and TA. Scale bars: (Ai, Bi) 100 µm; (Aiv, Biv) 20 µm.

Figure 2-figure supplement 3: Divergent premotor INs in the thoracic spinal cord following injections in antagonists LG and TA.

(A-B) Representative examples of thoracic transverse sections following injections in the LG (ΔG-Rab-eGFP) and TA (ΔG-Rab-mCherry) showing GFP (green) and mCherry (pink). A divergent premotor IN is highlighted in the dashed box. The filled arrowhead shows an

additional divergent premotor IN. The dashed lines drawn ouline the grey matter contour. **(ii-iv)** Higher magnification of a divergent premotor IN that has been infected by the ΔG-Rab-eGFP and ΔG-Rab-mCherry, showing (ii) mCherry, (iii) eGFP and (iv) the overlay. **(C-E)** Venn diagrams showing the distributions of thoracic infected premotor INs in the three samples injected in LG and TA. Scale bars: (Ai, Bi) 100 µm; (Aiv, Biv) 20 µm.

Figure 2-figure supplement 4: Rostro-caudal distributions of divergent thoracic premotor neurons.

(A-C) Rostro-caudal distributions of divergent premotor INs shown in the coronal (top) and sagittal (bottom) axes of the thoracic cord following injections in (A) LG and MG (n=2), (B) PL and TA (n=2), (C) LG and TA (n=3). Numbers along the axis indicate distances (in µm).

Figure 2-source data 2-figure supplement 4

Source data for Figure 2-figure supplement 4A,B,C

Figure 3: Organisation of divergent premotor LDPNs in the cervical spinal cord.

(Ai) Representative example of an upper cervical transverse section following an injection in the LG (ΔG-Rab-eGFP) and TA (ΔG-Rab-mCherry), showing ChAT (grey blue), GFP (green) and mCherry (pink). A divergent premotor LDPN is highlighted in the dashed box. The dashed line drawn outlines the grey matter contour. **(ii-iv)** Higher magnification of the divergent premotor LDPN, showing (ii) eGFP, (iii) mCherry and (iv) the overlay. More representative examples of cervical sections following injections in LG and MG, TA and PL, LG and TA are shown on Figure 3-figure supplement 1, 2 and 3 respectively. **(B-D)** Distribution of the cervical premotor LDPNs following injections in (C) LG and MG (n=2), (D) PL and TA (n=2) and (E) LG and TA (n=3). Divergent premotor LDPNs infected from both injections are labelled in black. The violin plots show the dorso-ventral and medio-lateral distributions of divergent (black), GFP positive (green) and mCherry positive (pink) premotor LDPNs along the medio-lateral and dorso-ventral axis. Each violin area is normalised to 1. **(E)** Overlap of the distribution of cervical divergent premotor LDPNs followings each pair of muscles injected. **(F)** Asymmetric violin plots showing the medio-lateral and dorso-ventral distributions of premotor divergent LDPNs. The halves correspond respectively to the dorsal (top) and ventral (bottom) distributions and to the ipsilateral (right) and contralateral (left) distributions of divergent premotor LDPNs in the cervical cord. Violin areas were normalized on the number of divergent neurons. (**G**) Pies showing the distribution of infected premotor LDPNs in each quadrant; the size of the pies is proportional to the number of infected premotor LDPNs in each quadrant. **(H)** Plot showing the distribution of the sectional areas of divergent premotor neurons in each region of the spinal cord. The dashed line (labelled cervical MN) corresponds to the mean sectional area of cervical

MNs (n=17 MNs). When not specified numbers along the axis indicate distances (in μm). Scale bars: (Ai) 200 μm; (Aiv) 20 μm. Raw number of eGFP, mCherry and double labelled premotor neurons per samples per muscle pair injected, are shown on the Figures 3-figure supplement 1, 2 and 3.

Figure 3-source data 1

Source data for Figure 3B-G, H

Figure 3-figure supplement 1: Divergent premotor INs in the cervical spinal cord following injections in synergists LG and MG.

(A-B) Representative examples of cervical transverse sections following injections in the LG (ΔG-Rab-eGFP) and MG (ΔG-Rab-mCherry) showing GFP (green) and mCherry (pink). A divergent premotor IN is highlighted in the dashed box. The dashed lines drawn outline the grey matter contour. **(ii-iv)** Higher magnification of a divergent premotor IN that has been infected by the ΔG-Rab-eGFP and ΔG-Rab-mCherry, showing (ii) mCherry, (iii) eGFP and (iv) the overlay. **(C-D)** Venn diagrams showing the distributions of cervical infected premotor INs in the two samples injected in LG and MG. Scale bars: (Ai, Bi) 200 μm; (Aiv, Biv) 20 μm.

Figure 3-figure supplement 2: Divergent premotor INs in the cervical spinal cord following injections in synergists PL and TA.

(A-B) Representative examples of cervical transverse sections following injections in the PL (ΔG-Rab-eGFP) and TA (ΔG-Rab-mCherry) showing GFP (green) and mCherry (pink). A divergent premotor IN is highlighted in the dashed box. The dashed lines drawn outline the grey matter contour. **(ii-iv)** Higher magnification of a divergent premotor IN that has been infected by the ΔG-Rab-eGFP and ΔG-Rab-mCherry, showing (ii) mCherry, (iii) eGFP and (iv) the overlay. **(C-D)** Venn diagrams showing the distributions of cervical infected premotor INs in the two samples injected in PL and TA. Scale bars: (Ai, Bi) 200 μm; (Aiv, Biv) 20 μm.

Figure 3-figure supplement 3: Divergent premotor INs in the cervical spinal cord following injections in antagonists LG and TA.

(A-B) Representative examples of cervical transverse sections following injections in the LG (ΔG-Rab-eGFP) and TA (ΔG-Rab-mCherry) showing GFP (green) and mCherry (pink). A divergent premotor IN is highlighted in the dashed box. The dashed lines drawn outline the grey matter contour. **(ii-iv)** Higher magnification of a divergent premotor IN that has been infected by the ΔG-Rab-eGFP and ΔG-Rab-mCherry, showing (ii) mCherry, (iii) eGFP and (iv)

the overlay. **(C-E)** Venn diagrams showing the distributions of cervical infected premotor INs in the three samples injected in LG and TA. Scale bars: (Ai, Bi) 200 µm; (Aiv, Biv) 20 µm.

Figure 3-figure supplement 4: Rostro-caudal distributions of divergent cervical premotor neurons.

(A-C) Rostro-caudal distributions of divergent premotor INs along the coronal (top) and sagittal (bottom) coronal axes of the cervical cord following injections in (A) LG and MG (n=2), (B) PL and TA (n=2), (C) LG and TA (n=3). Numbers along the axis indicate distances (in µm).

Figure 3-source data 2-figure supplement 4

Source data for Figure 3-figure supplement 4A,B,C

Figure 4: Non-glycinergic, non-cholinergic cervical premotor LDPNs and mixed populations of inhibitory and non-inhibitory thoracic premotor neurons revealed by injections in GlyT2-eGFP; RΦGT mice.

(A) Experimental strategy to determine whether thoracic and cervical premotor neurons are inhibitory. **(B, D)** Representative example of (Bi) a cervical and (Di) a thoracic transverse section following an injection in the LG (ΔG-Rab-mCherry) using GlyT2-eGFP; RΦGT mice, showing ChAT (blue), GFP (green) and mCherry (pink). The dashed boxes highlight the infected premotor LDPNs. The dashed lines drawn outlines the grey matter contours. **(Bii-iv, Dii-iv)** Higher magnification of the dashed box areas, highlighting (Bii-iv) a GFP-, mCherry+ cervical premotor LDPN on the contralateral Lamina VIII and (Dii-iv) a GFP+, mCherry+ thoracic premotor neuron in ipsilateral intermediate lamina. **(C, E)** Distribution of the (C) cervical and (E) thoracic premotor neurons infected, following injections in the LG of GlyT2-eGFP; RΦGT mice (n=3). The violin plots show the dorso-ventral and medio-lateral distributions of GFP+, mCherry+ (black) and GFP+, mCherry- (pink) premotor neurons along the medio-lateral and dorso-ventral axis. Each violin area is normalised to 1. **(F)** Proportions of inhibitory premotor neurons in the thoracic and the cervical region of GlyT2-eGFP; RΦGT mice following injections in the LG (n=3). When not specified numbers along the axis indicate distances (in µm). Scale bars: (Bi) 200 µm; (Di) 100 µm; (Biv,Div) 10 µm.

Figure 4-source data 1

Source data for Figure 4C,E

Figure 4-figure supplement 1: Lumbar V0c INs innervate multiple motor pools.

(A) Representative example of one of the few divergent V0c INs observed in the lumbar cord following injections in muscle pairs. The dashed lines drawn outlines the grey matter. The

higher magnifications show (ii) mCherry, (iii) eGFP, (iv) ChAT and (iv) the overlay. Scale bars: (Ai) 200 µm; (Av) 20 µm

Figure 5: A subpopulation of cervical premotor LDPNs expresses Lhx1.
(A) Experimental strategy to determine whether cervical premotor LDPNs express Lhx1. (**Bi**) Representative example of a transverse section from the cervical cord following an injection in GS (ΔG-Rab-eGFP) muscles, showing a cervical premotor LDPN infected (pink) expressing Lhx1. The premotor LDPN expressing Lhx1 is highlighted in the dashed box. The dashed line drawn outlines the grey matter contour. (**ii-iv**) Higher magnification of the premotor LDPN Lhx1+ that has been infected by the ΔG-Rab-mCherry, showing (ii) mCherry, (iii) Lhx1 and (iv) the overlay. (**C**) Distribution of the cervical premotor LDPNs following injections in GS whether they are Lhx1+ (black) or not (pink). Numbers along the axis indicate distances (in µm).Scale bars: (Bi) 200 µm; (Biv) 20 µm. The efficiency of Lhx1 staining along post-natal development is shown figure 5-figure supplement 1.

Figure 5-source data 1
Source data for Figure 5C

Figure 5-figure supplement 1: The number of neurons labelled with anti-Lhx1 antibody decreases in the spinal cord over postnatal development.
Lhx1 staining at P2, P6 and P10 showing the decrease in the number of Lhx1 positive cells in the spinal cord through early postnatal development. The dashed lines drawn outline the grey matter. Scale bars: 100 µm.

Figure 6: Cervical premotor LDPNs innervate homolateral lumbar and cervical MNs.
(A) Experimental strategy to determinewhether divergent cervical premotor LDPNs that innervate homolateral lumbar and cervical MNs do exist. **(Bi**) Representative example of a transverse section from the cervical cord following an injection in FMs (ΔG-Rab-mCherry) and GS (ΔG-Rab-eGFP) muscles, showing a premotor LDPN infected from the two contralateral motor pools. The dashed box highlights the divergent premotor LDPN. The dashed line drawn outlines the grey matter contour. **(ii-iv)** Dashed box area at higher magnification, showing (ii) eGFP, (iii) mCherry and (iv) the overlay. **(C)** Distribution of the premotor LDPNs infected from the homolateral injections in GS and FMs. The violin and box plots show the distribution of divergent premotor LDPNs innervating homolateral local FMs and distant GS motor pools along the medio-lateral and dorso-ventral axis. Each violin area is normalised to 1. **(D)** Proportion of cervical premotor LDPNs that also project to FM motor pools per animal. **(E)** Plot showing the sectional area of the cervical divergent premotor LDPNs that diverge to two pools

of lumbar MNs (hind_hind) and to the pools of GS and FM MNs (fore_hind). When not specified numbers along the axis indicate distances (in μm). Scale bars: (Bi) 200 μm; (Biv) 10 μm.

Figure 6-source data 1

Source data for Figure 6C-E

Figure 6-figure supplement 1: Cervical premotor LDPNs innervate ipsilateral cervical and contralateral lumbar MNs

(A) Experimental strategy to examine whether divergent cervical premotor LDPNs innervate ipsilateral cervical and contralateral lumbar motor pools. **(Bi**) Representative example of a transverse section from the cervical cord following injections in contralateral GS (ΔG-Rab-eGFP) and ipsilateral FM (ΔG-Rab-mCherry) muscles, showing a double labelled premotor LDPN. The dashed box highlights the divergent premotor LDPN. The dashed line drawn outlines the grey matter. **(ii-iv)** Dashed box area at higher magnification, showing (ii) mCherry, (iii) eGFP and (iv) the overlay . Scale bars: (Bi) 200 μm; (Biv) 20 μm.

Figure 6-figure supplement 2: Premotor LAPNs are distributed in the thoracic, lumbar, and sacral spinal cord, and diverge to homolateral lumbar and cervical MNs.

(Ai, Ci, Ei) Representative examples of transverse sections from the (A) thoracic, (C) lumbar and (E) sacral spinal cord following injections in homolateral GS (ΔG-Rab-eGFP) and FMs (ΔG-Rab-mCherry), showing ChAT (blue grey), GFP (green) and mCherry (pink). Dashed boxes highlight INs that were infected from the injections in homolateral GS and FMs. The dashed lines drawn indicate the grey matter. **(Aii-iv, Cii-iv, Eii-iv)** High-magnification of the dashed boxes showing double infected premotor neurons in the (Aii-iv) thoracic, (Cii-iv) lumbar and (Eii-iv) sacral cord. **(B, D, F)** Distributions of the ascending single labelled (pink) and divergent (black) premotor neurons in the (B) thoracic, (D) lumbar and (F) sacral cord following injections in homolateral GS (ΔG-Rab-eGFP) and FMs (ΔG-Rab-mCherry). **(G)** Plot showing the size of the sacral premotor LAPNs infected from GS and FMs injections (black) or from the injection in FMs only (pink). When not specified numbers along the axis indicate distances (in μm). Scale bars: (Ai, Ei) 100 μm; (Ci) 200 μm (Aiv, Civ, Eiv) 10 μm.

Figure 6-source data 2-figure supplement 2

Source data for Figure 6-figure supplement 2B,D,F,G

Figure 7: Divergence rates throughout the spinal cord and circuits

(A) Schematic summarizing the projections determined. **(B)** Plot showing the increase of the apparent divergence rate with the distance between innervated MNs and premotor neurons.

Figure 7-source data 1

Source data for Figure 7B

Figure 8: Simulation comparing observed vs real rates of divergence depending on transsynaptic mRV efficiency.

Simulation of the spreading of mRV in premotor circuits following double injections, extracted from a binomial distribution. Plot showing the relation between observed rate of divergence depending on the real rate of divergence within premotor spinal circuits. This simulation was run with the simplifying assumption that the efficiencies of viral transfer are equal and independent from each other across spinal cord regions.

Supplementary file 1: Numbers of MNs and premotor neurons, and medio-lateral and dorso-ventral distributions of divergent premotor neurons across individual experiments.

Distribution of divergent premotor neurons per region of the spinal cord across individual experiments, expressed as median ± first/third quartile.

Supplementary file 2: Details of muscles infected following forearm injections. (+) means that a fluorescent signal was found in muscle fibers, (-) means that no fluorescence was observed following muscle dissections.

Supplementary file 3: List of the mice used for each experiment, including genotype and figure in which they are shown.

A

ChAT+-G+

Ipsilateral injections:

ΔG-rab-mCherry

ΔG-rab-eGFP

B

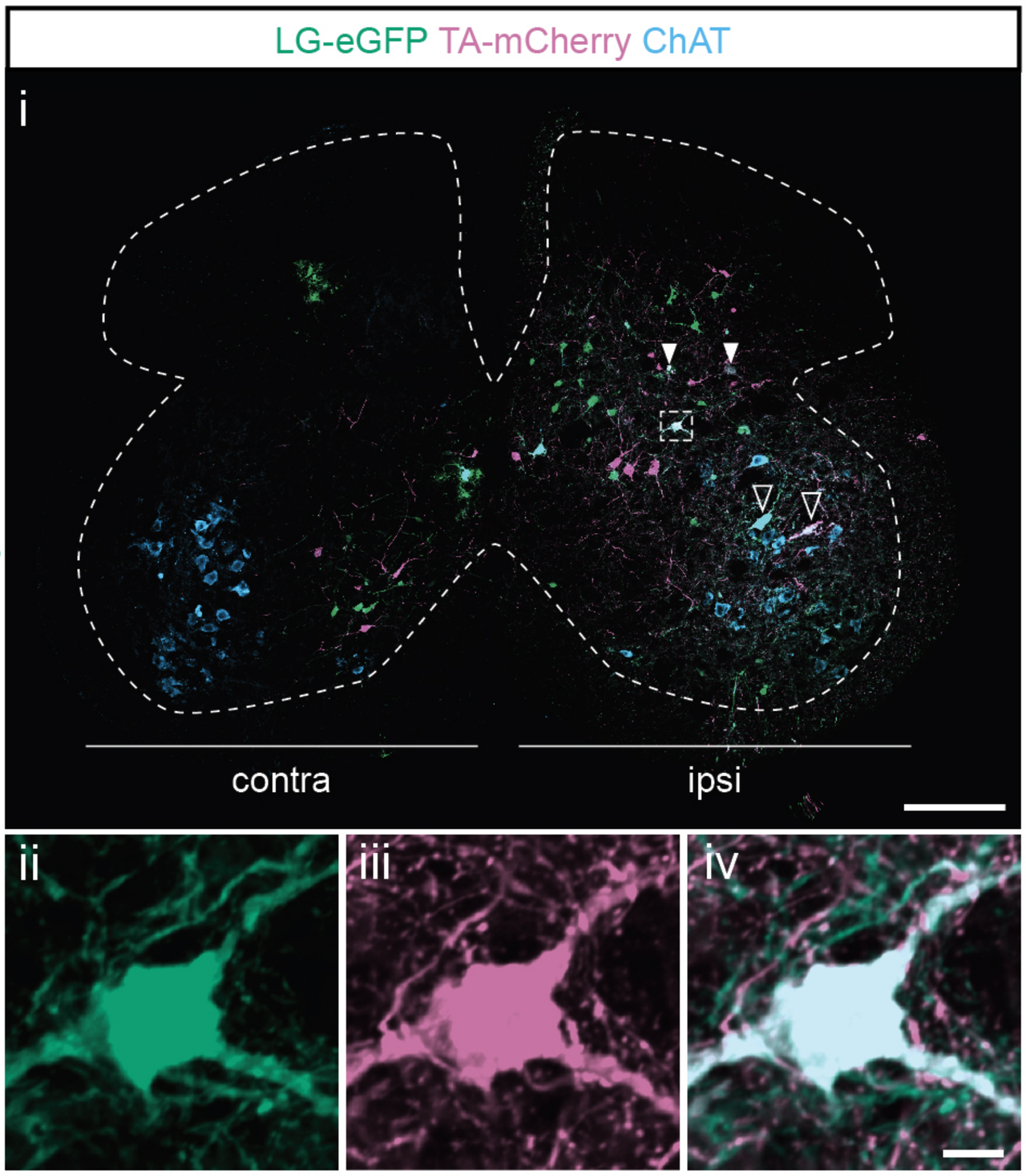

C

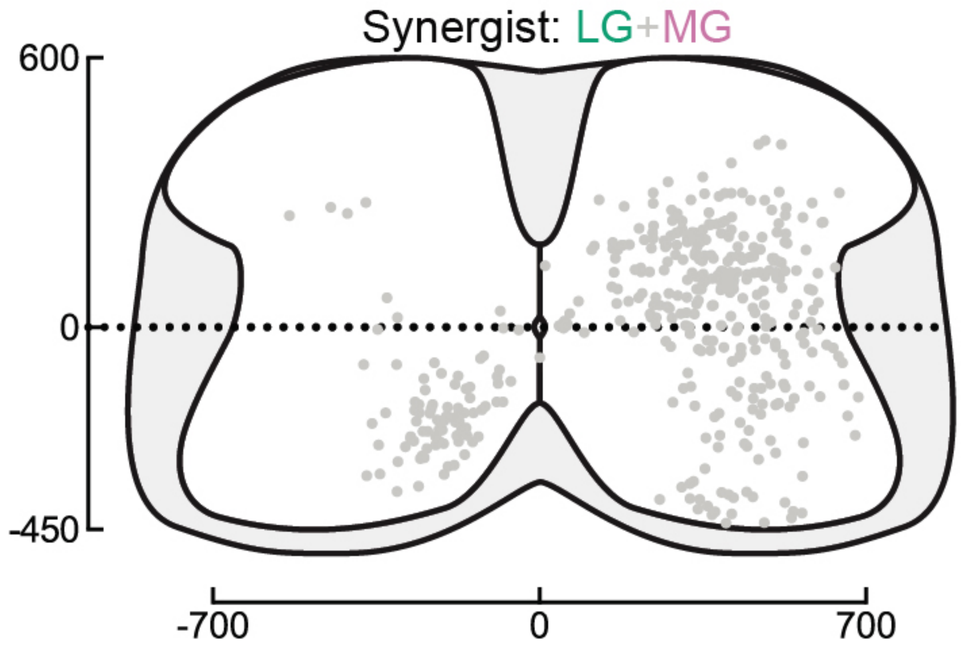

D

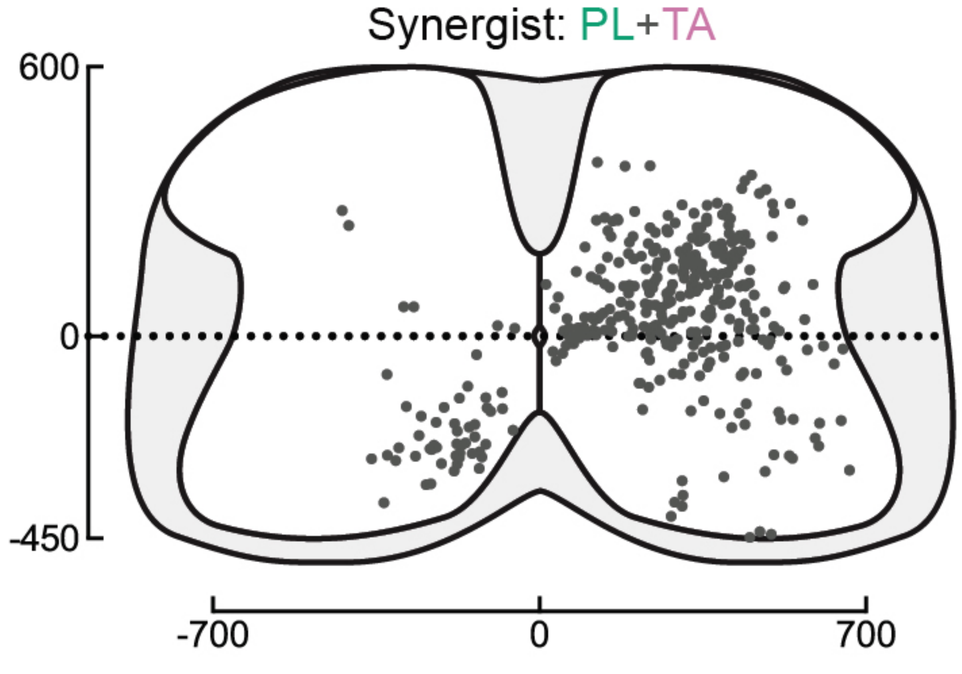

E

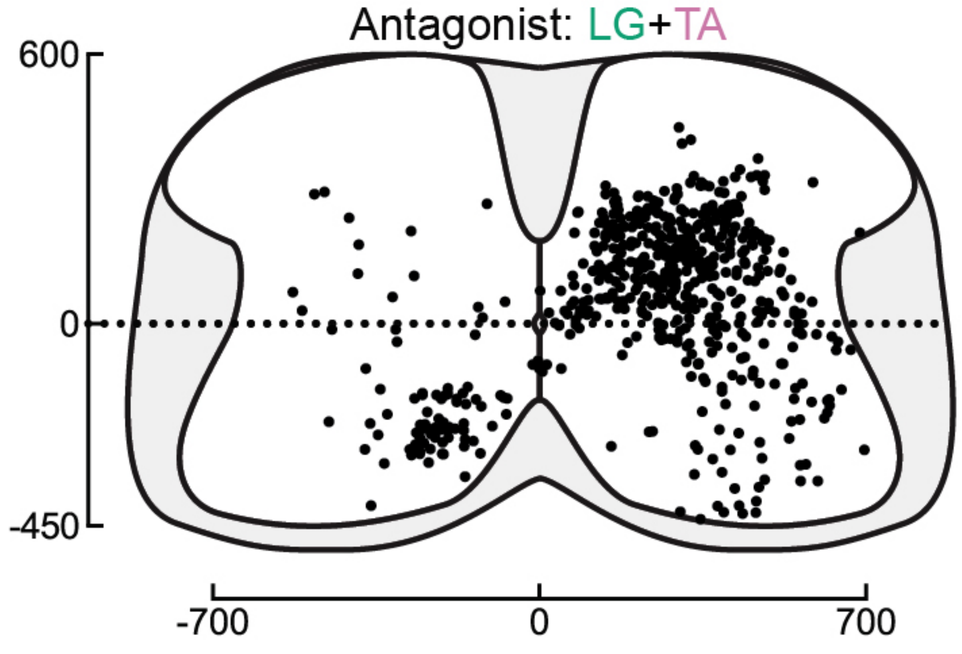

F

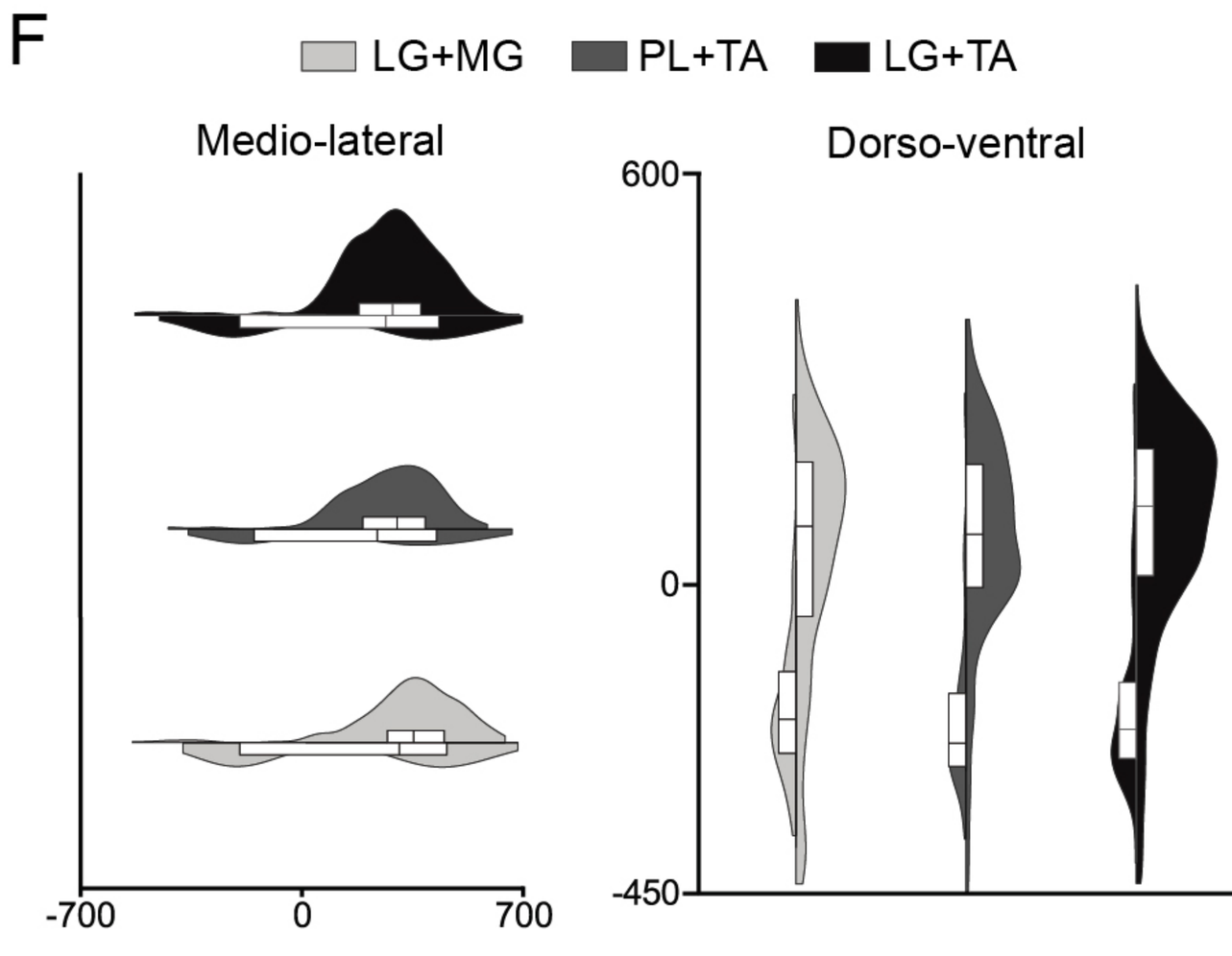

G

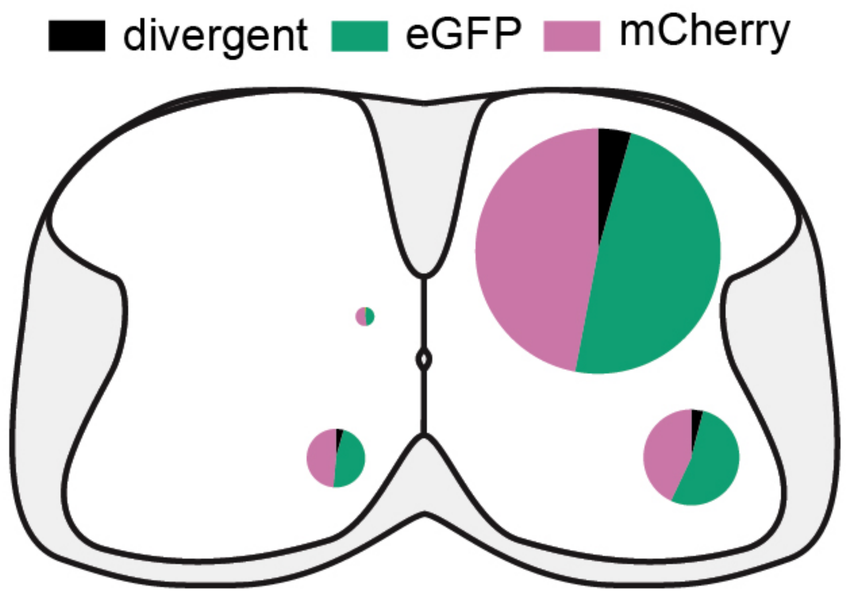

Figure 1

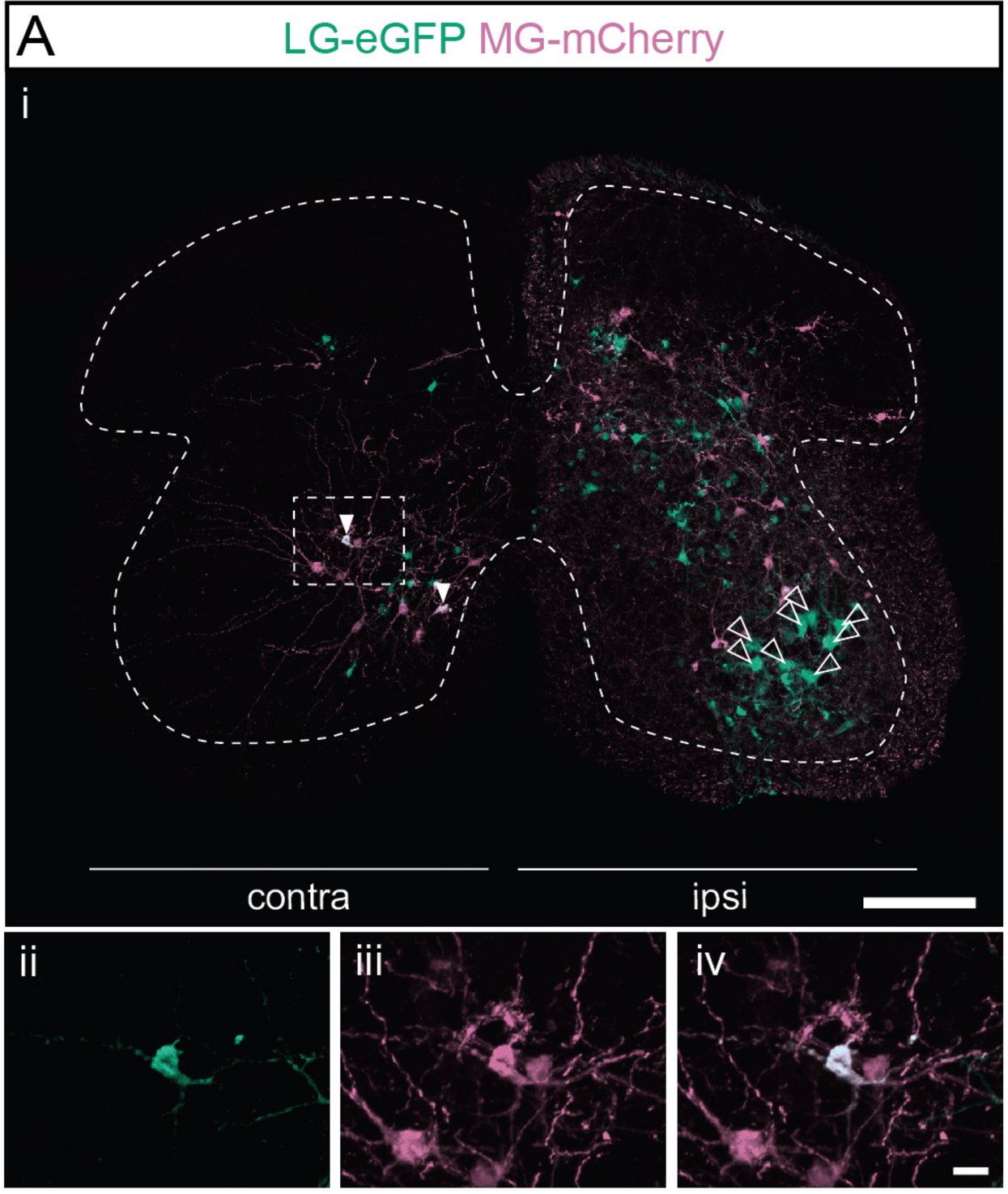

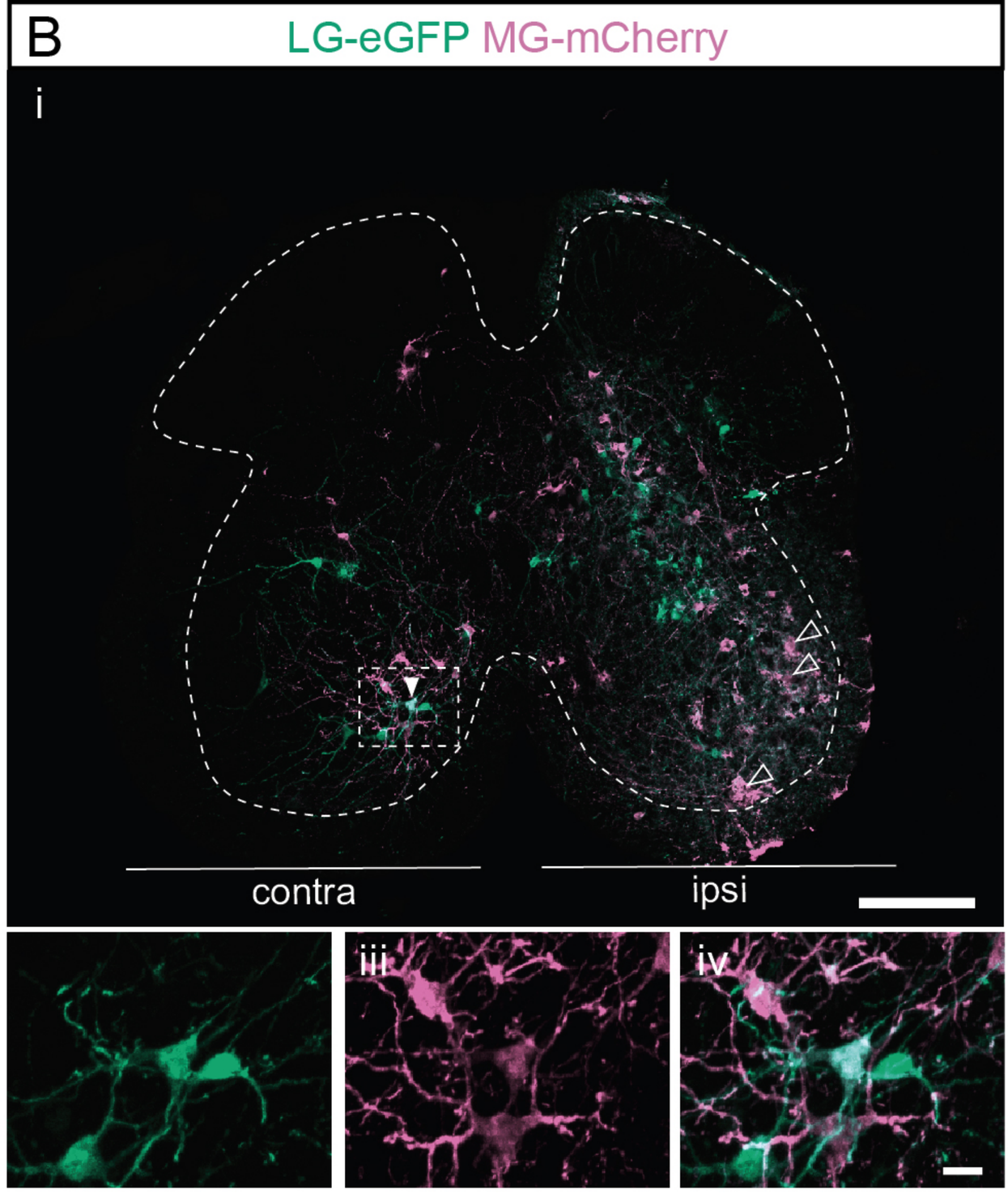

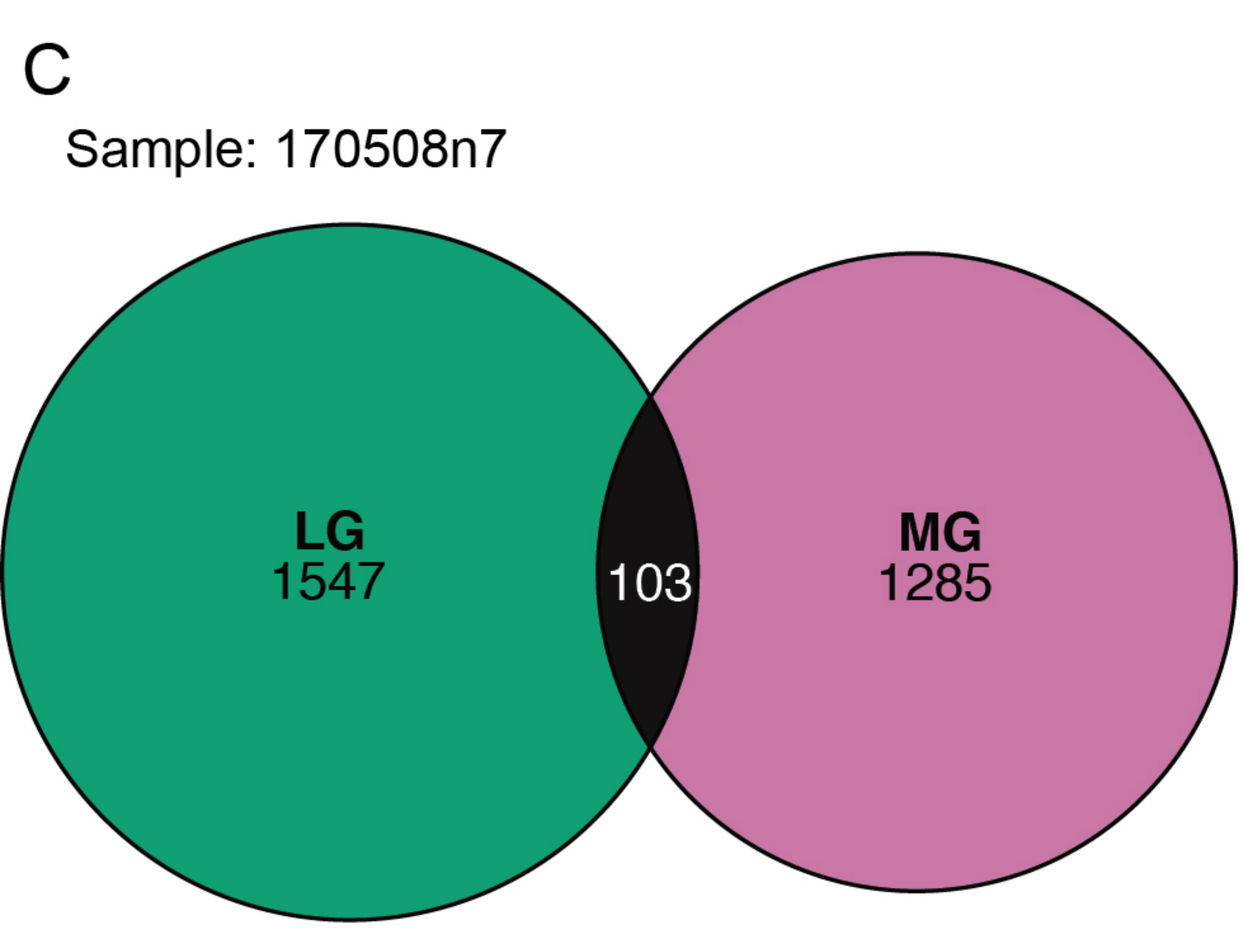

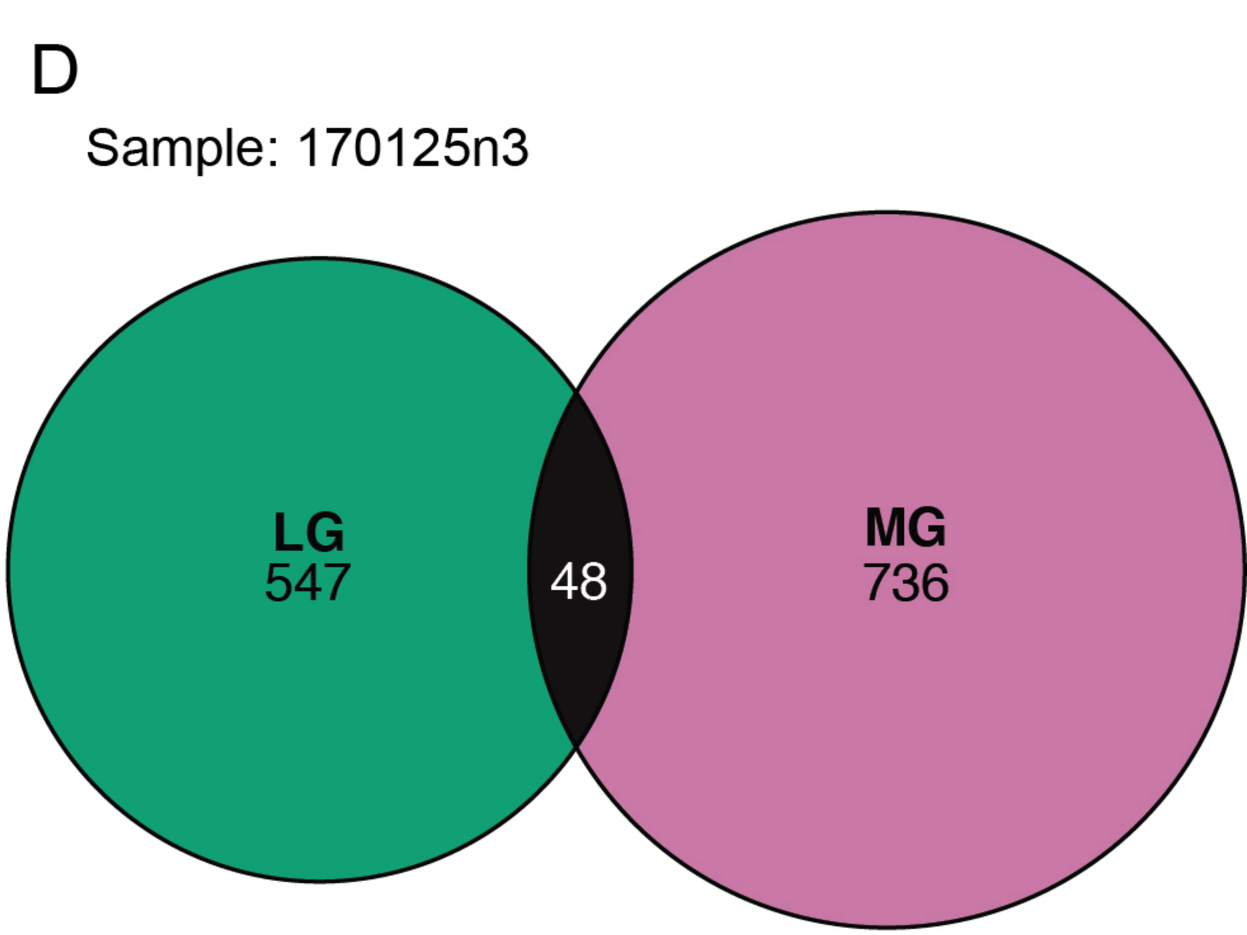

Figure 1-figure supplement 1

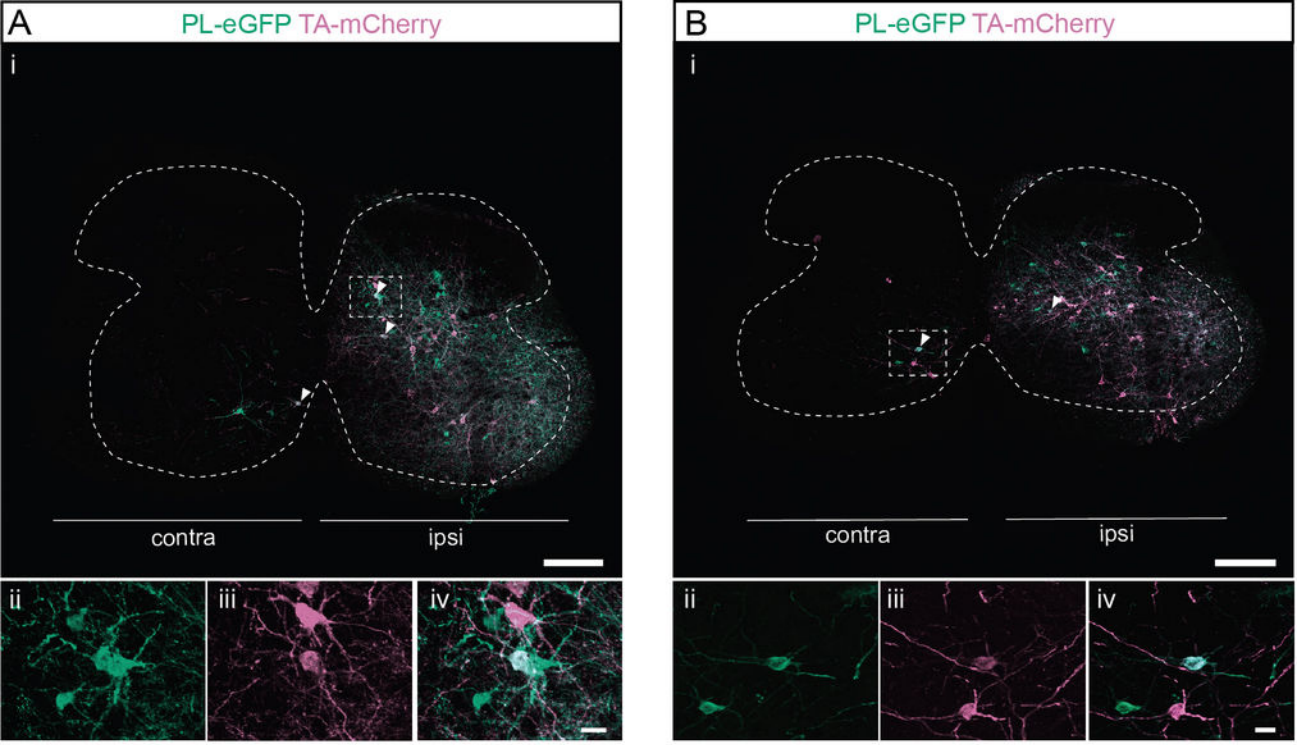

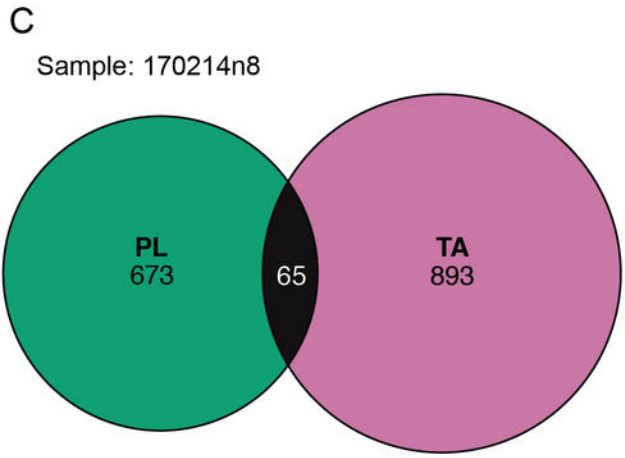

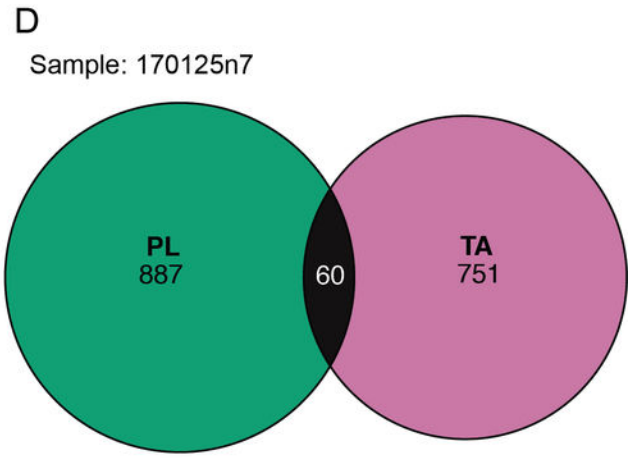

Figure 1-figure supplement 2

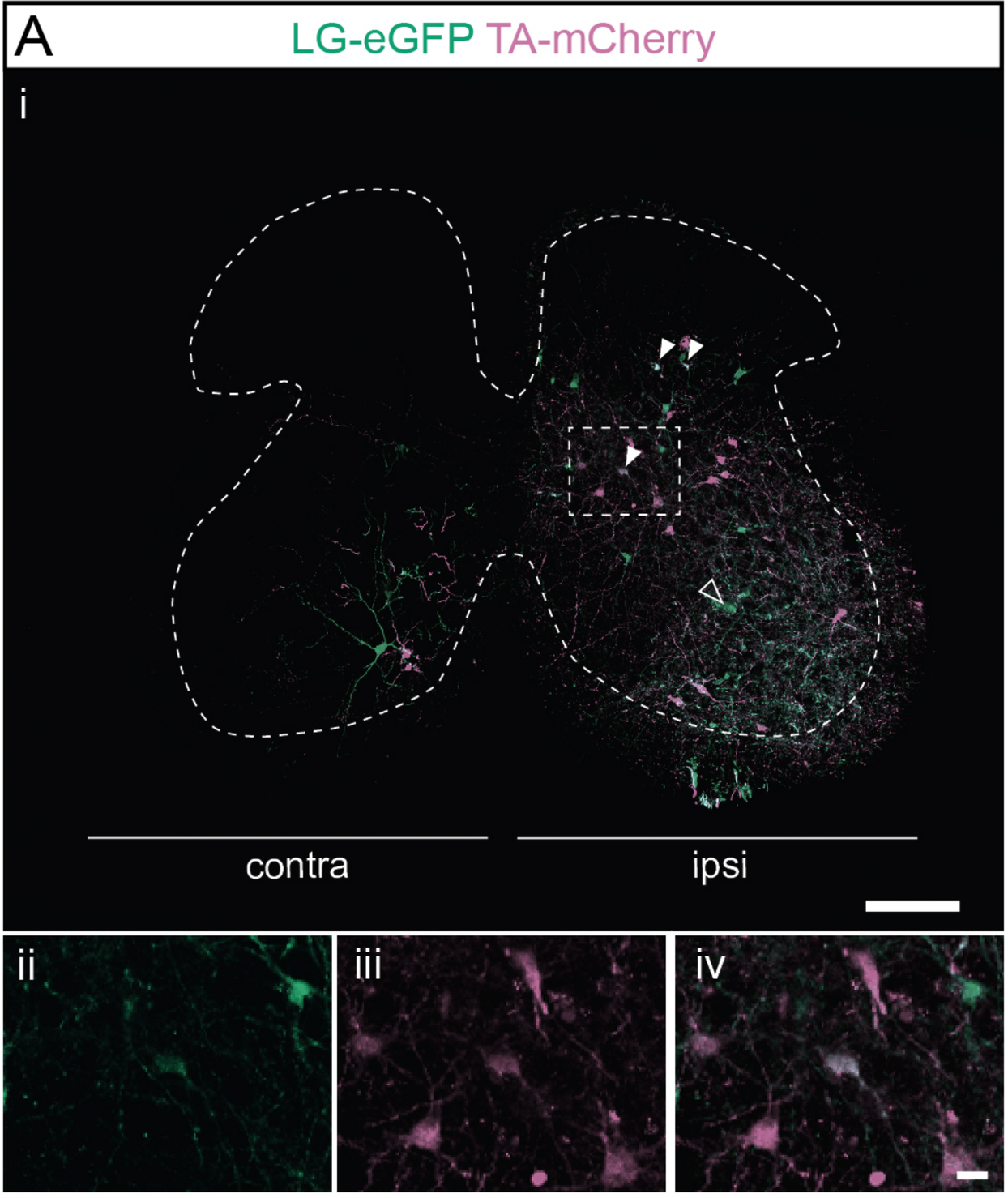

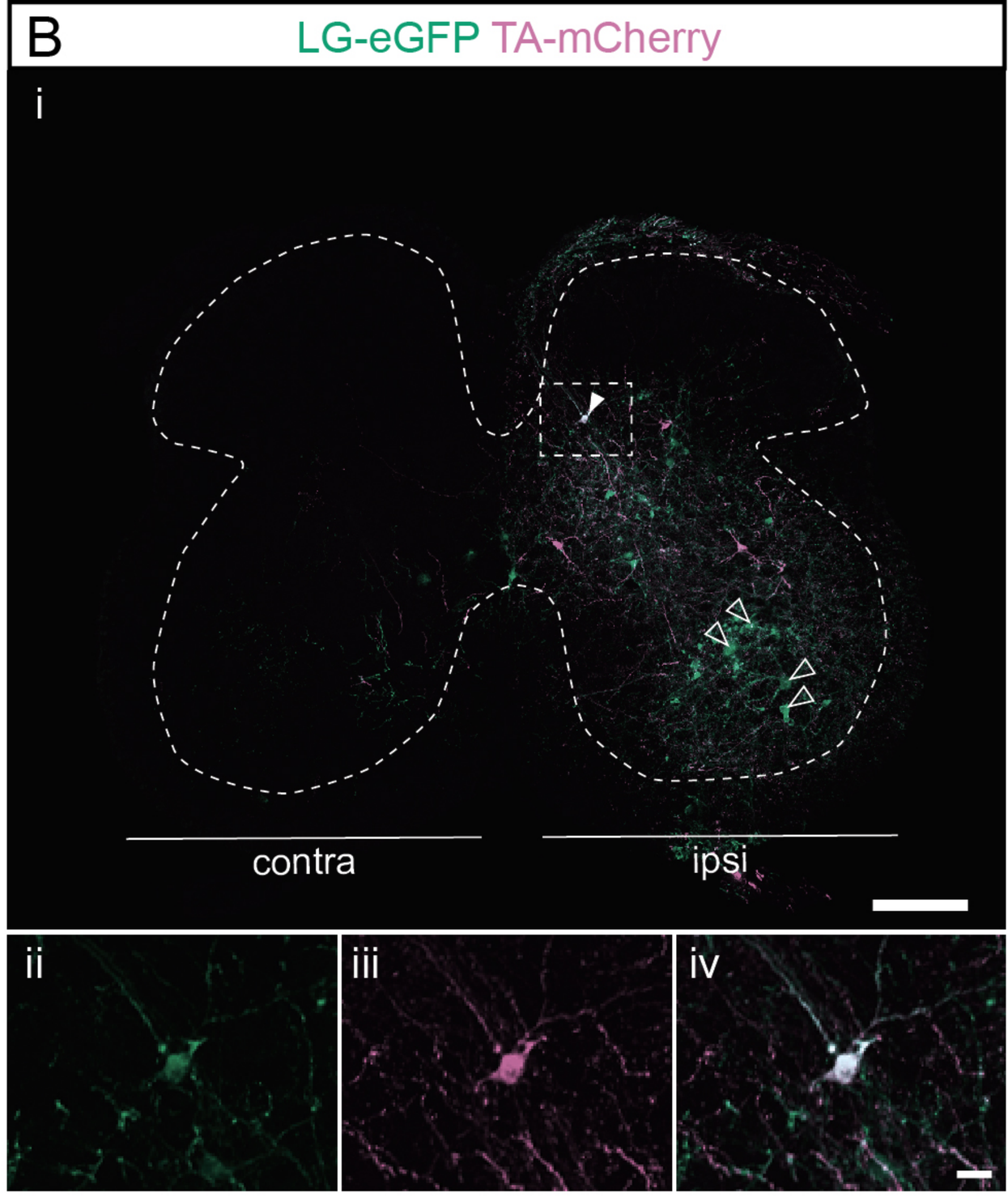

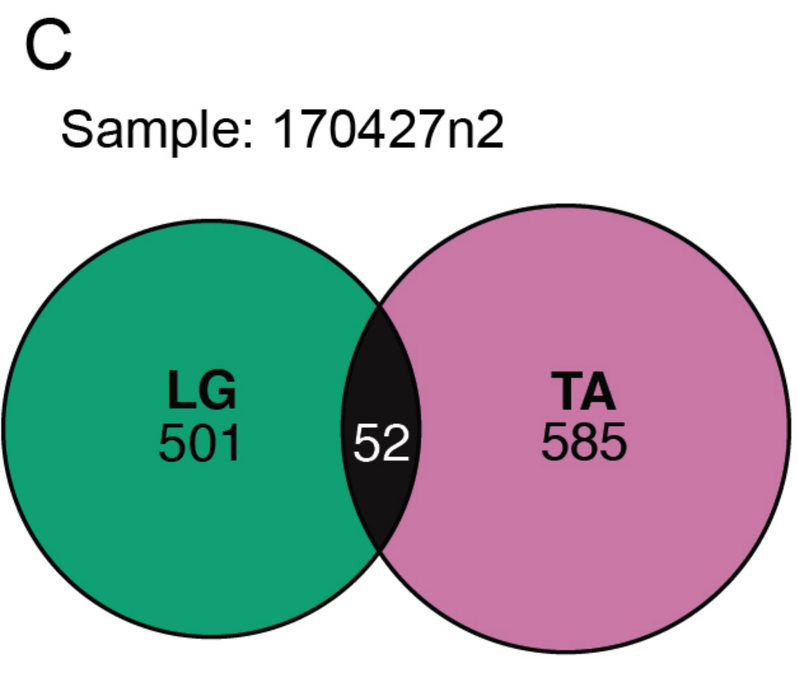

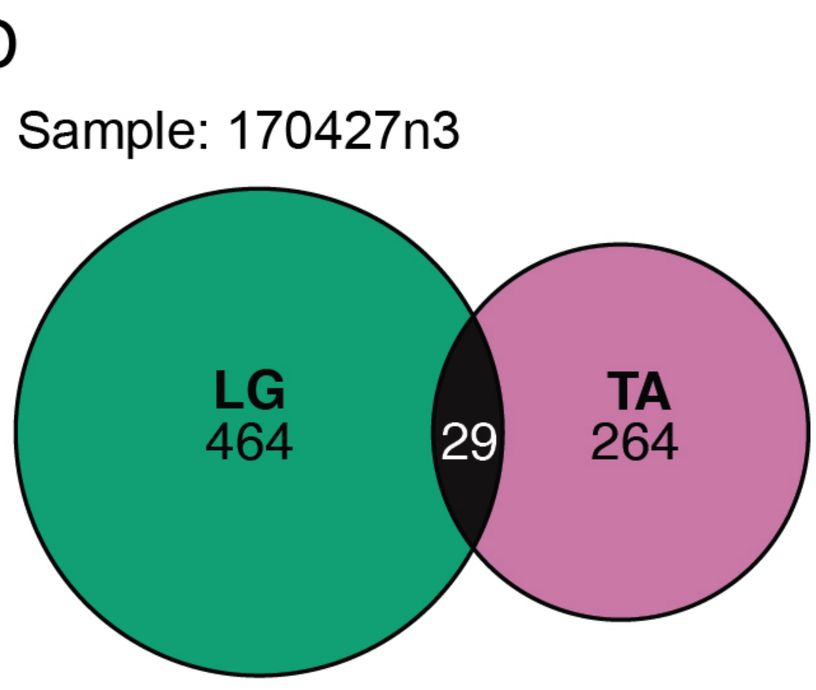

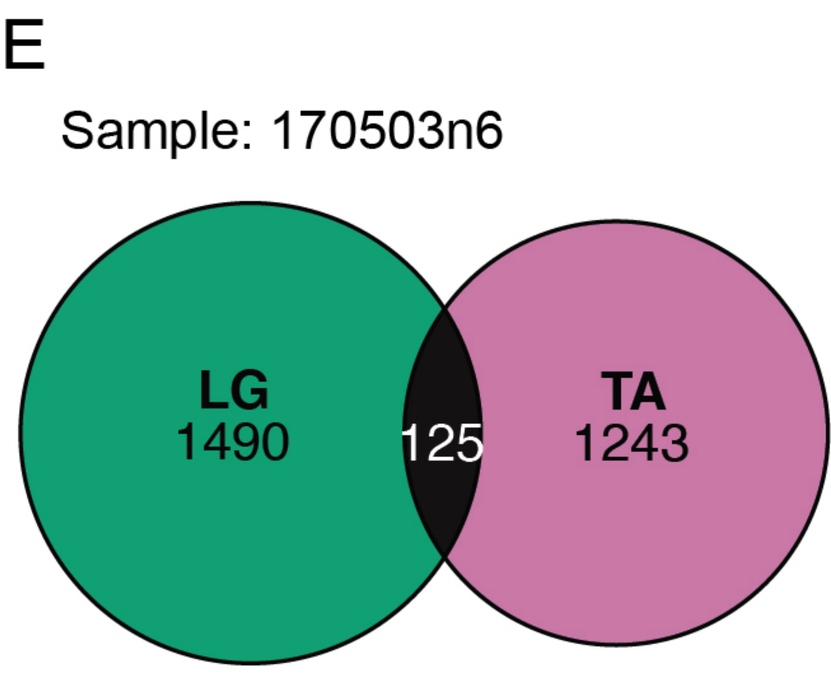

Figure 1-figure supplement 3

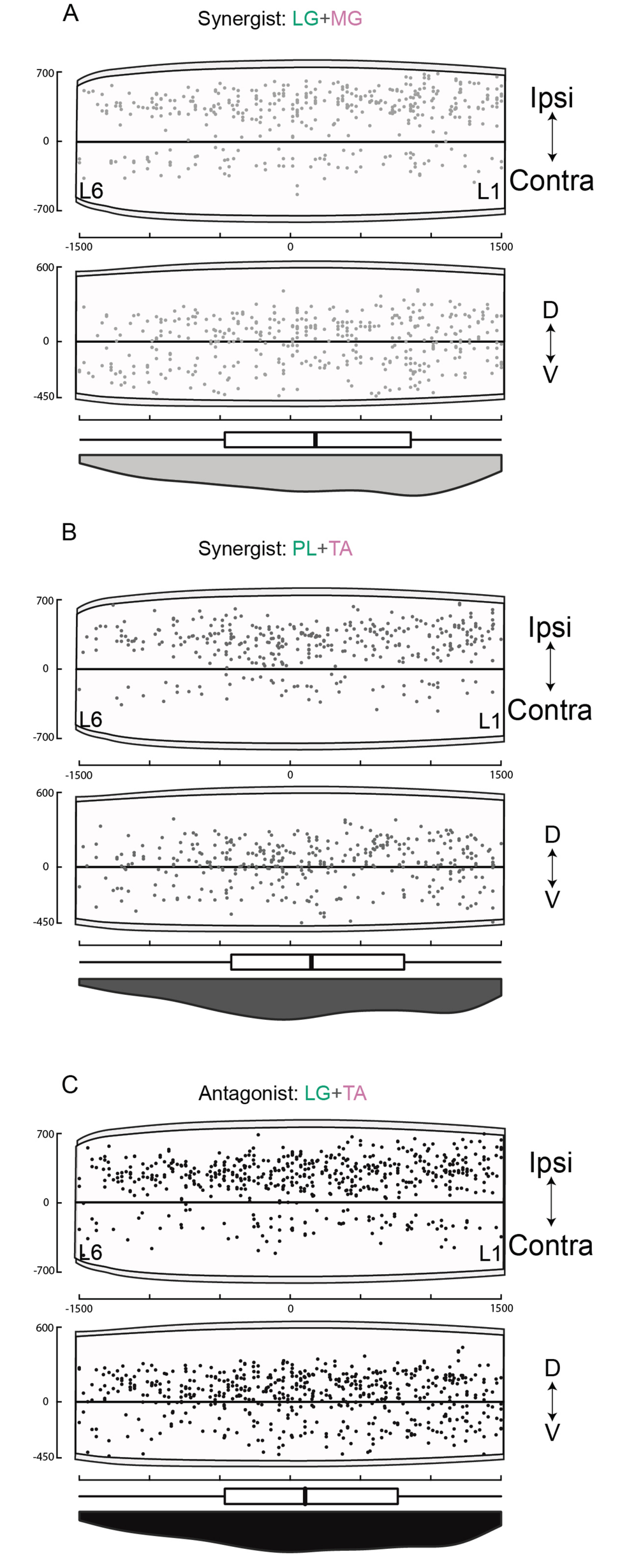

Figure 1-figure supplement 4

Medio-Lateral

Dorso-Ventral

A

LG+MG PL+TA LG+TA

Lumbar

170503n6
170427n3
170427n2
170125n8
170125n7
170508n7
170125n3

−700 0 700

600 0 −450

170125n3 170508n7 170125n7 170125n8 170427n2 170427n3 170503n6

B

Thoracic

170503n6
170427n3
170427n2
170125n8
170125n7
170508n7
170125n3

−500 0 500

550 0 −350

170125n3 170508n7 170125n7 170125n8 170427n2 170427n3 170503n6

C

Cervical

170503n6
170427n3
170427n2
170125n8
170125n7
170508n7
170125n3

−800 0 800

650 0 −450

170125n3 170508n7 170125n7 170125n8 170427n2 170427n3 170503n6

Figure 1-figure supplement 5

A

thoracic T9-T11

lumbar L1-L2

lumbar L4-L5

$ChAT^{+}$-G^{+}

TA

ChAT mCherry vGluT2

B

contra

ipsi

Ci

ii

iii

iv

v

vi

vii

D

ipsi

Ei

ii

iii

iv

v

vi

vii

Figure 1-figure supplement 6

A

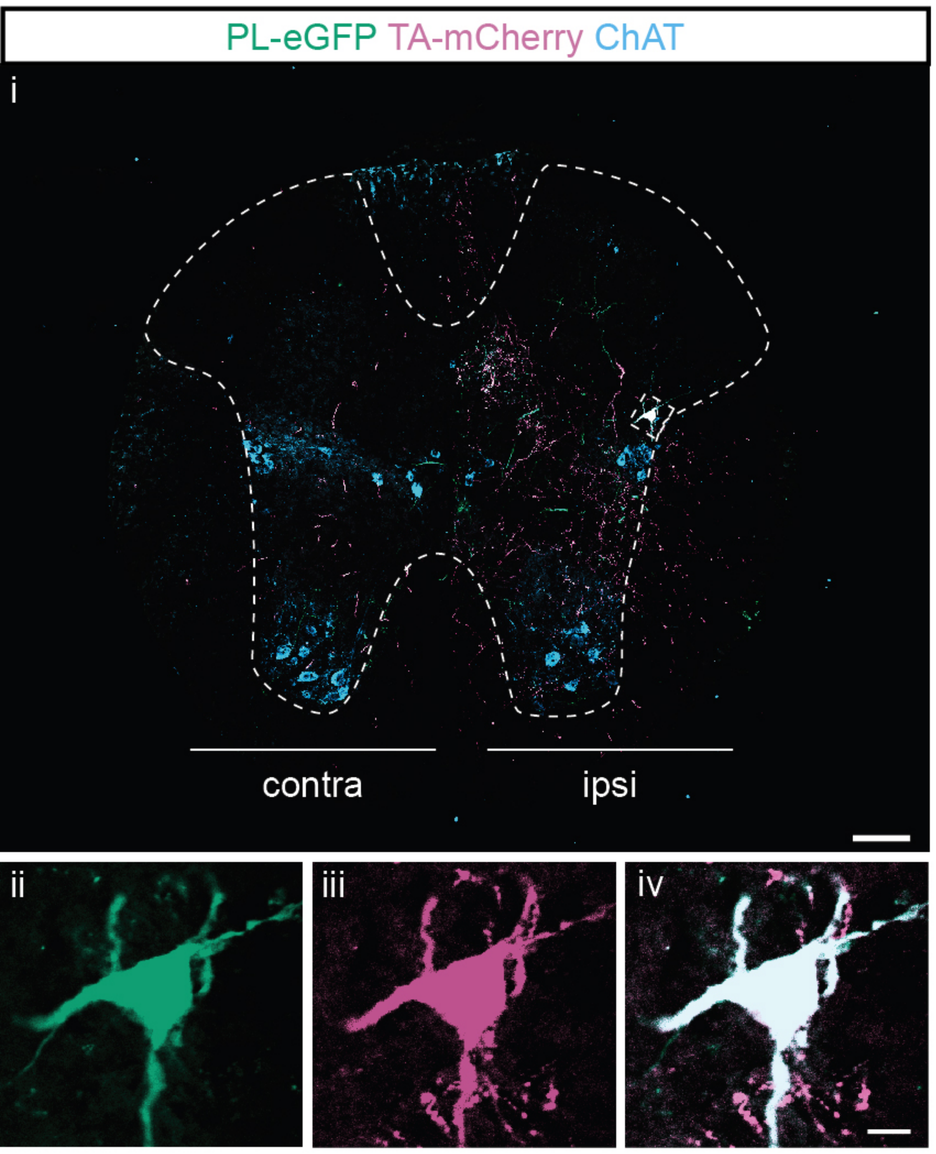

B

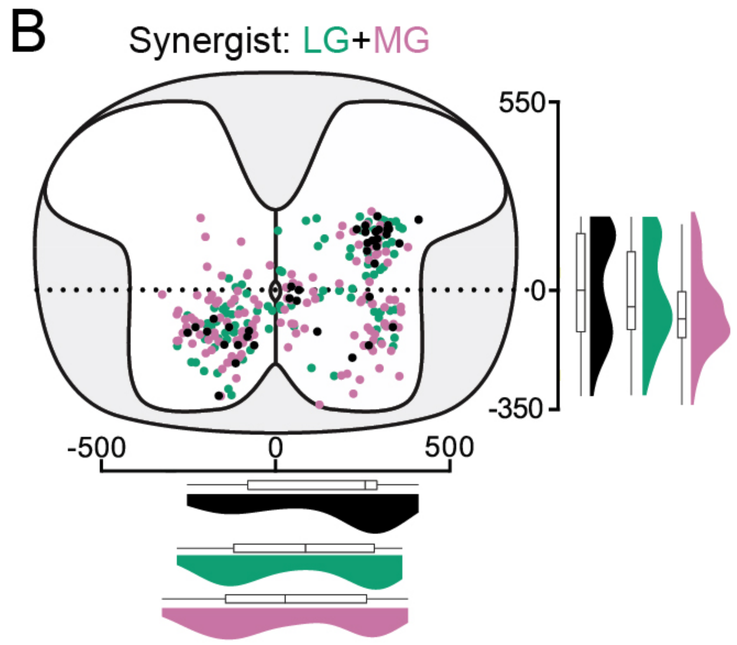

C

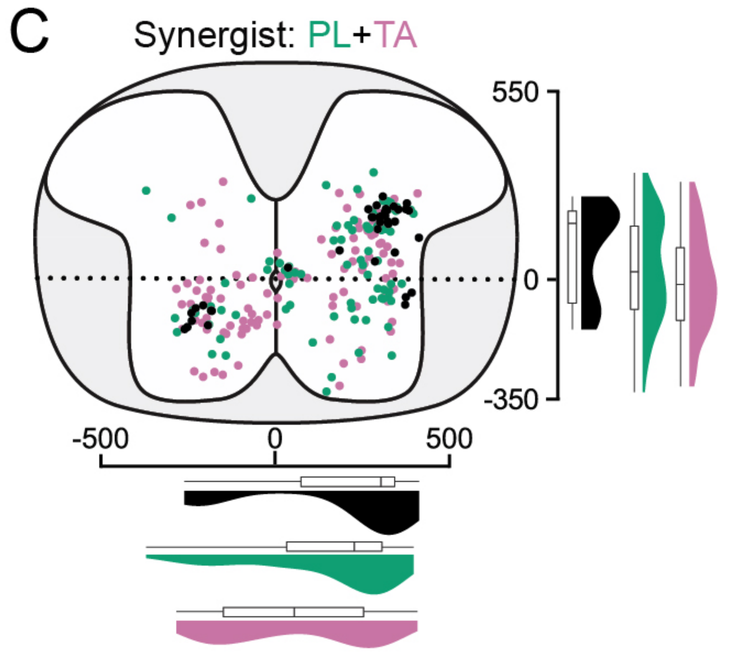

D

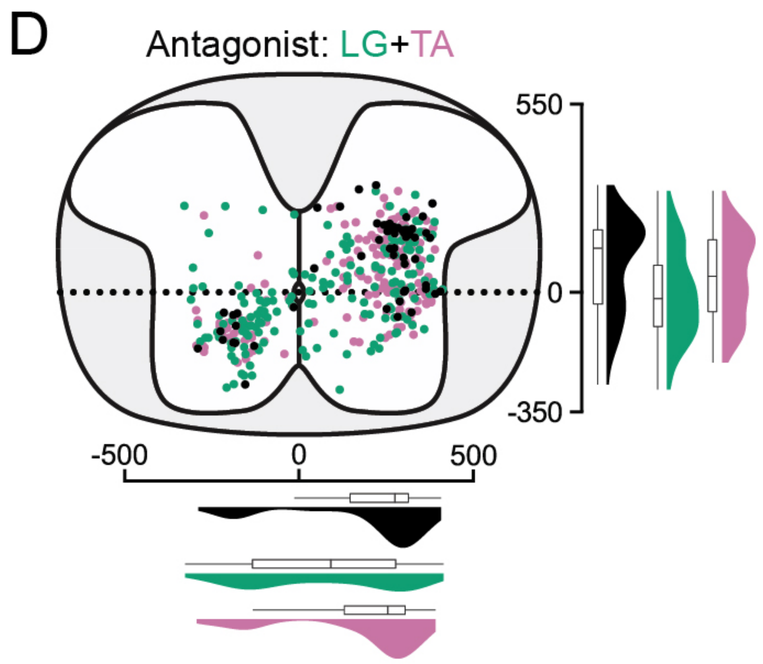

E

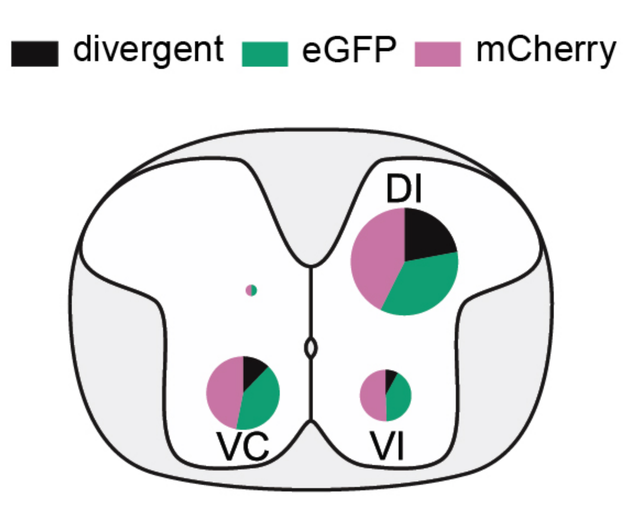

F

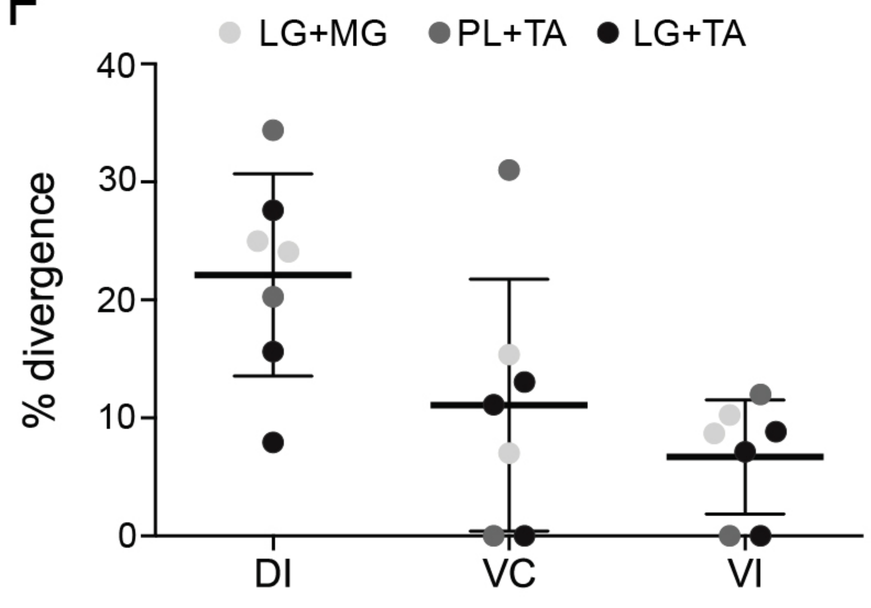

G

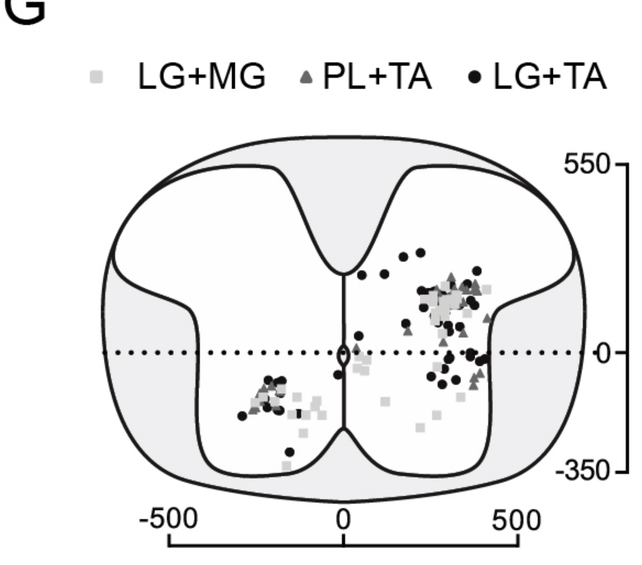

H

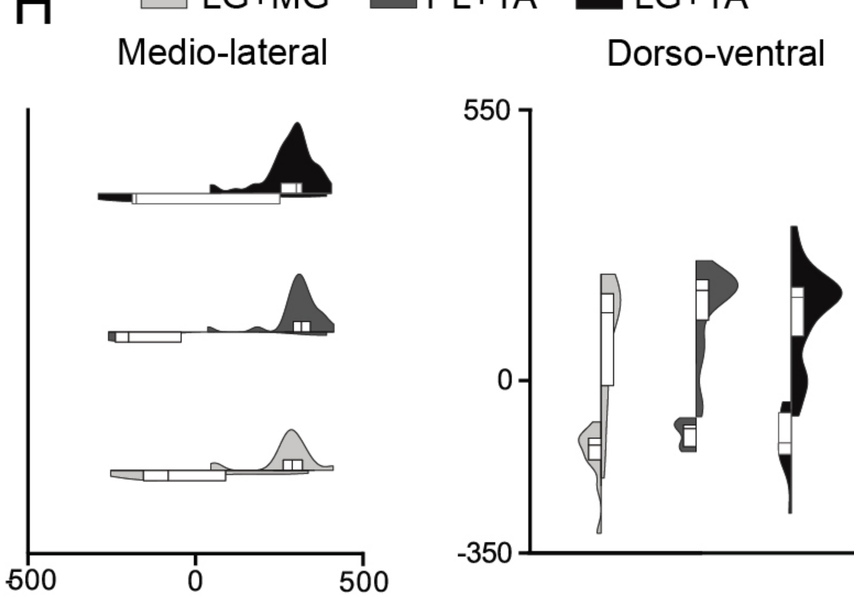

Figure 2

A

LG-eGFP MG-mCherry

i

contra

ipsi

ii

iii

iv

B

LG-eGFP MG-mCherry

i

contra

ipsi

ii

iii

iv

C

Sample: 170508n7

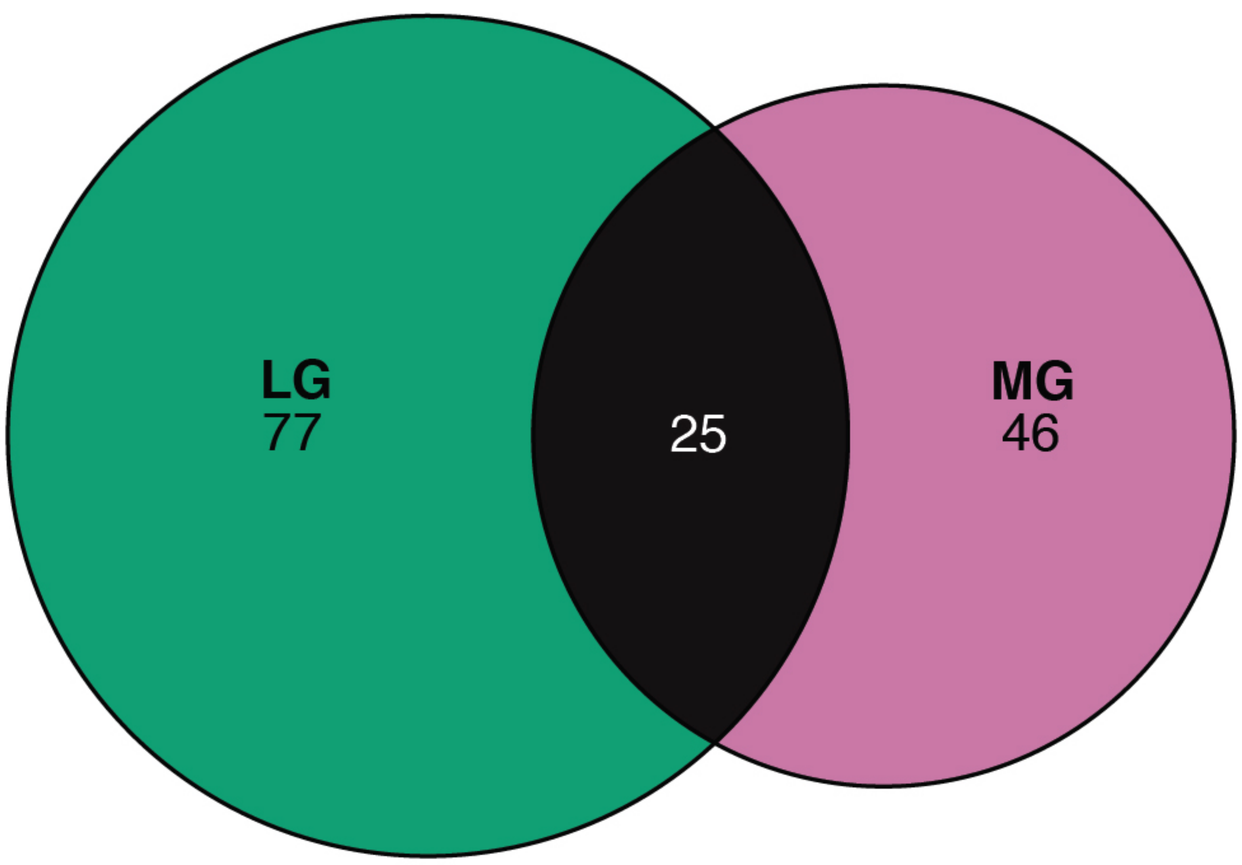

D

Sample: 170125n3

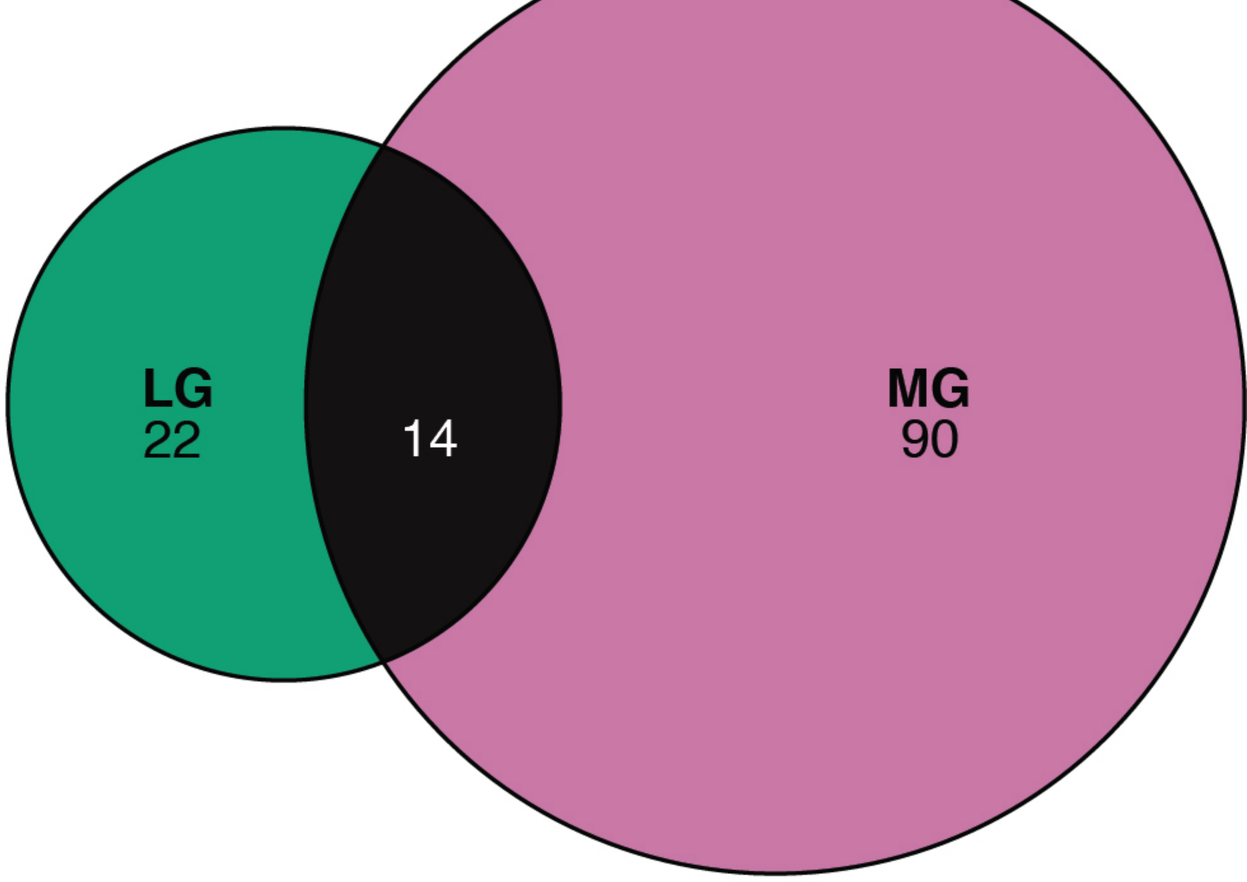

Figure 2-figure supplement 1

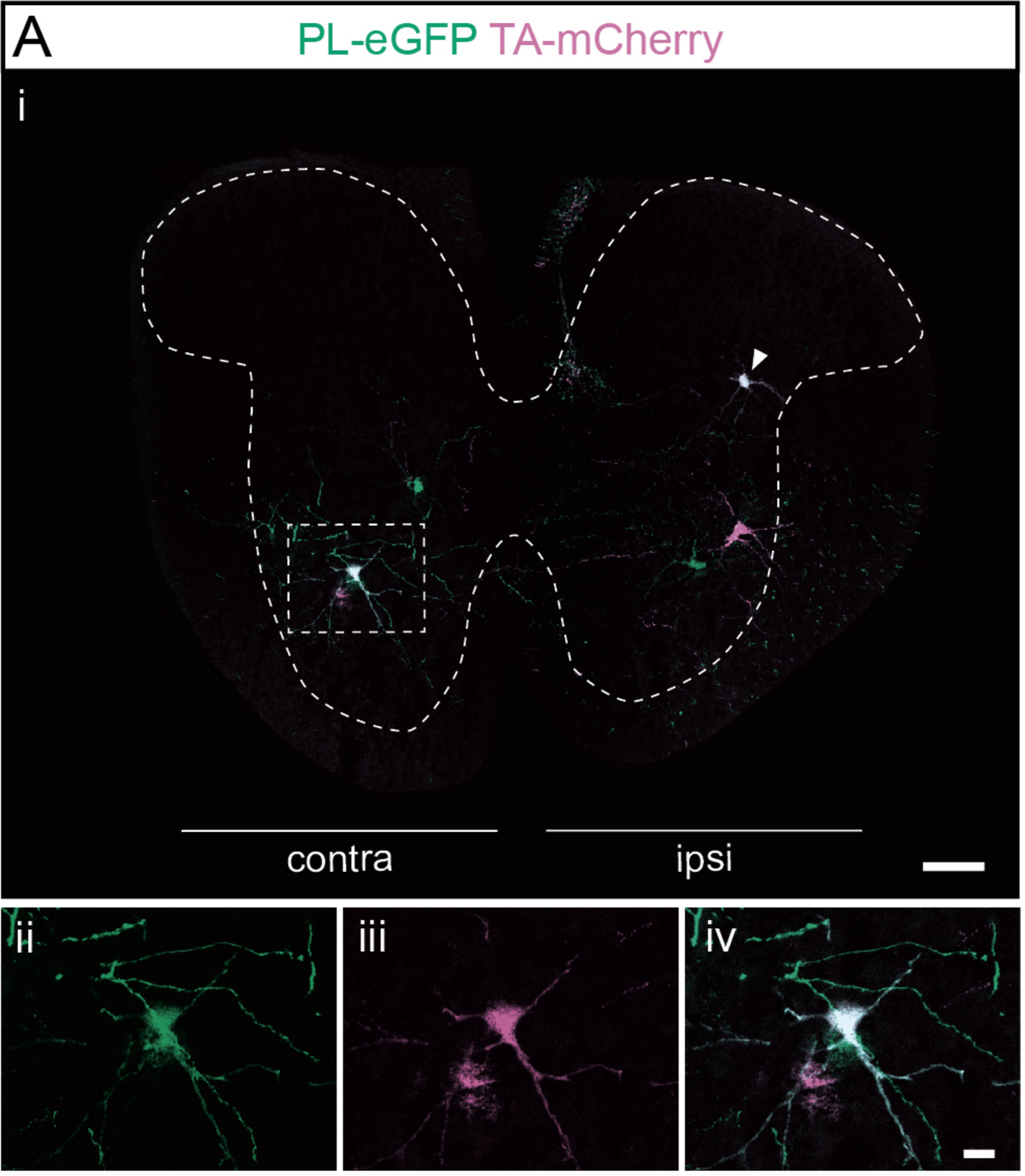

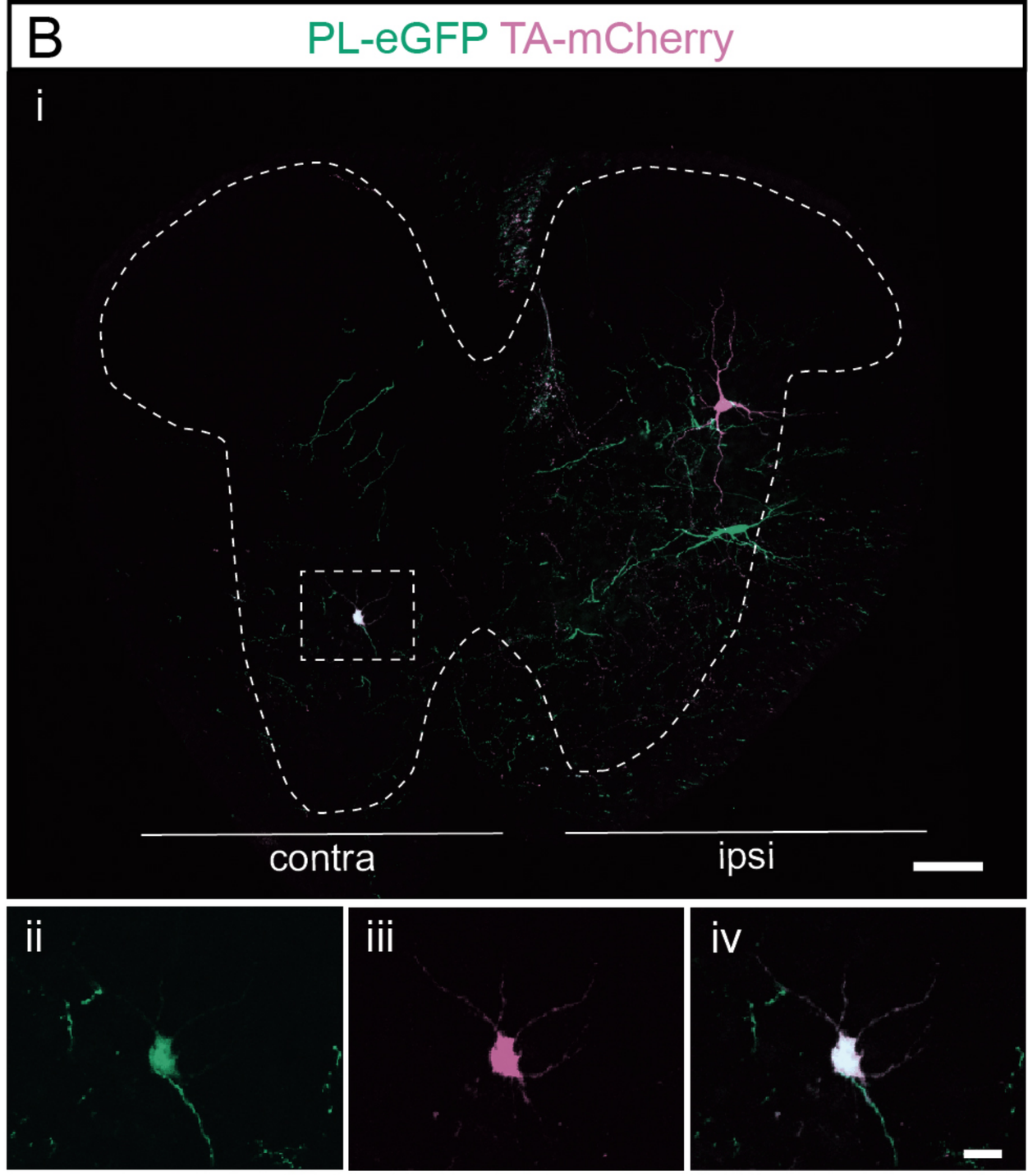

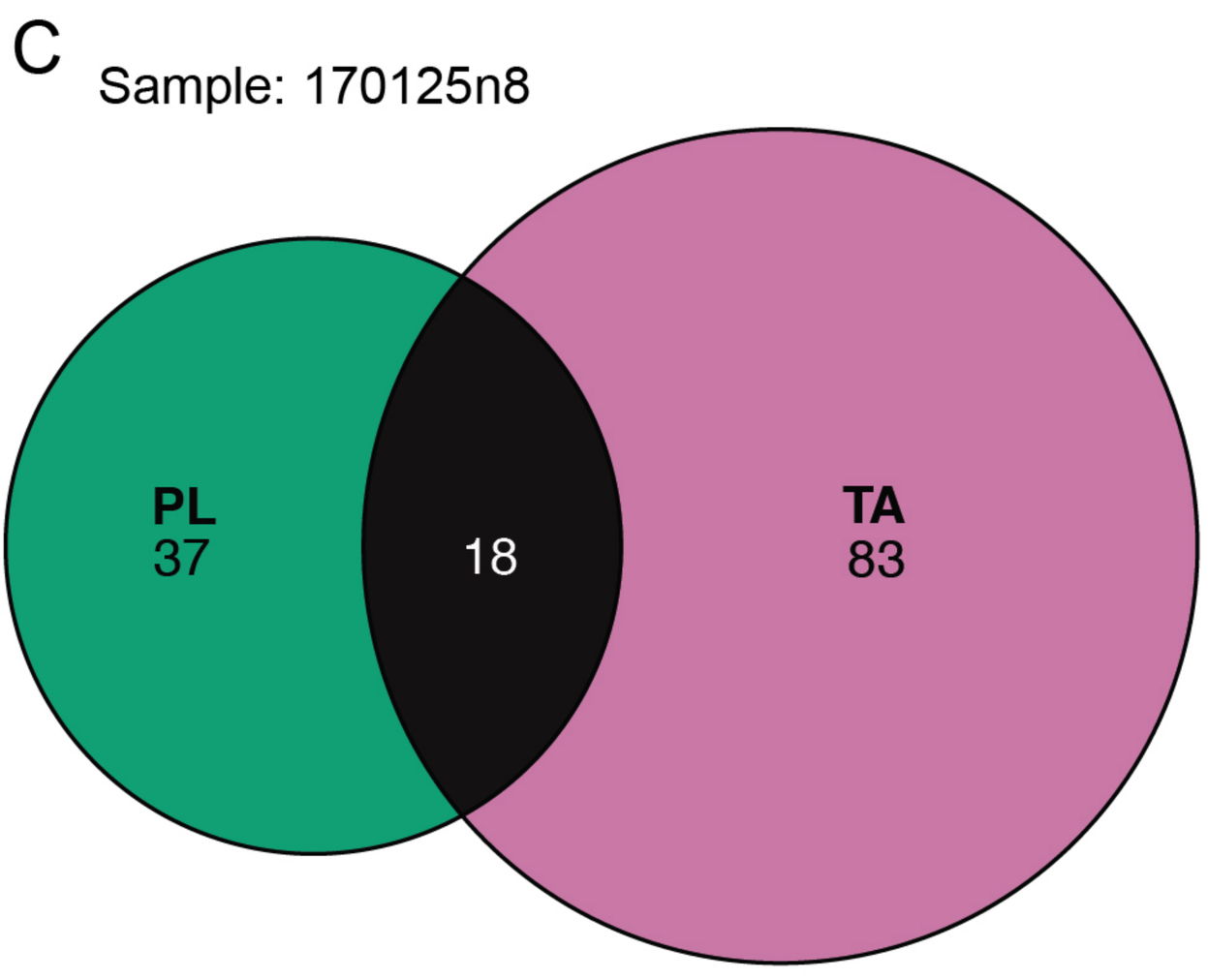

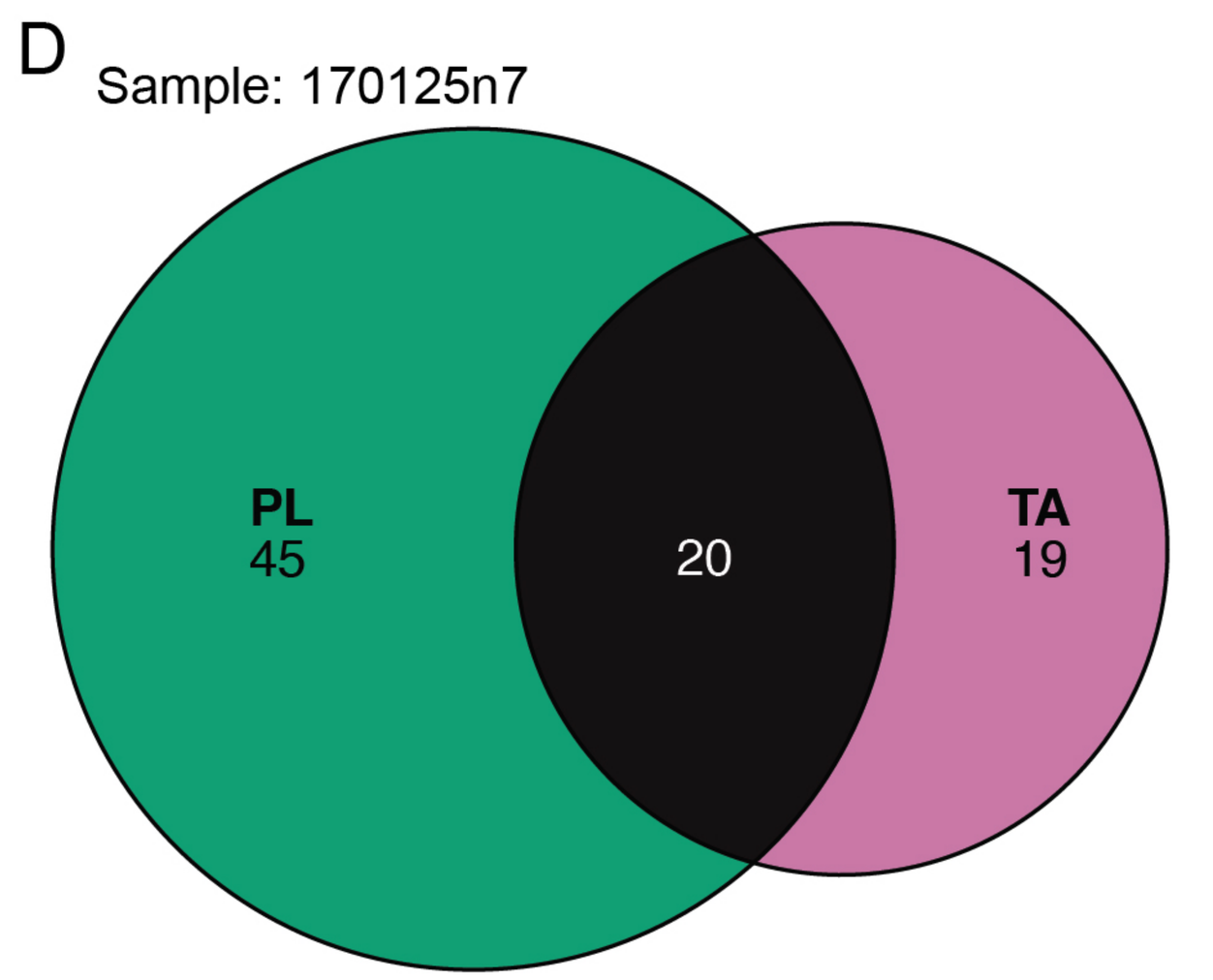

Figure 2-figure supplement 2

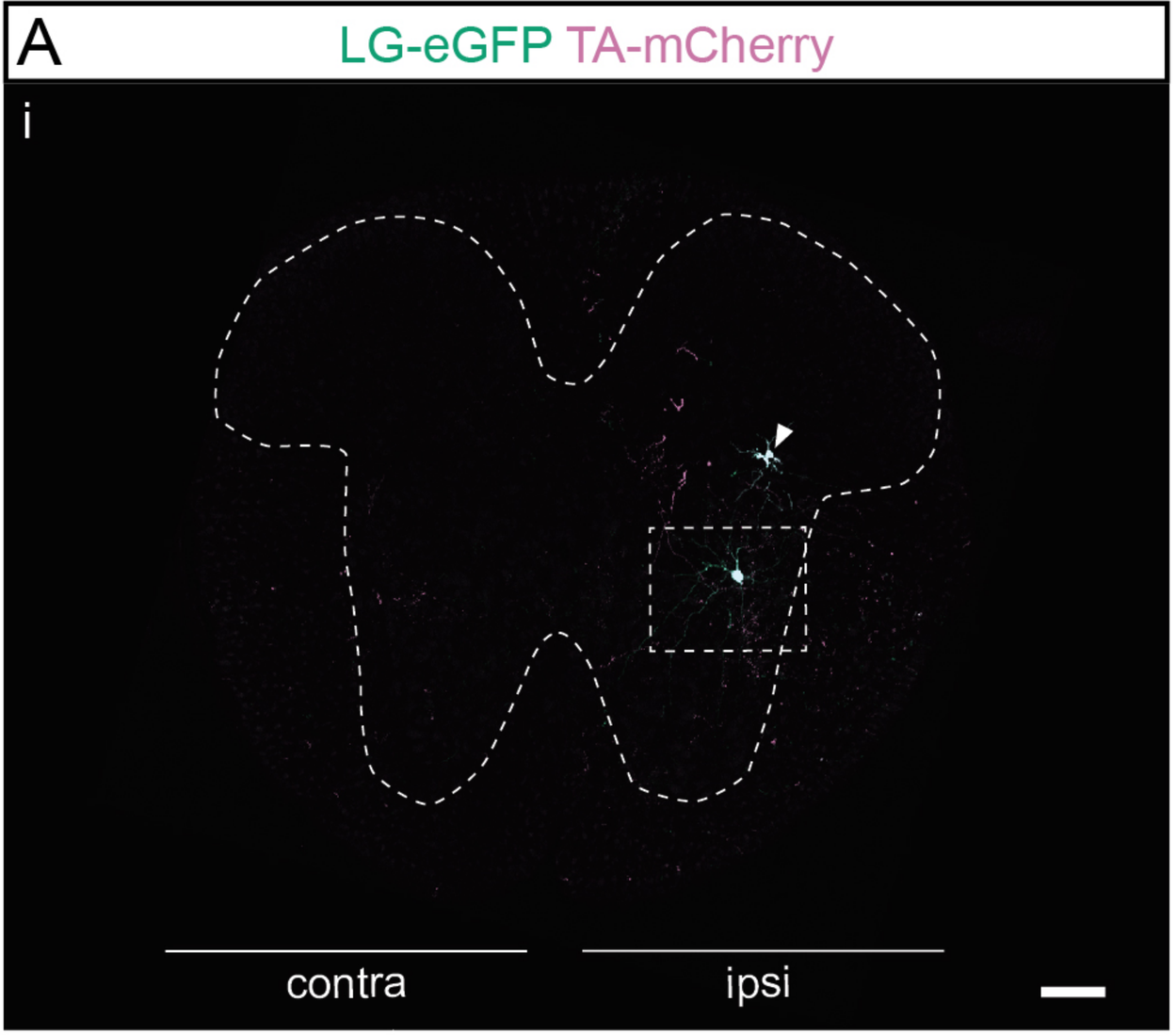

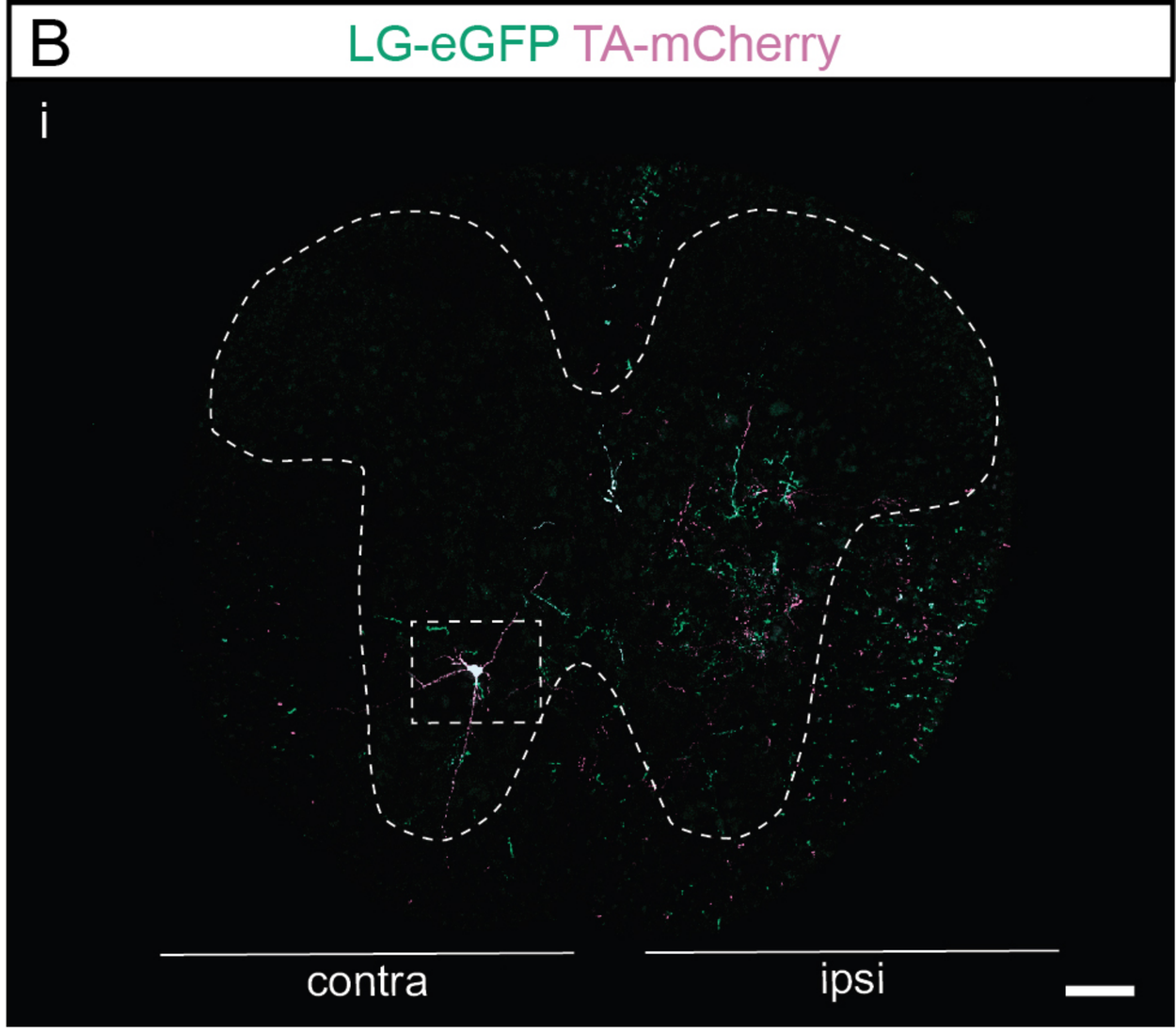

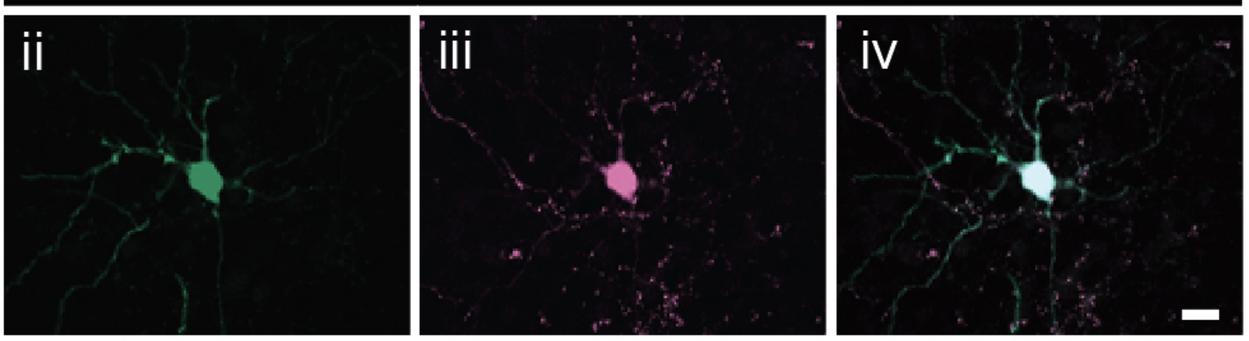

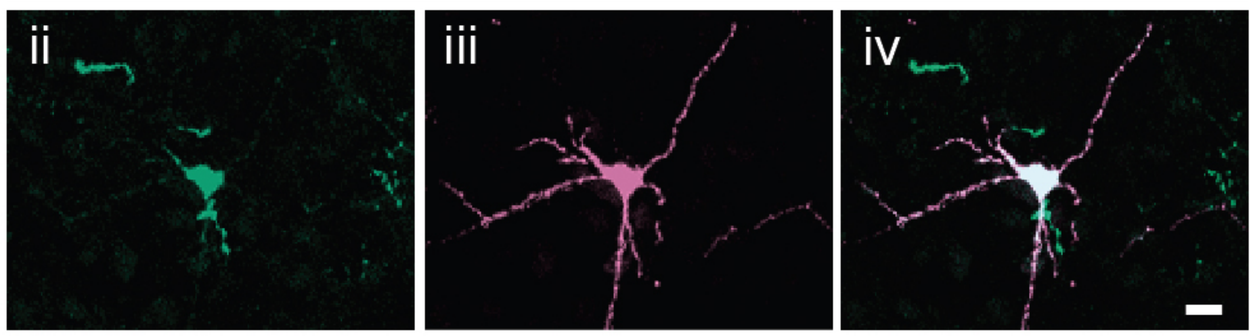

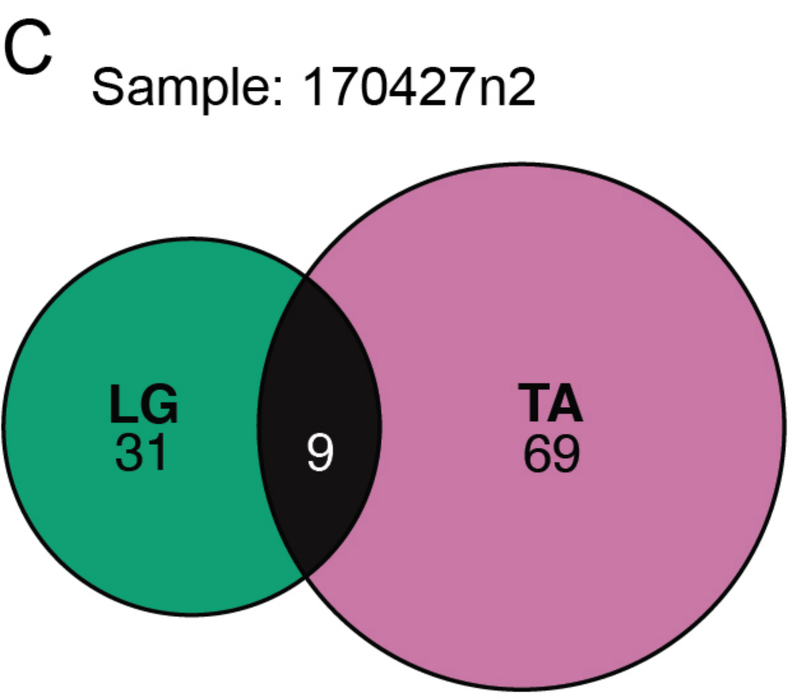

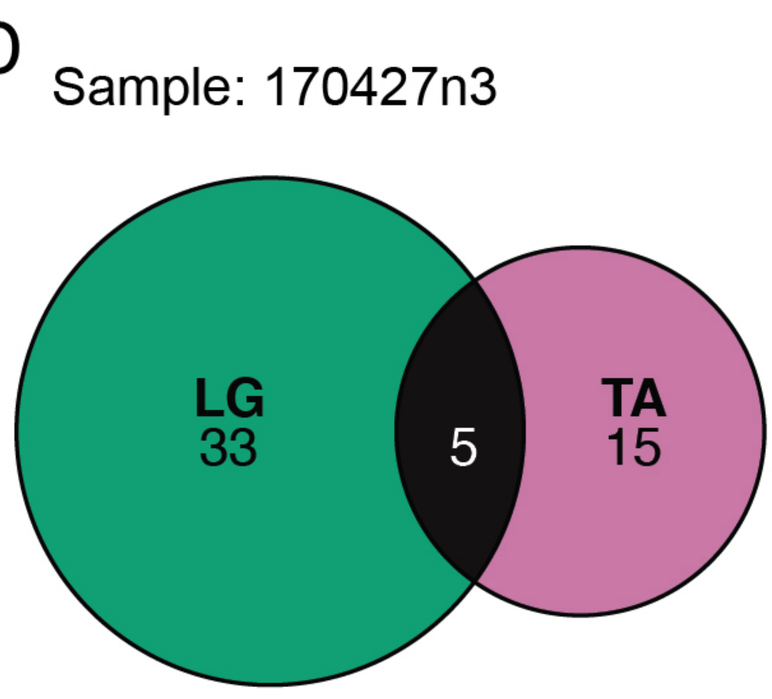

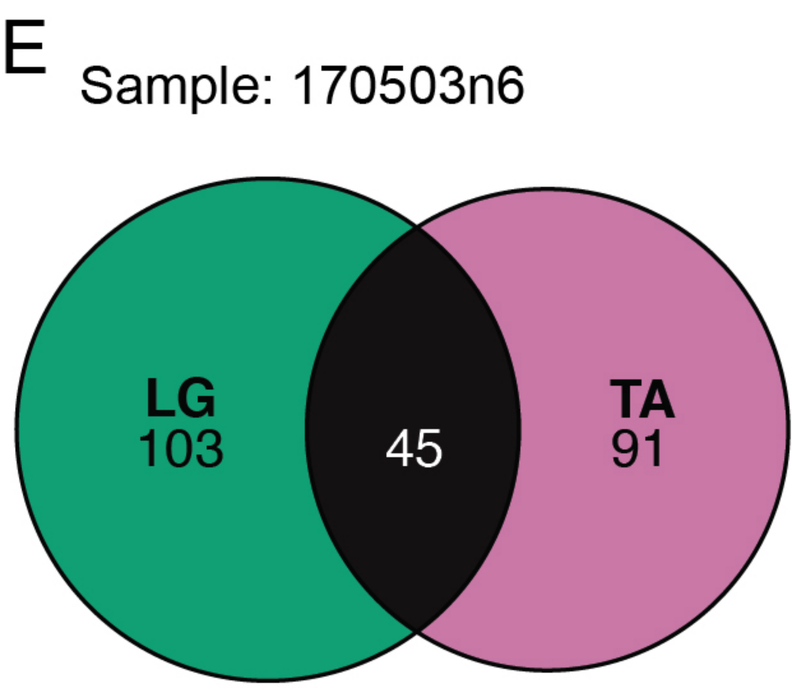

Figure 2-figure supplement 3

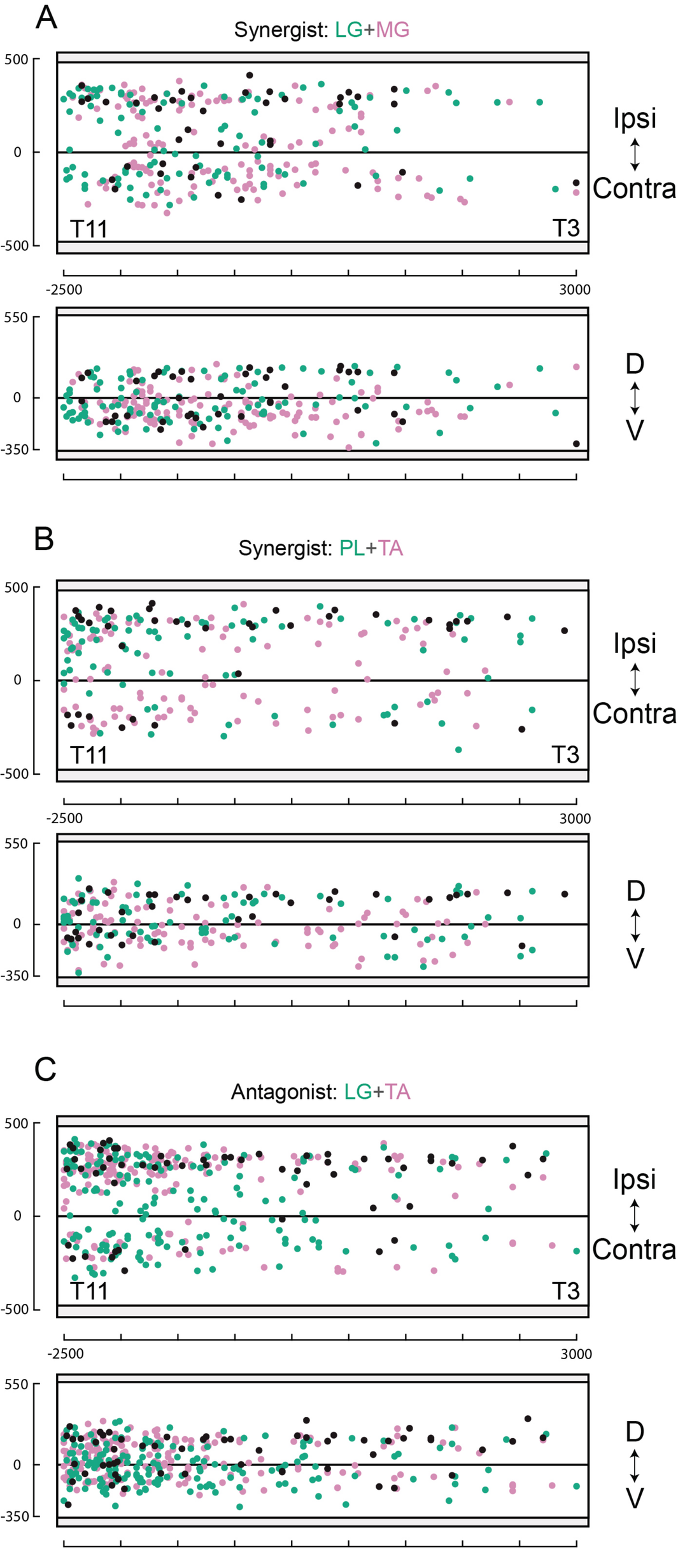

Figure 2-figure supplement 4

A

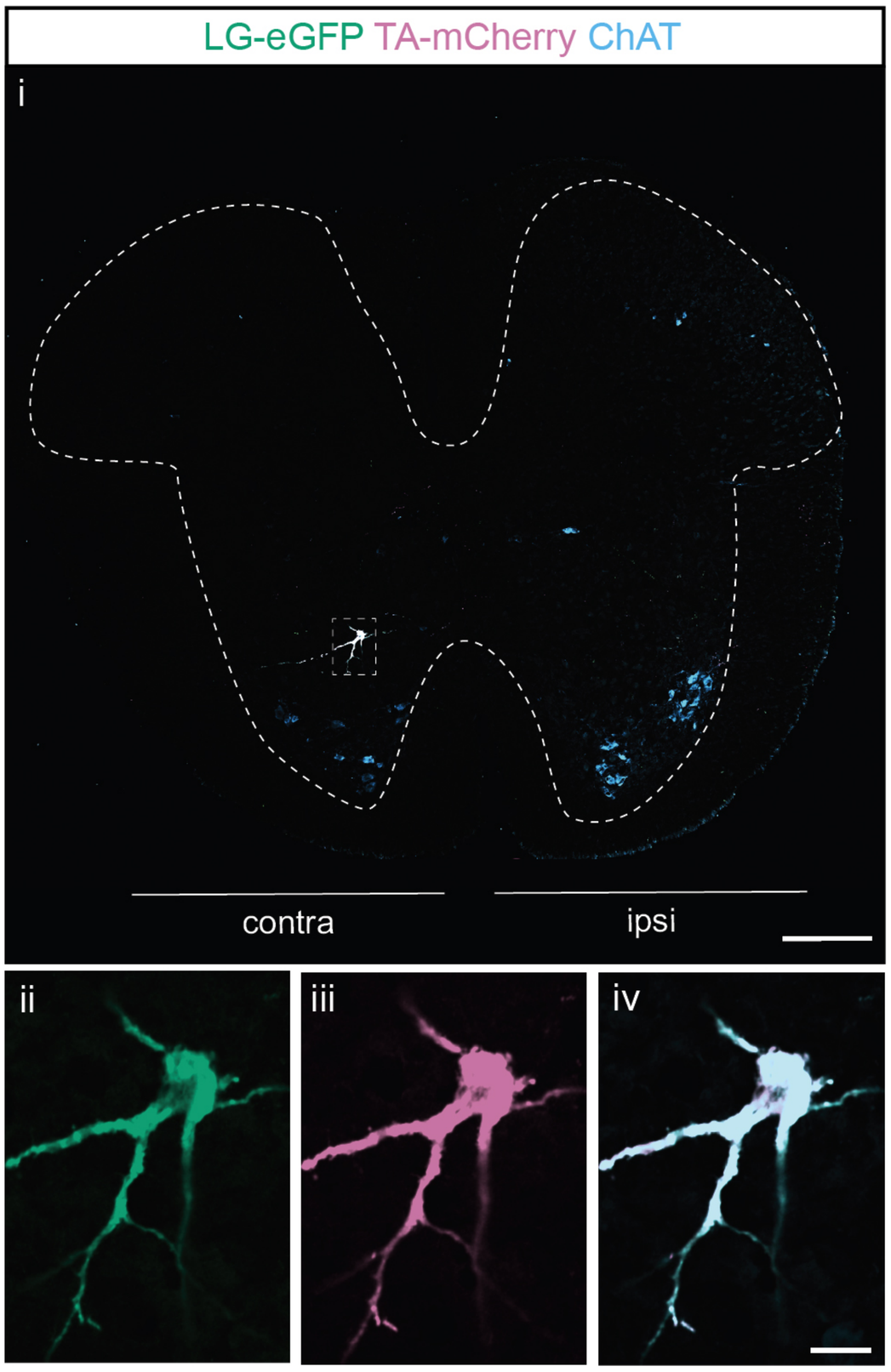

B

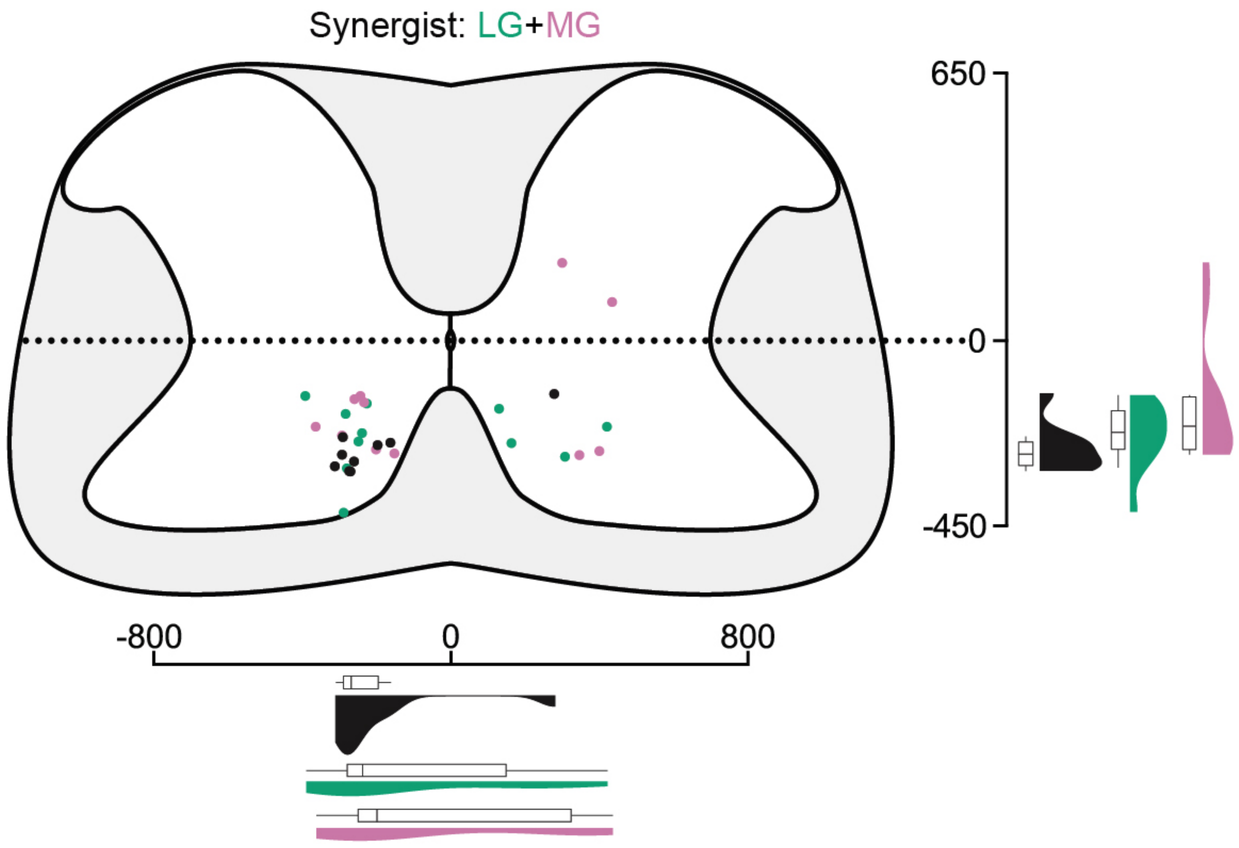

C

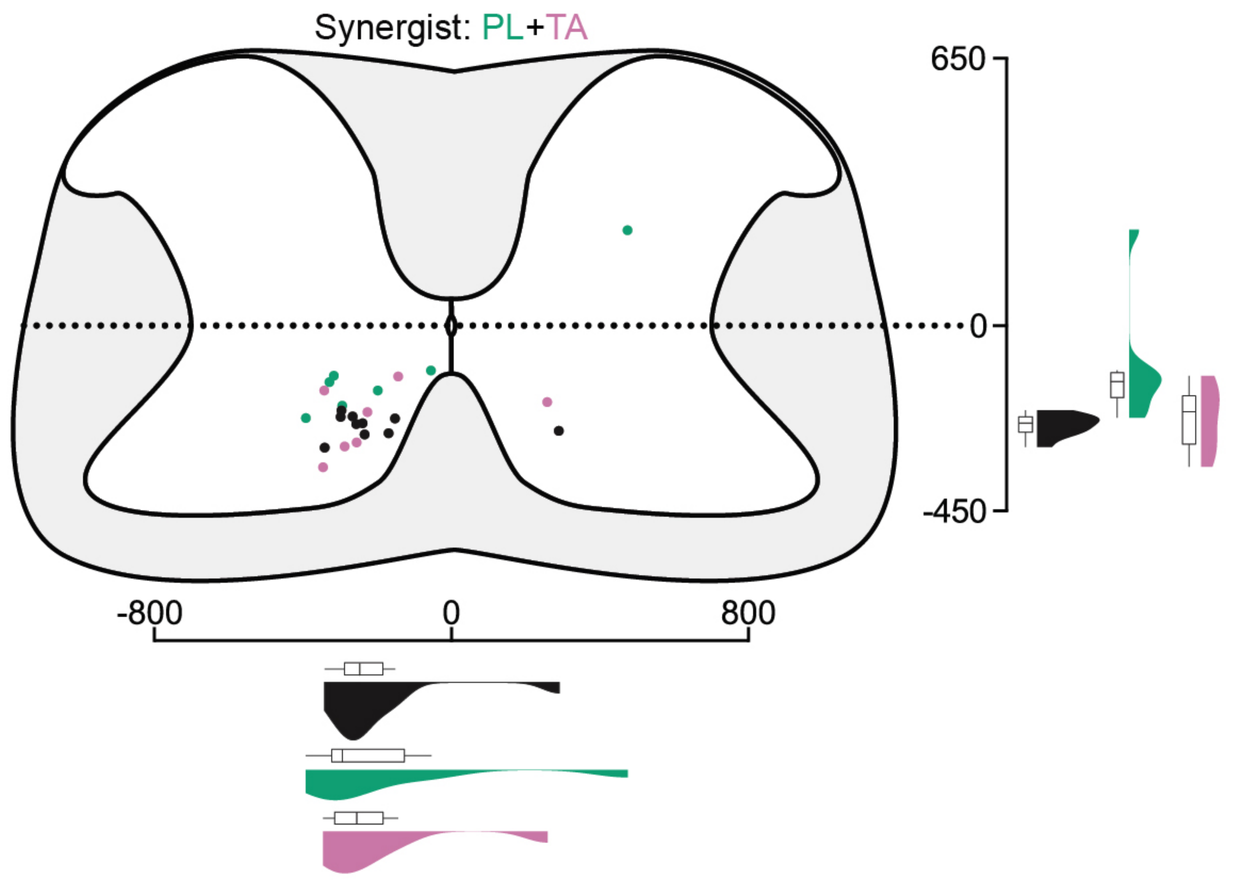

D

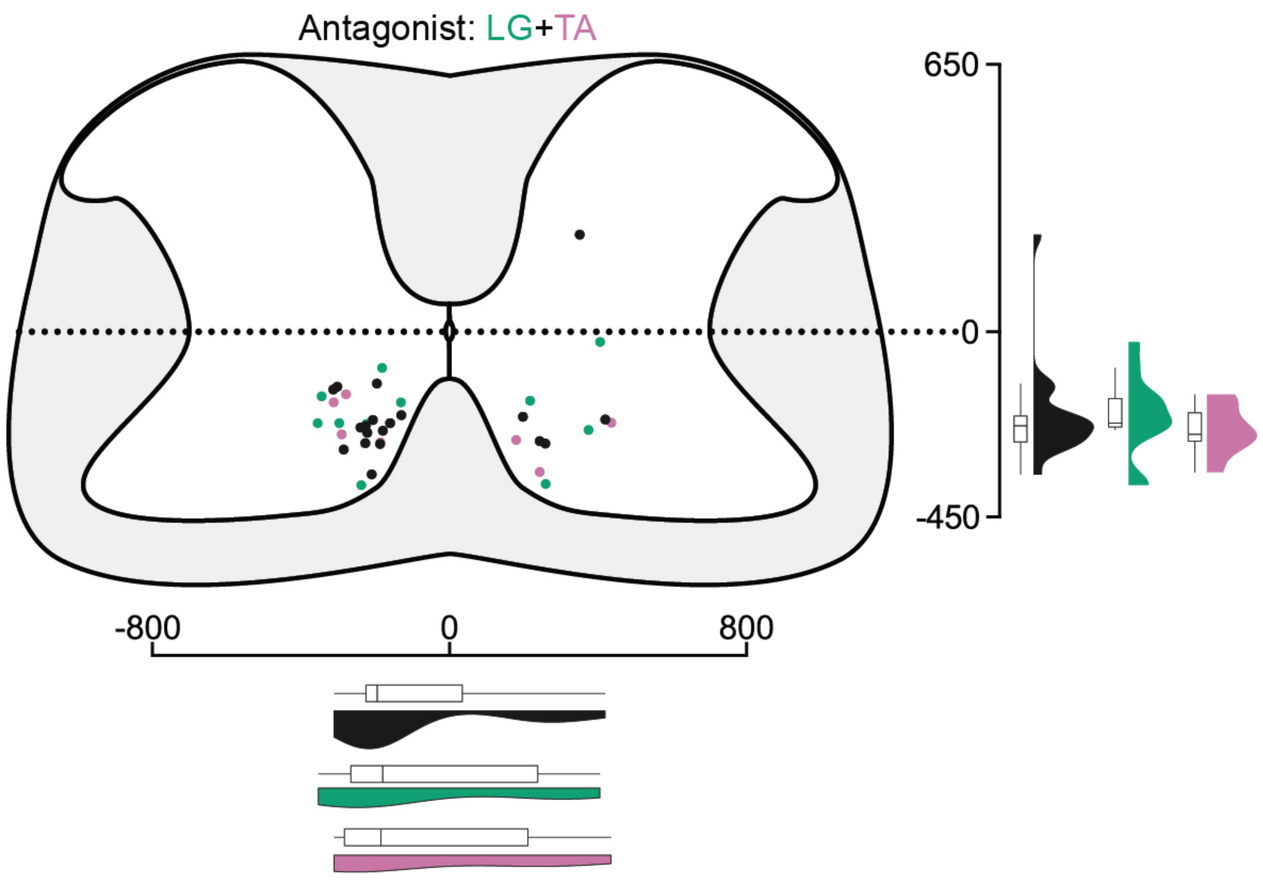

E

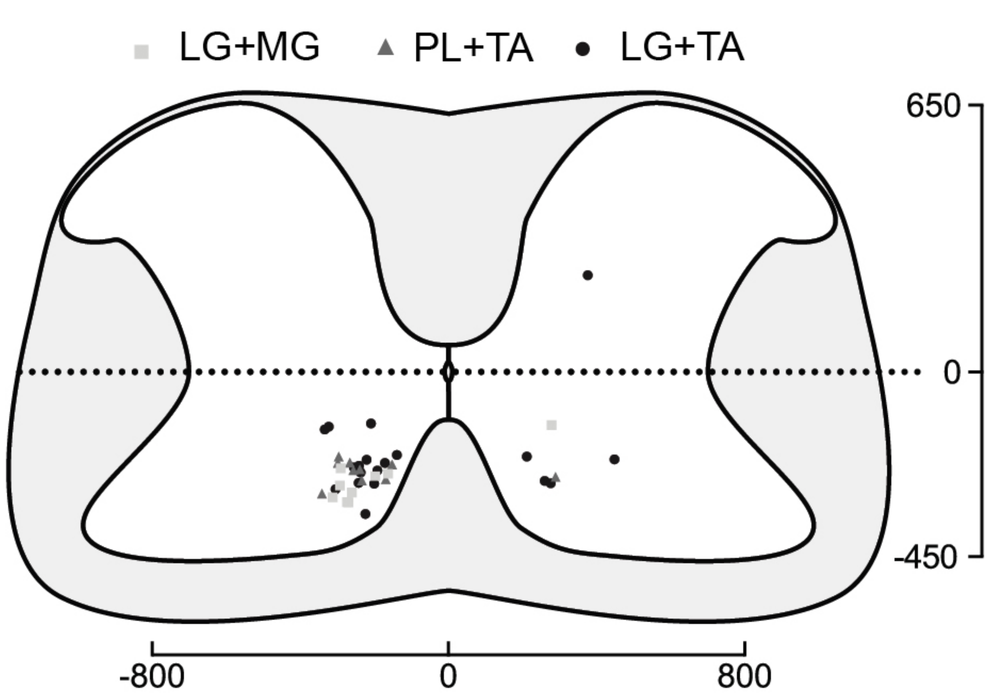

F

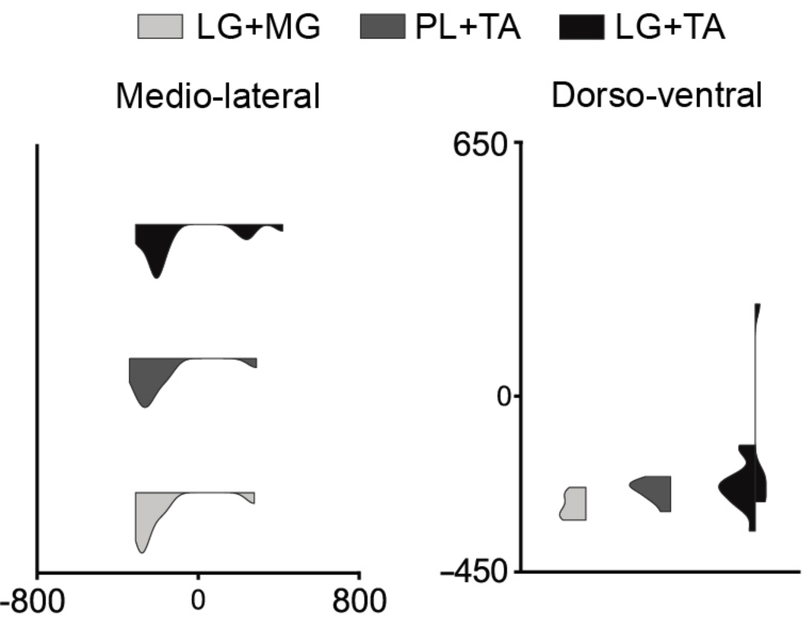

G

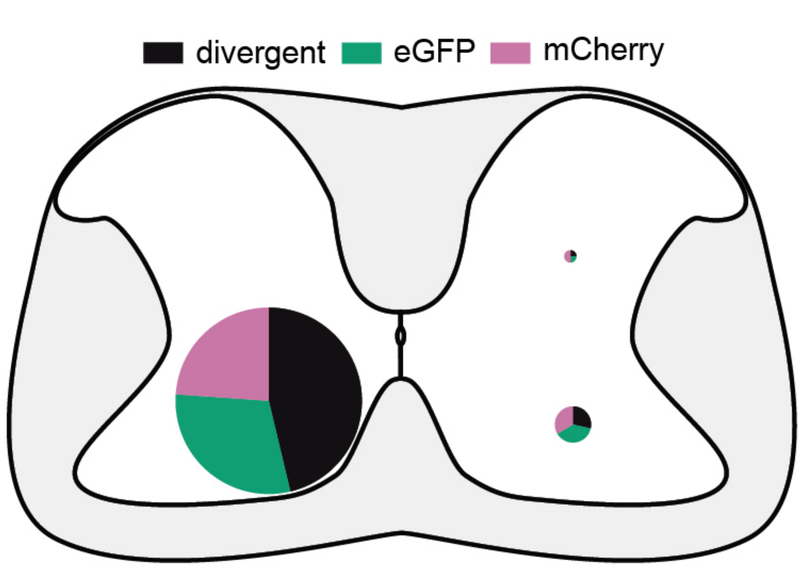

H

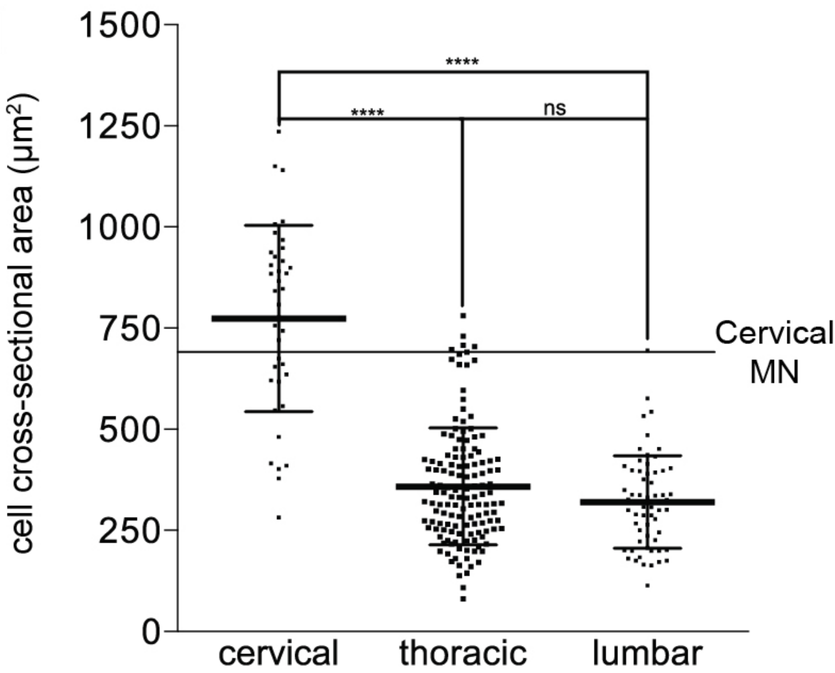

Figure 3

A

LG-eGFP MG-mCherry

i

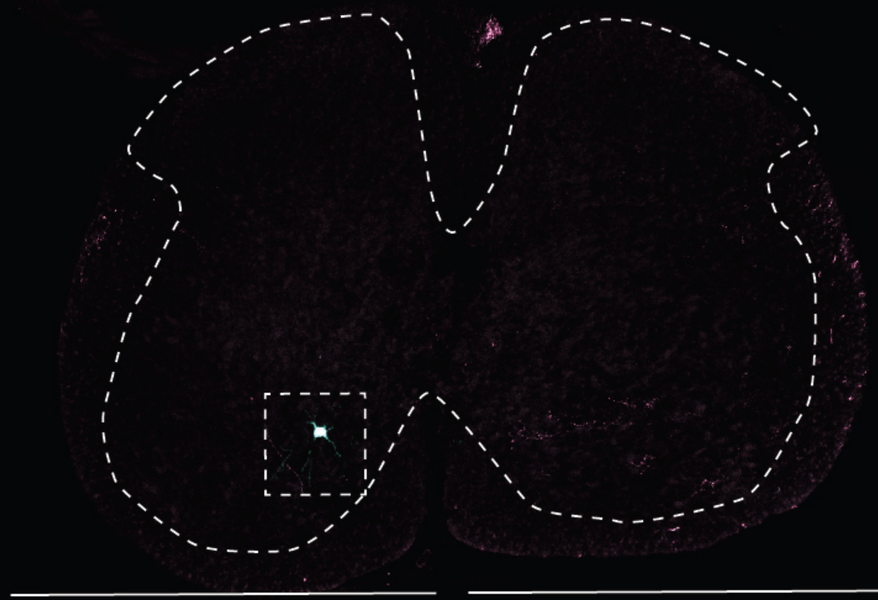

B

LG-eGFP MG-mCherry

i

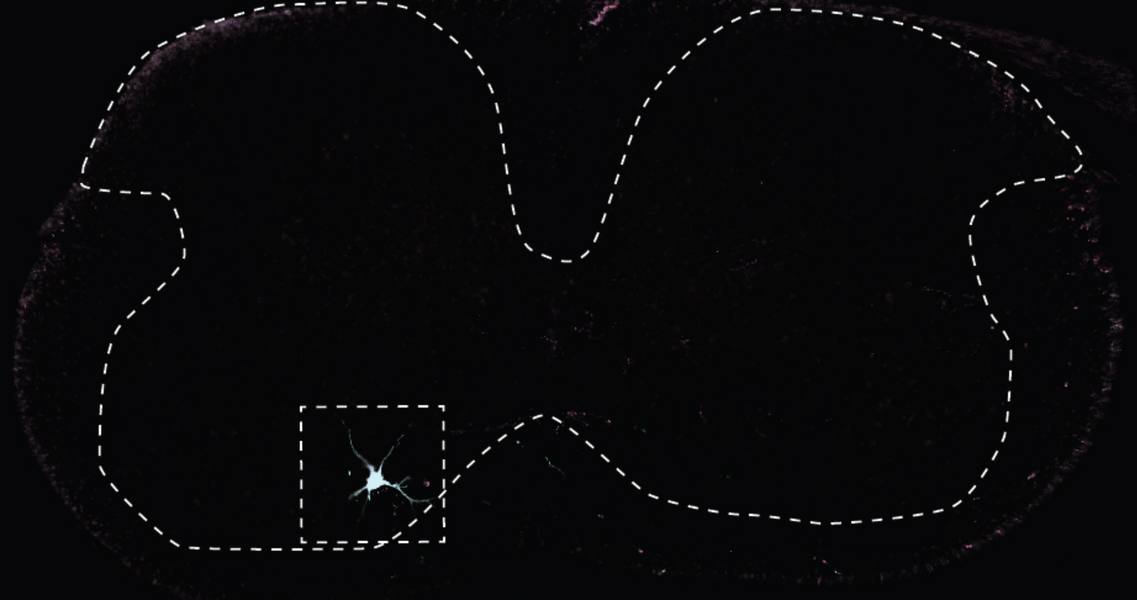

ii iii iv

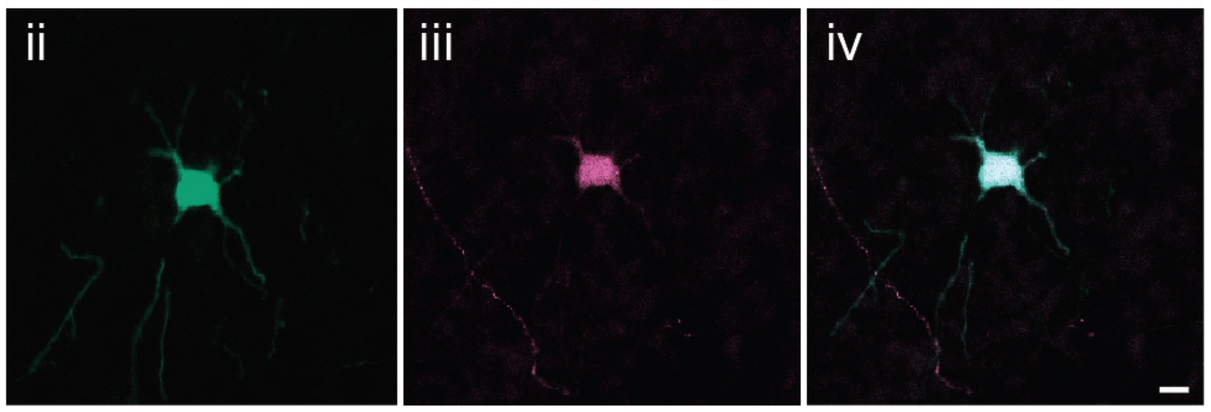

ii iii iv

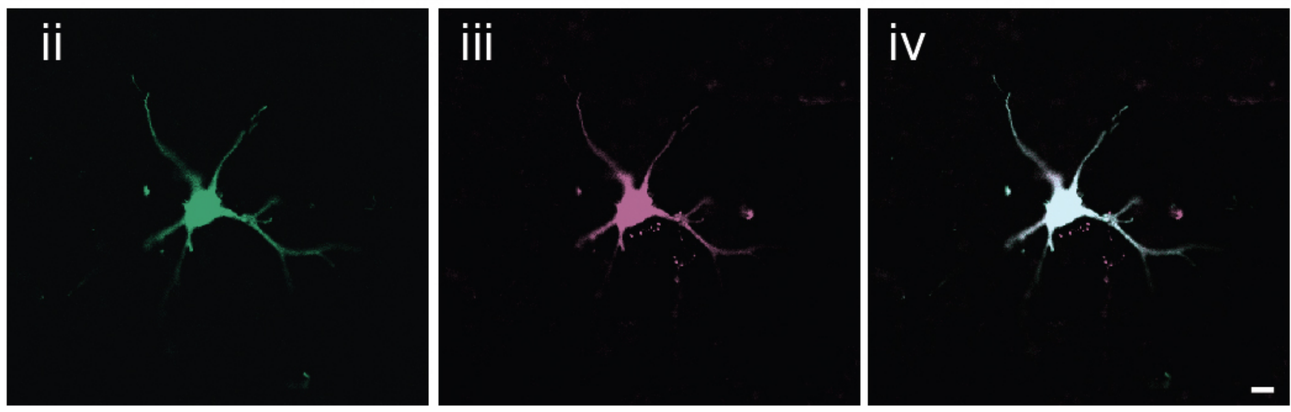

C

Sample: 170508n7

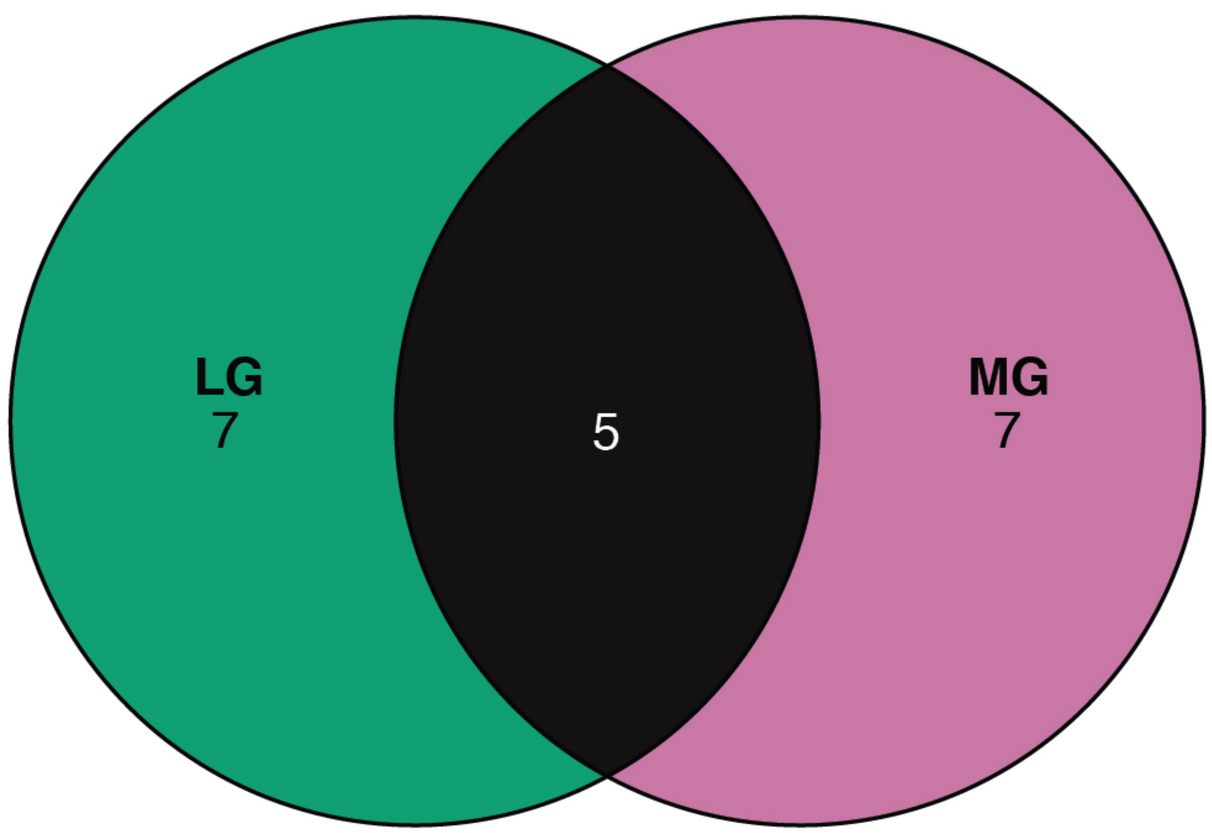

D

Sample: 170125n3

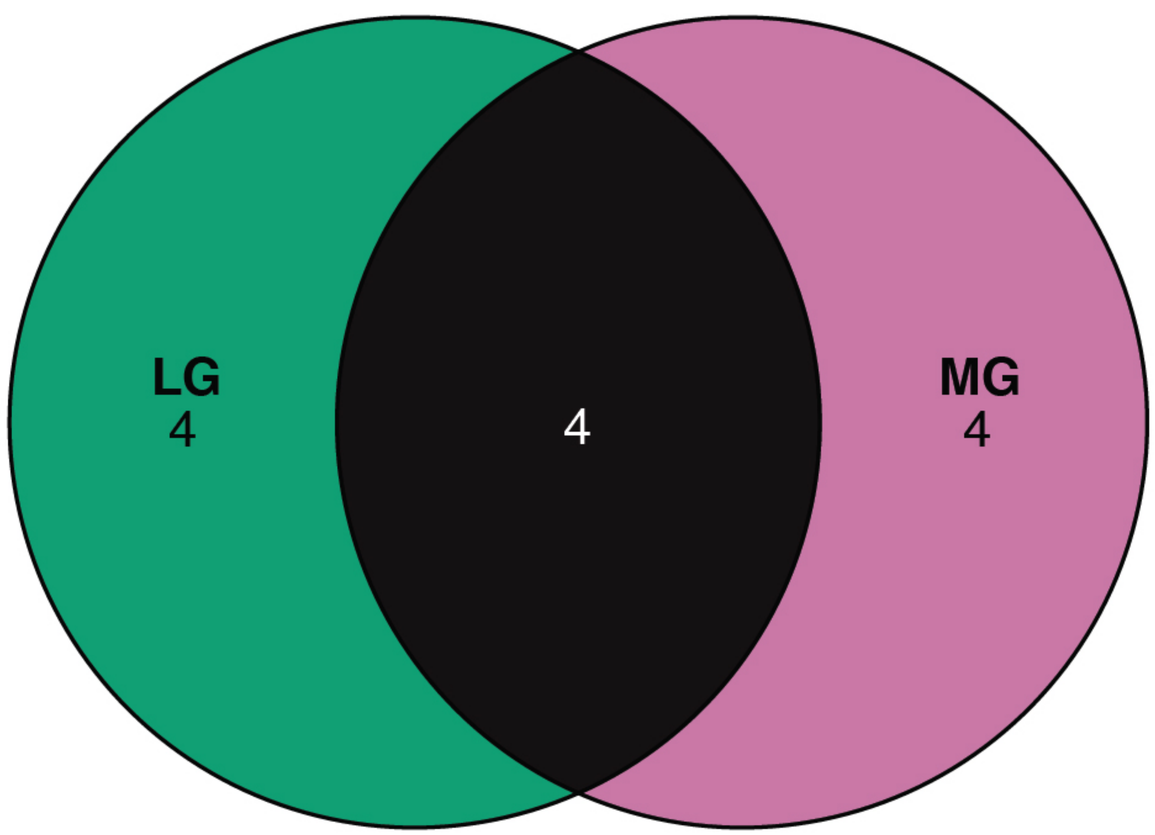

Figure 3-figure supplement 1

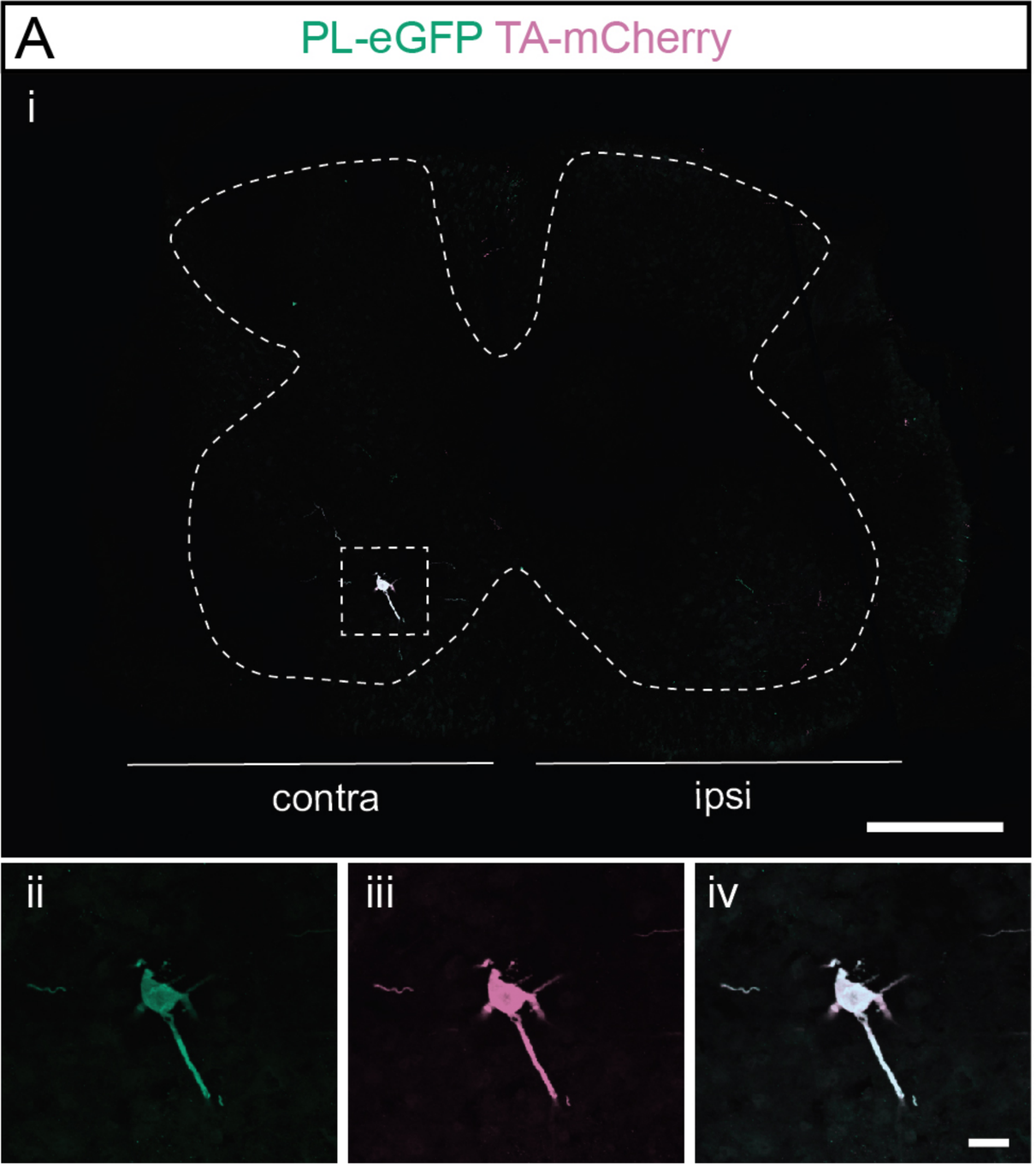

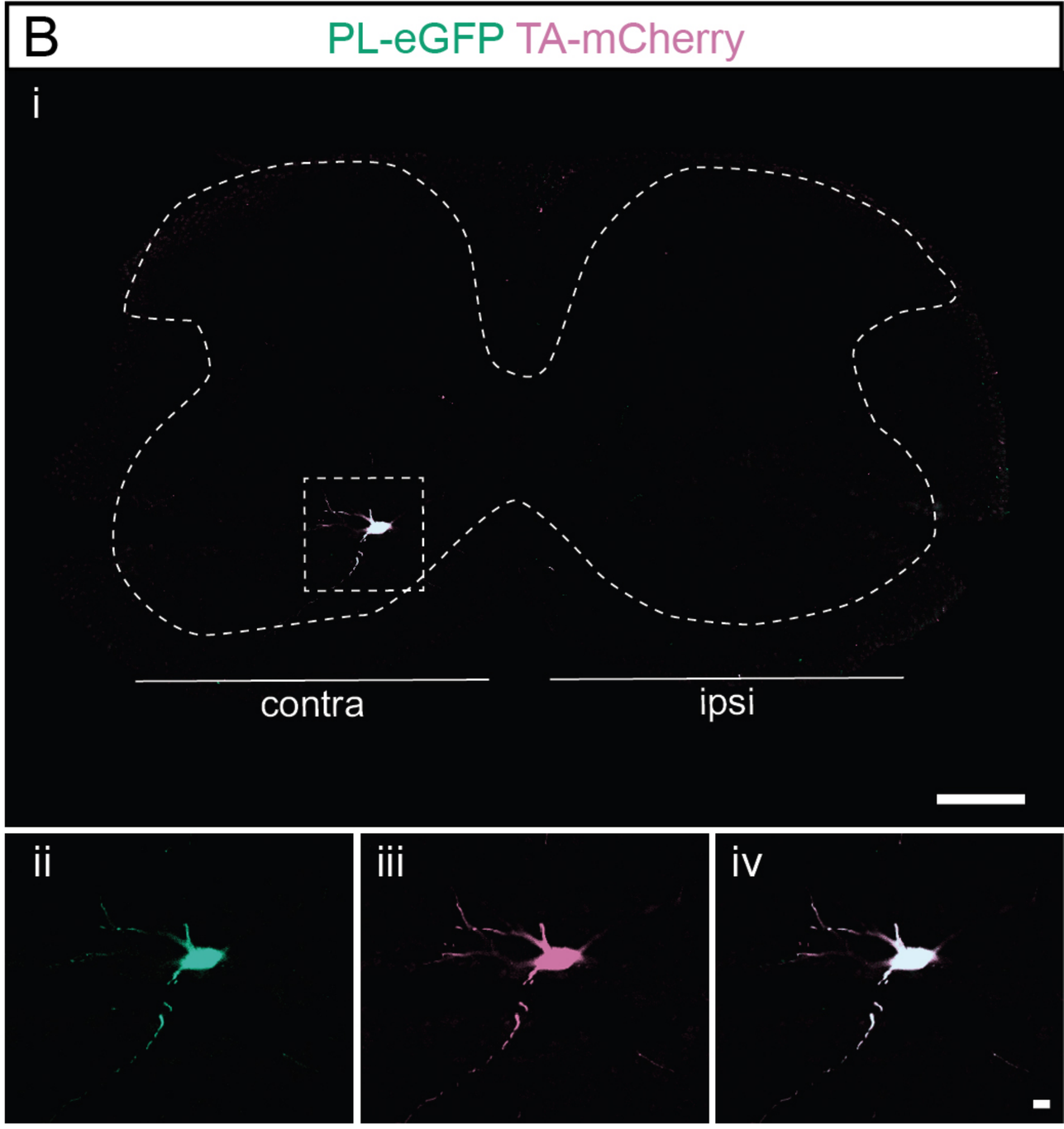

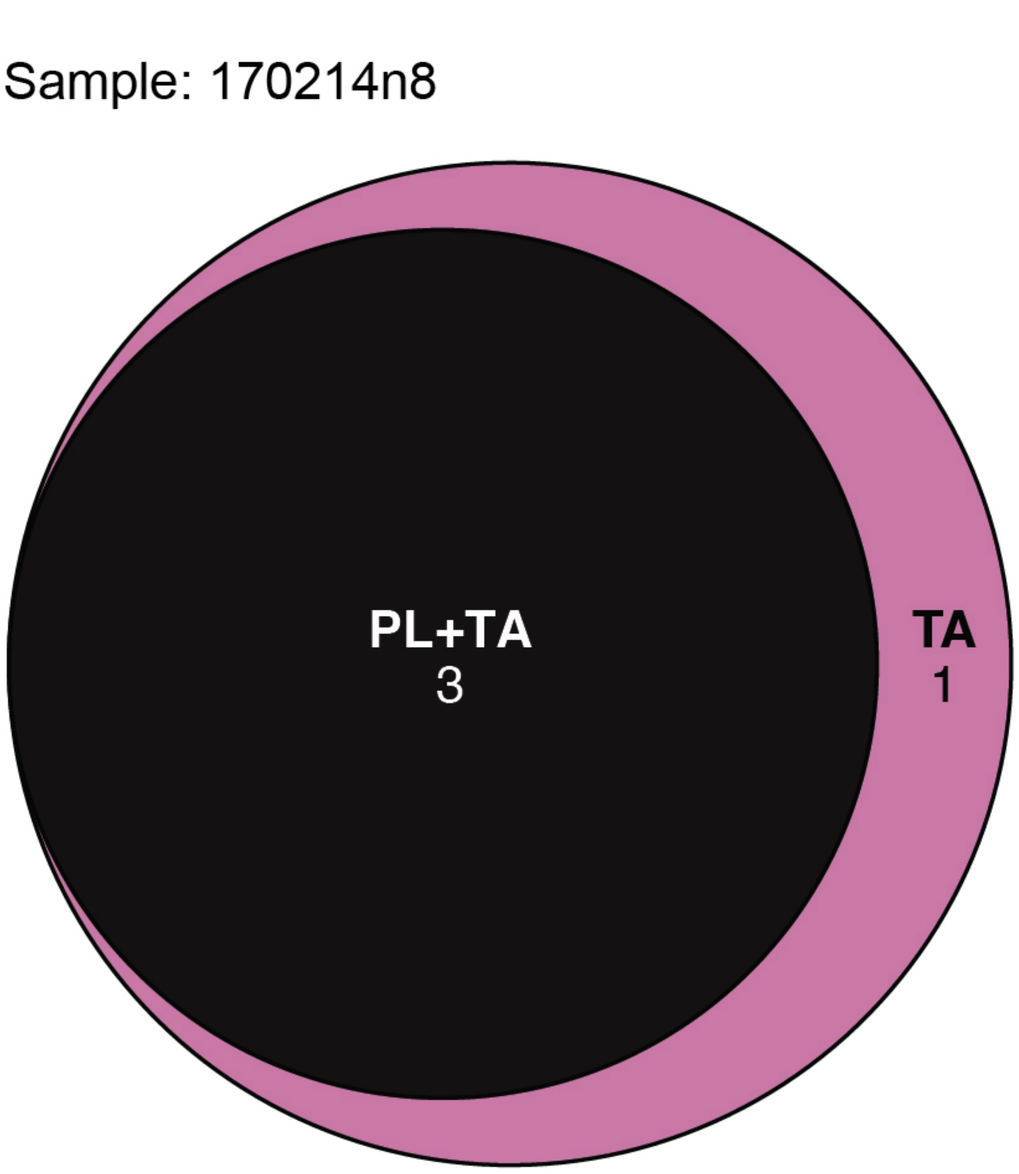

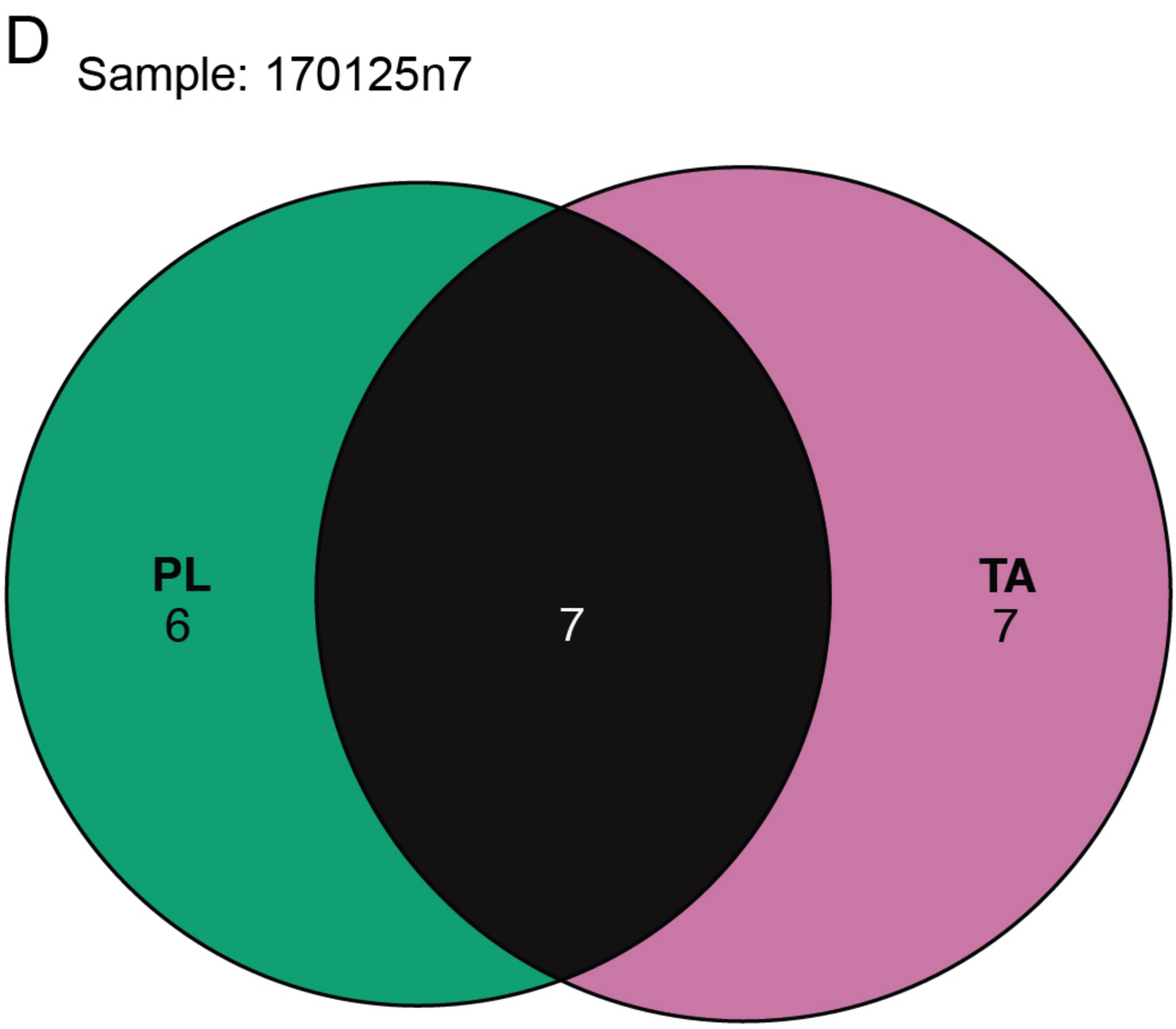

Figure 3-figure supplement 2

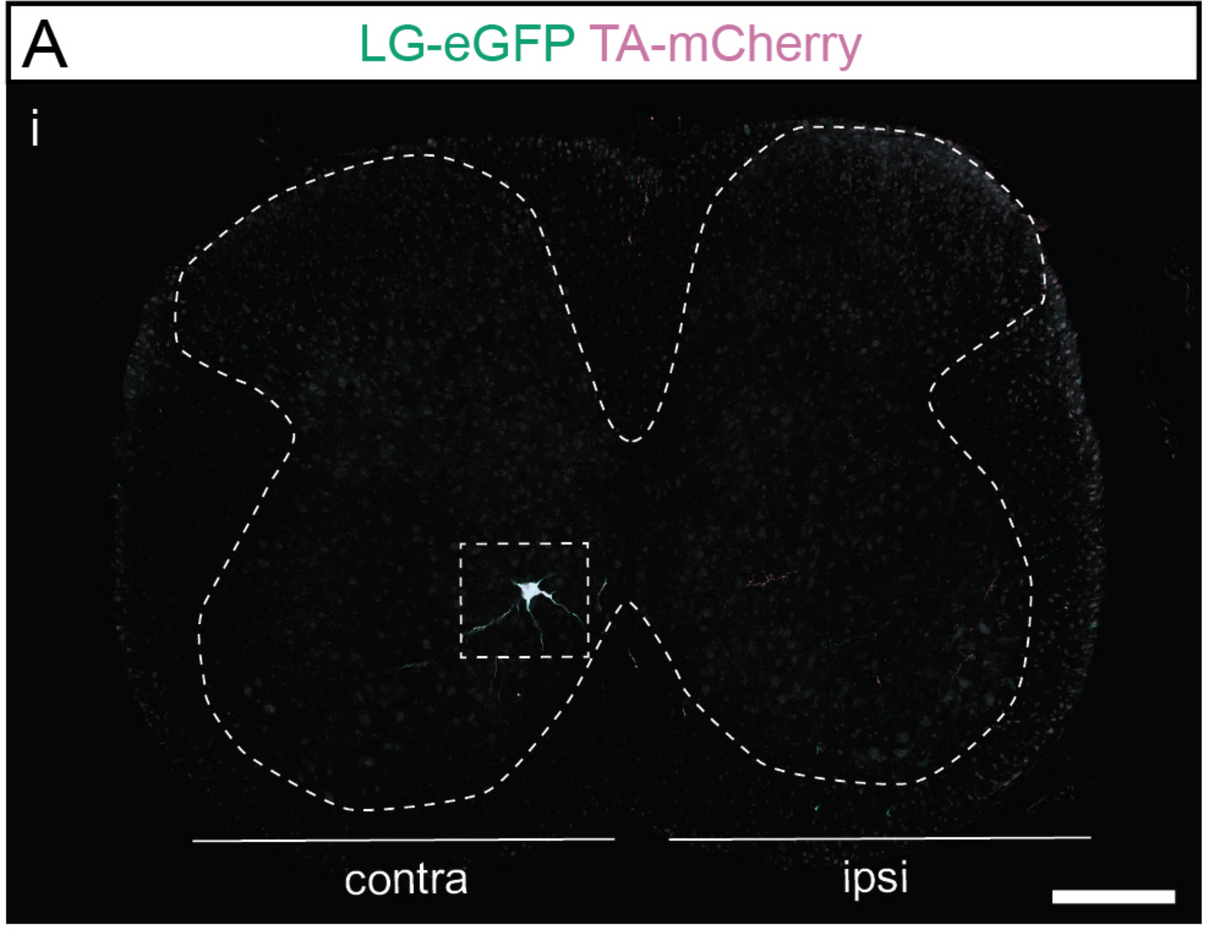

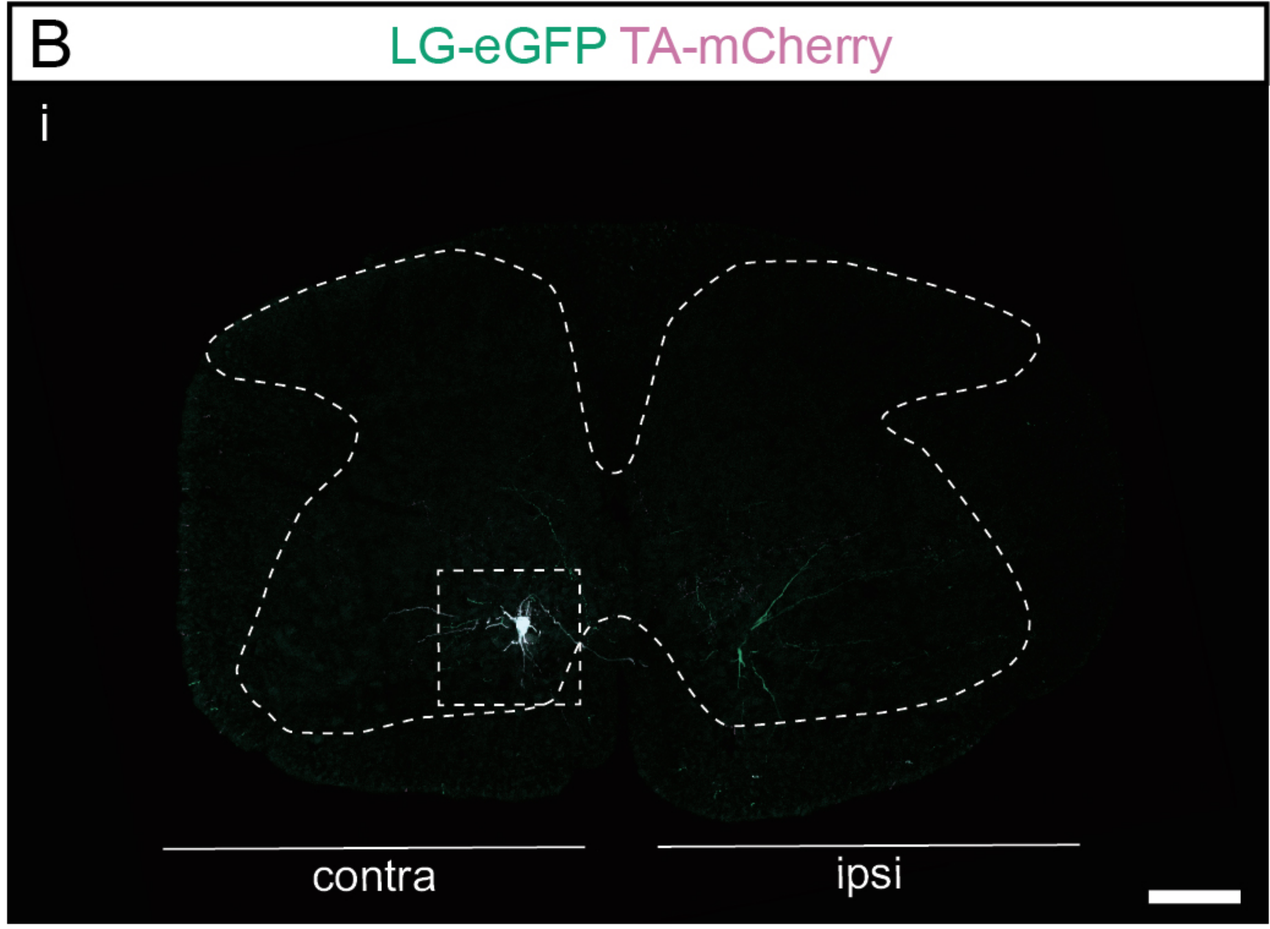

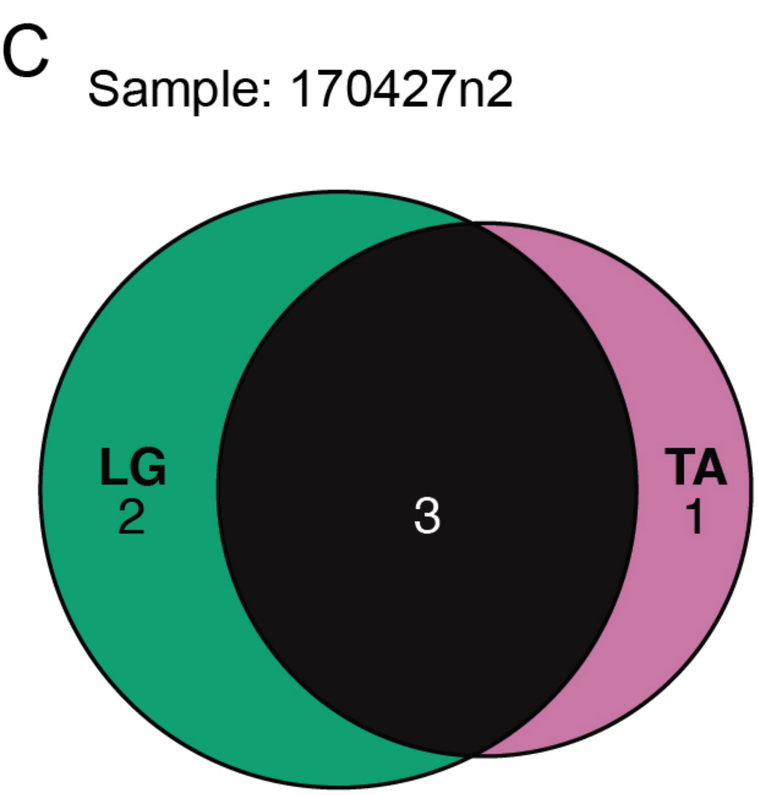

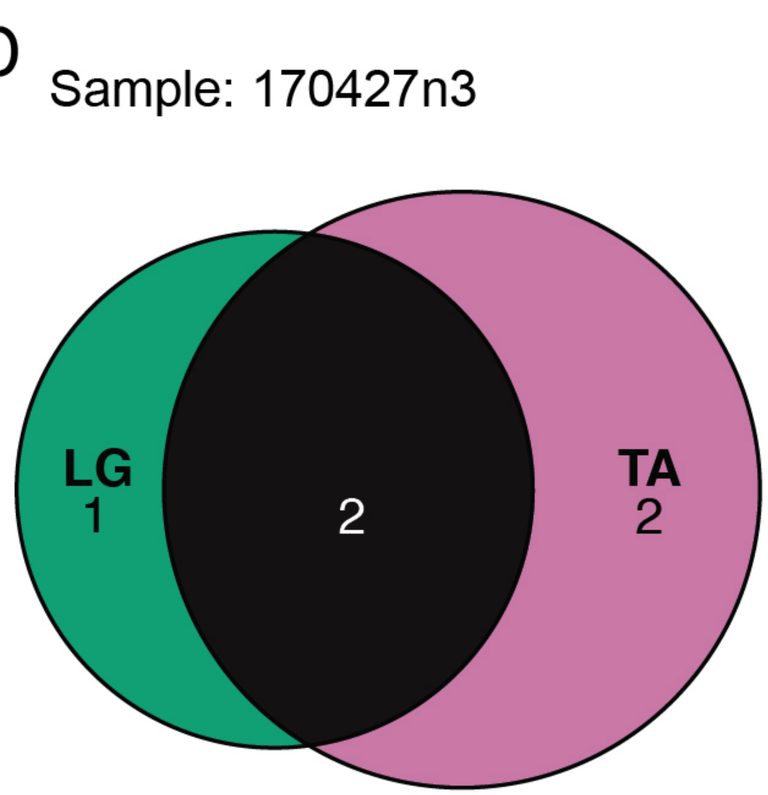

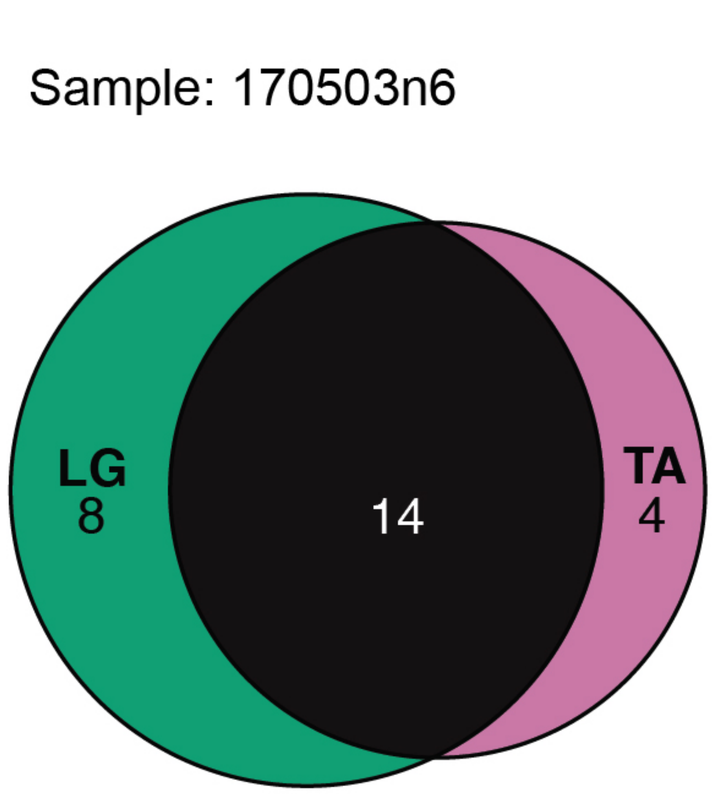

Figure 3-figure supplement 3

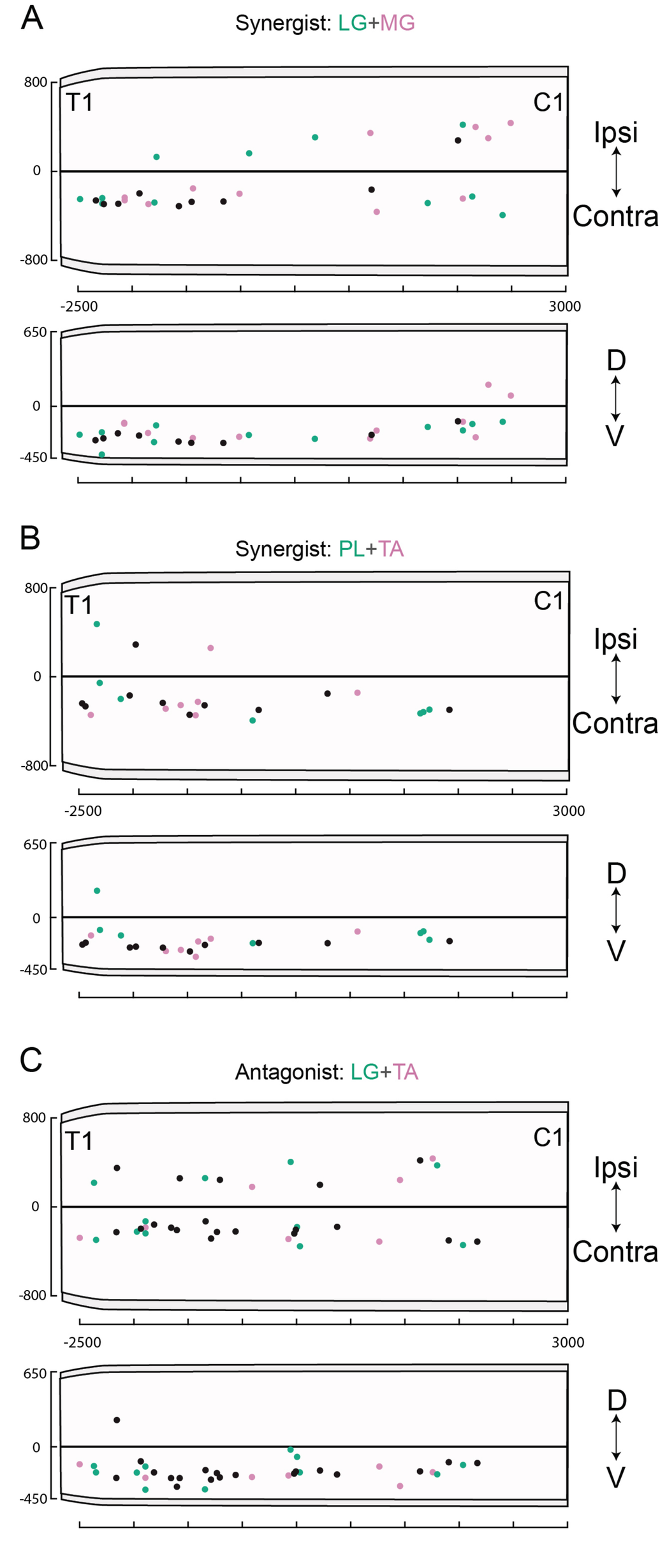

Figure 3-figure supplement 4

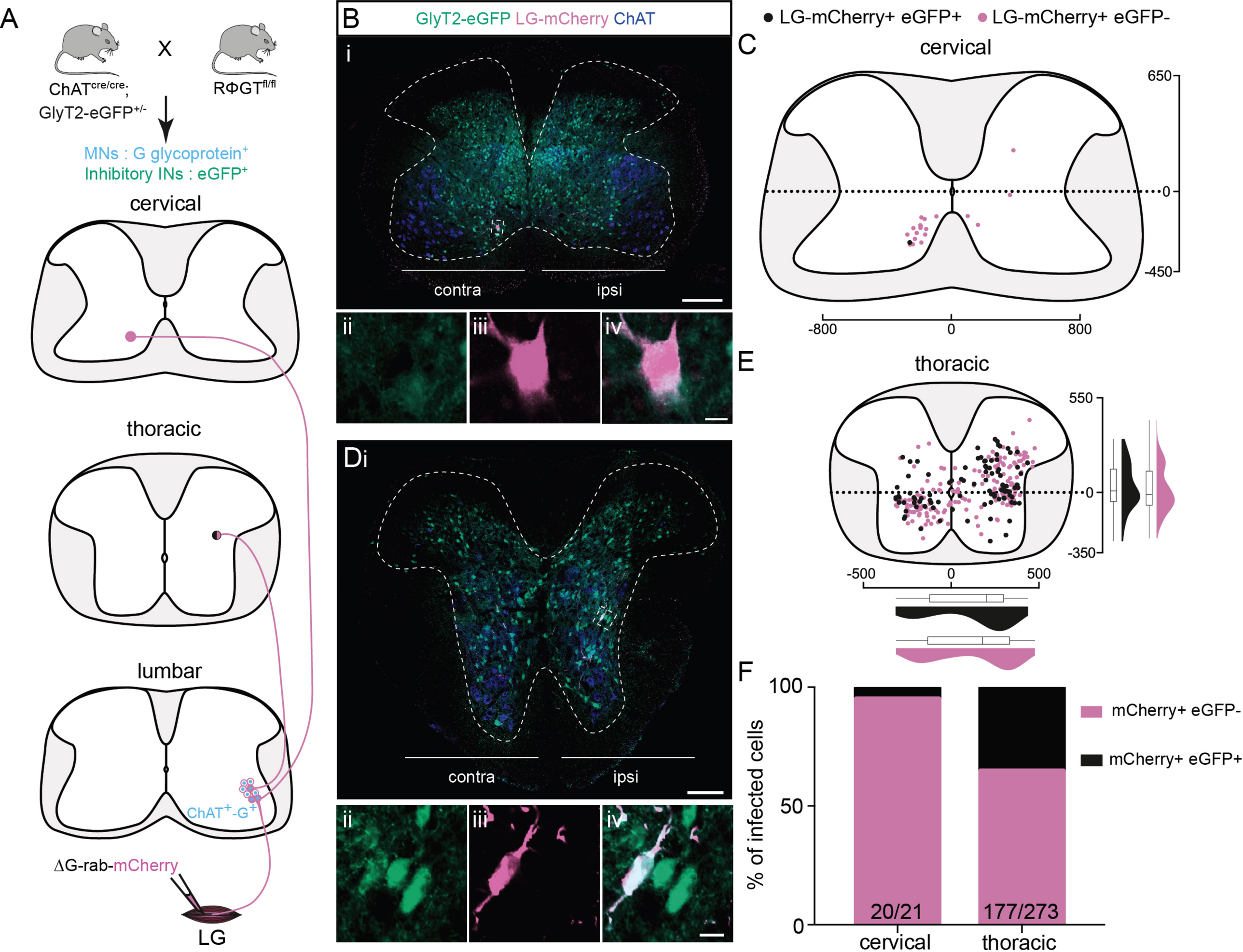
A
ChAT^cre/cre; GlyT2-eGFP^+/-
x
RΦGT^fl/fl
MNs : G glycoprotein+
Inhibitory INs : eGFP+
cervical
thoracic
lumbar
ChAT+-G+
ΔG-rab-mCherry
LG
B
GlyT2-eGFP LG-mCherry ChAT
i
contra
ipsi
ii
iii
iv
Di
contra
ipsi
ii
iii
iv
LG-mCherry+ eGFP+
LG-mCherry+ eGFP-
C
cervical
650
0
-450
-800
0
800
E
thoracic
550
0
-350
-500
0
500
F
100
50
0
% of infected cells
20/21
177/273
cervical
thoracic
mCherry+ eGFP-
mCherry+ eGFP+

Figure 4

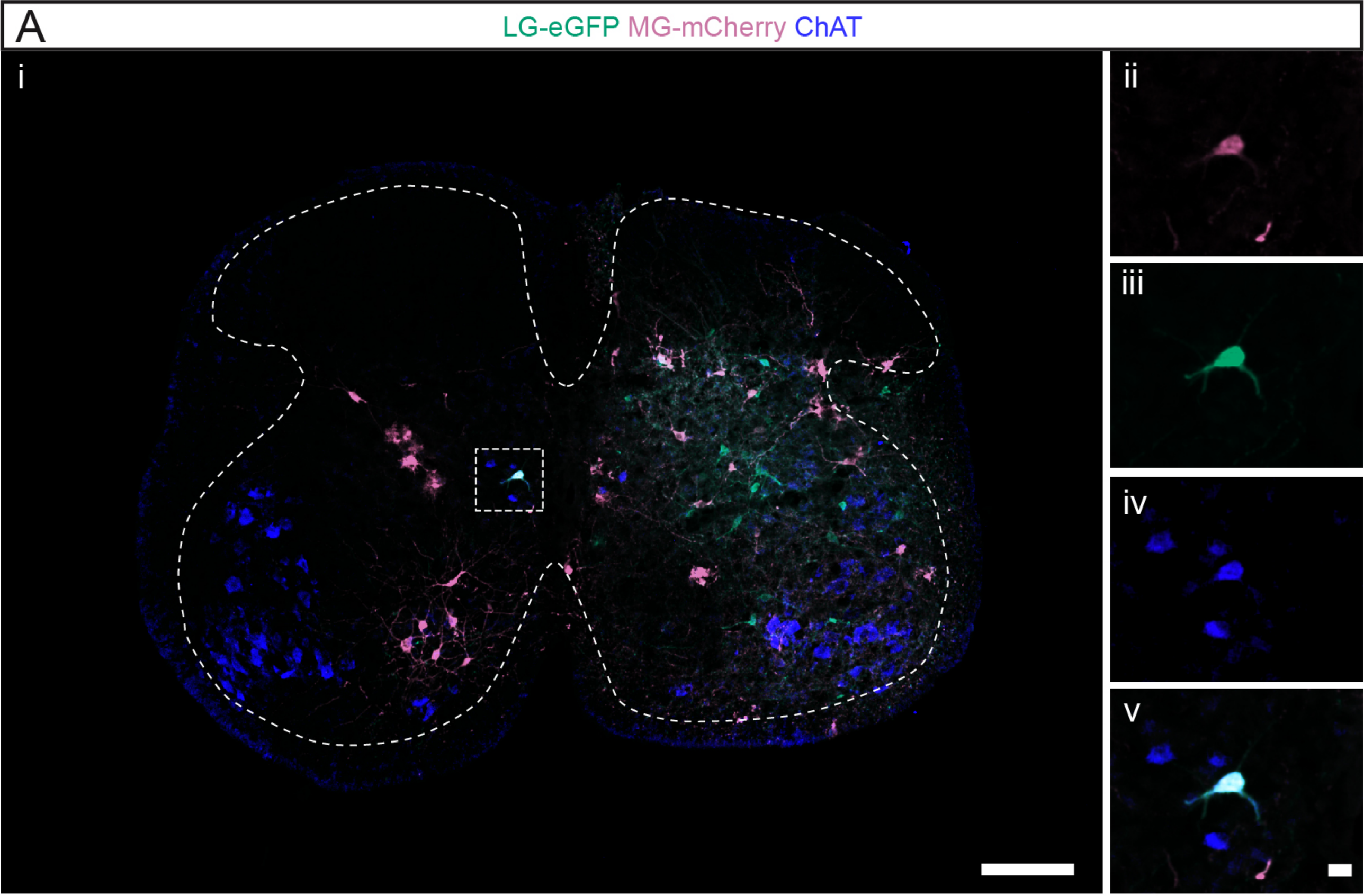

Figure 4-figure supplement 1

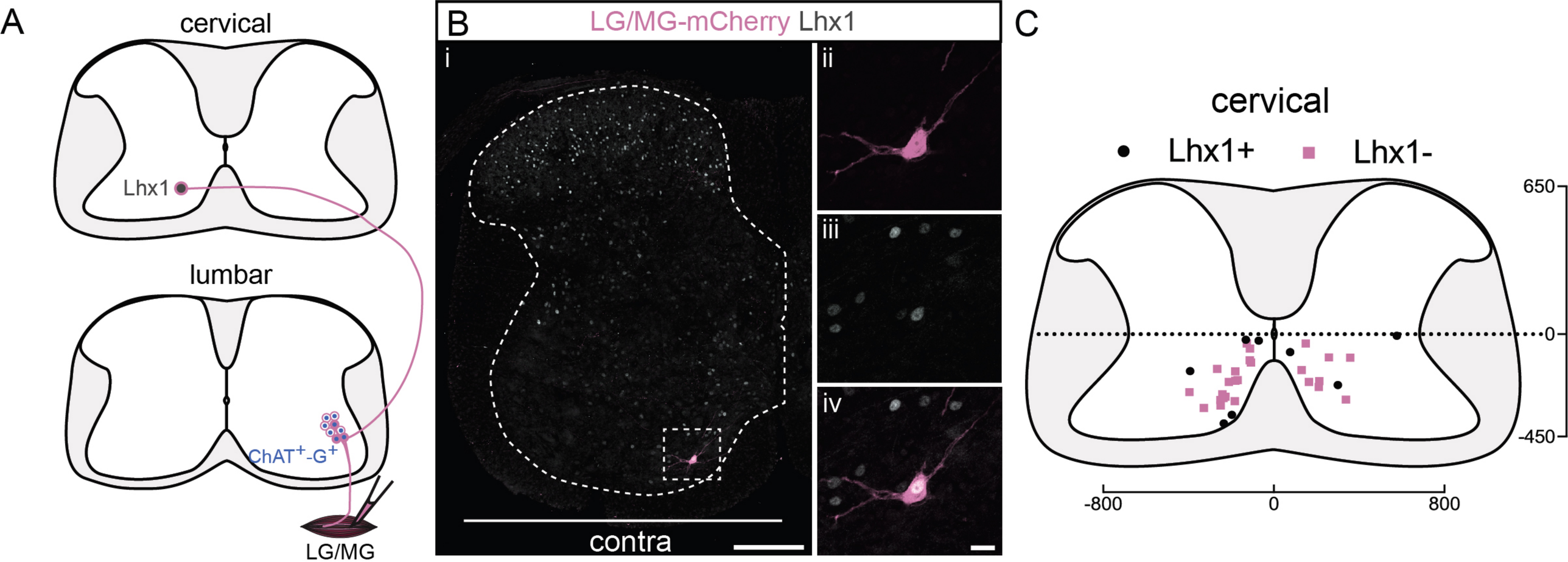
A
cervical
Lhx1
lumbar
ChAT+-G+
LG/MG
B
LG/MG-mCherry Lhx1
i
ii
iii
iv
contra
C
cervical
Lhx1+
Lhx1-
650
0
-450
-800
0
800

Figure 5

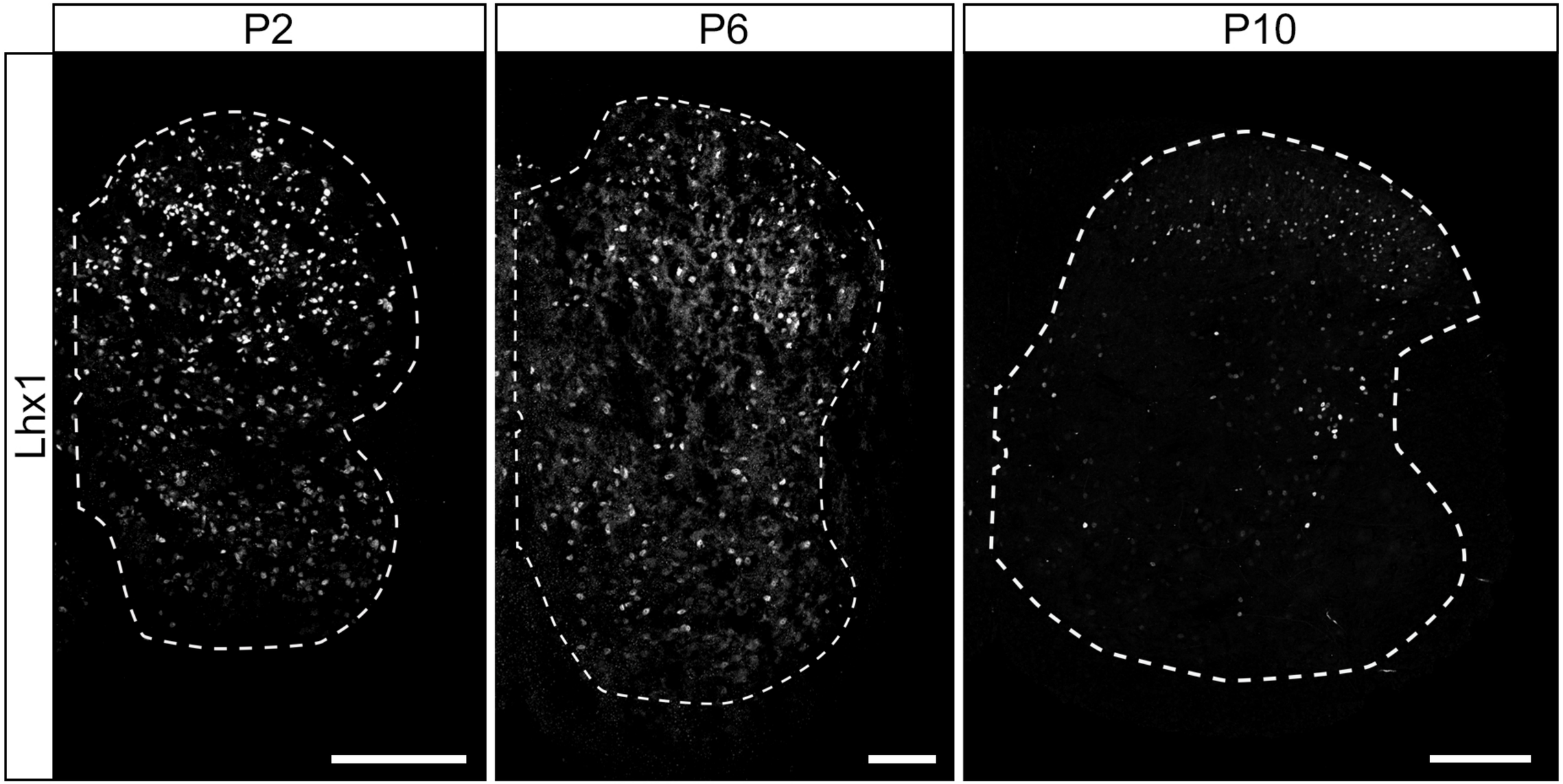

Figure 5-figure supplement 1

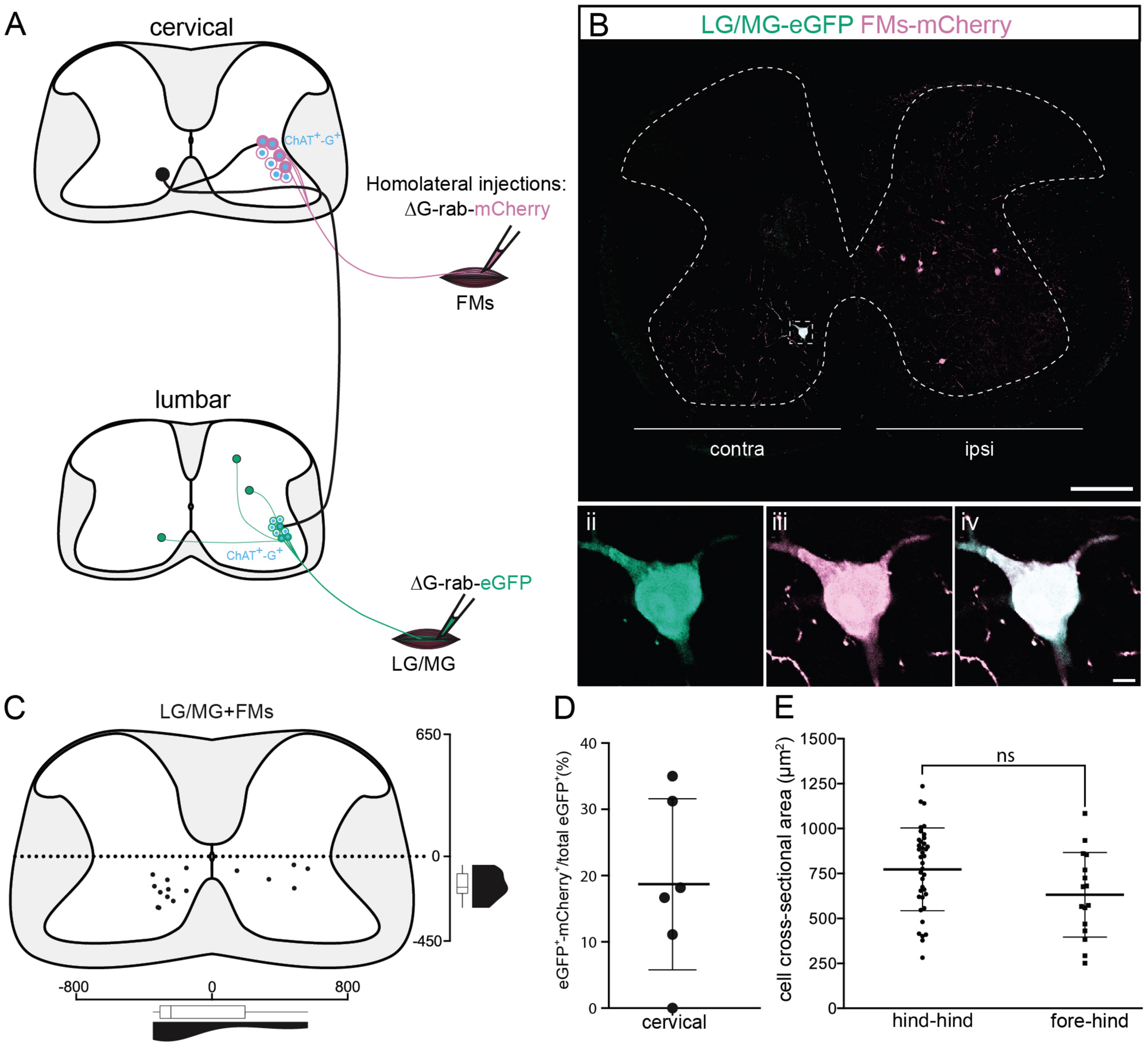
A
cervical
ChAT+-G+
Homolateral injections:
ΔG-rab-mCherry
FMs
lumbar
ChAT+-G+
ΔG-rab-eGFP
LG/MG
B
LG/MG-eGFP FMs-mCherry
contra
ipsi
ii
iii
iv
C
LG/MG+FMs
650
0
-450
-800
0
800
D
eGFP+-mCherry+/total eGFP+(%)
40
30
20
10
0
cervical
E
cell cross-sectional area (μm2)
1500
1250
1000
750
500
250
0
ns
hind-hind
fore-hind

Figure 6

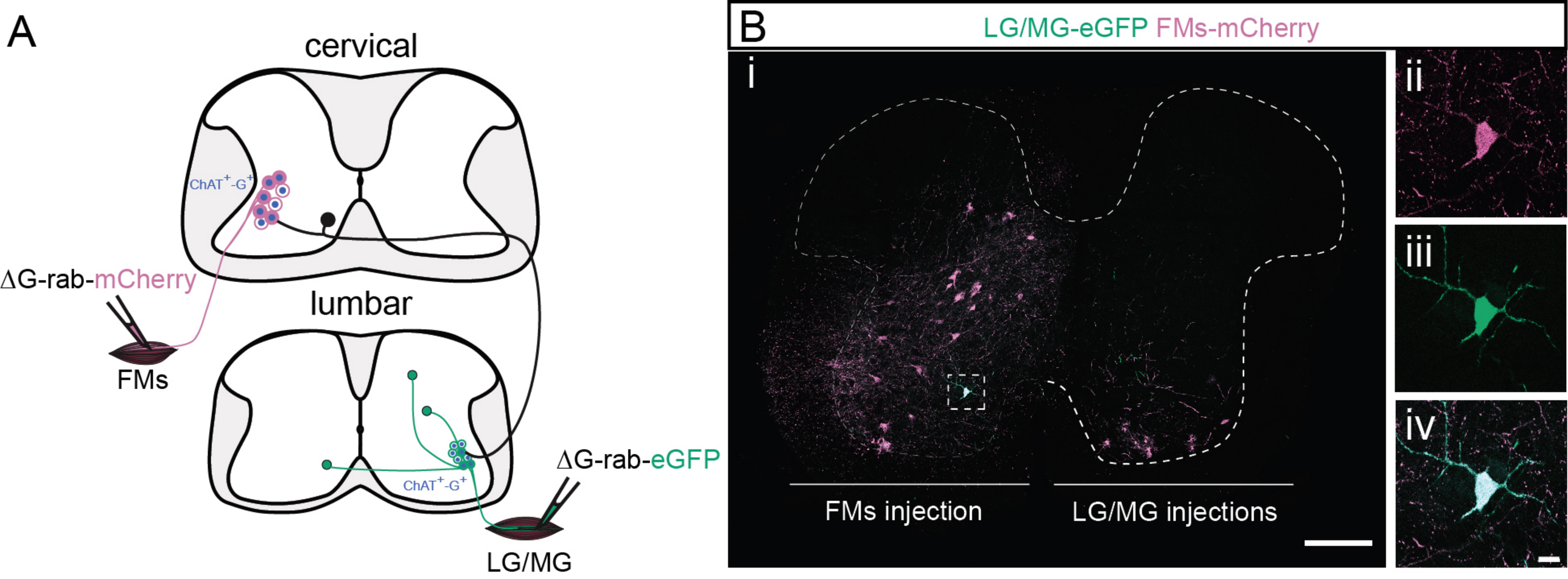

Figure 6-figure supplement 1

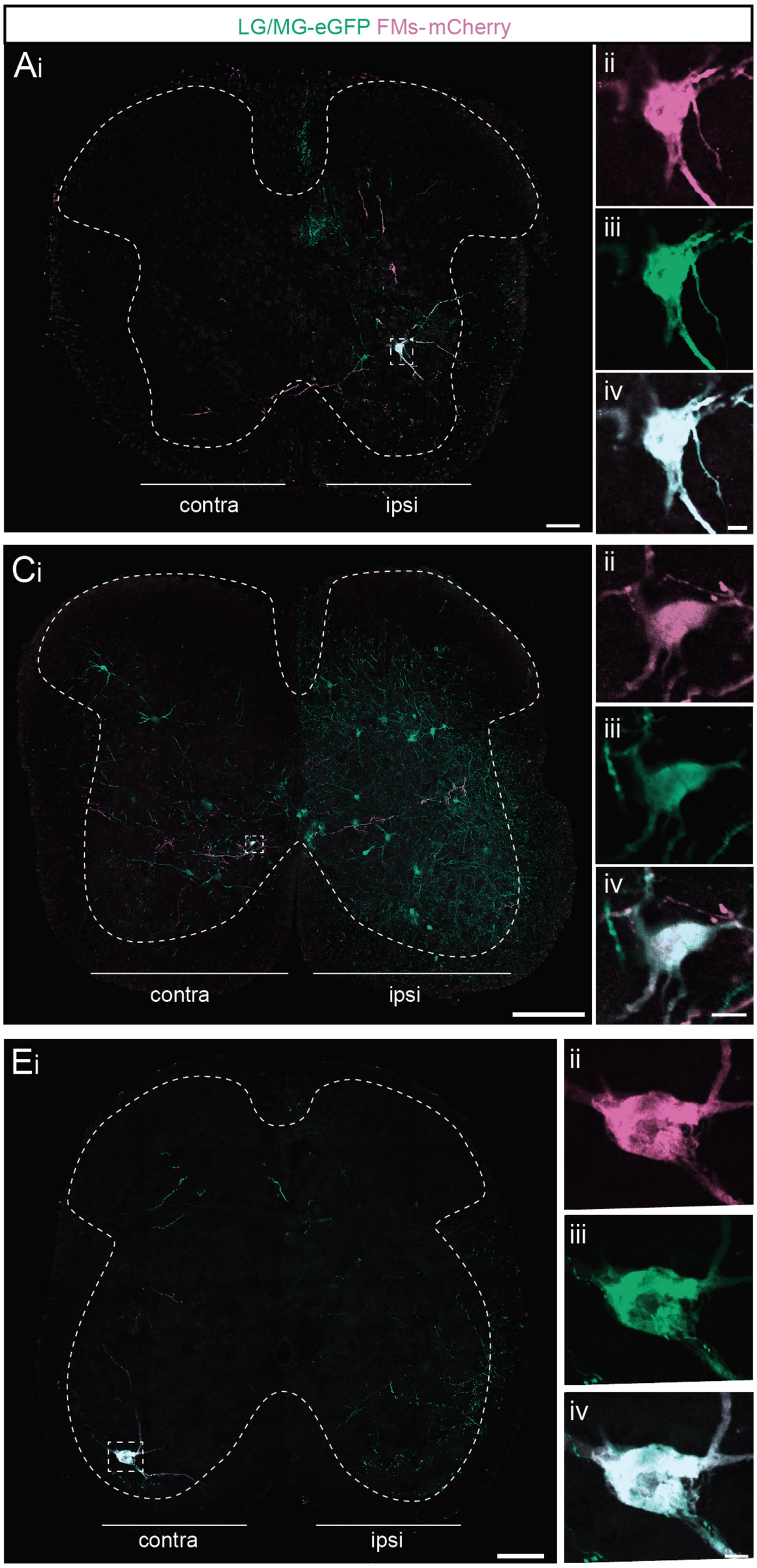

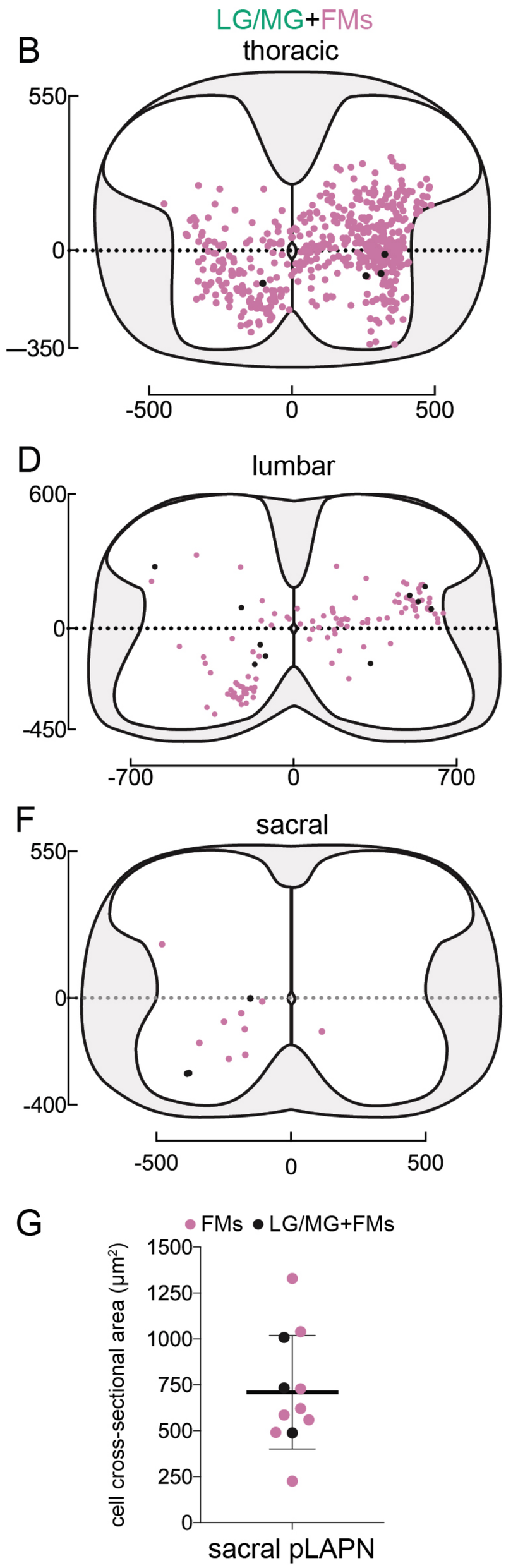

Figure 6-figure supplement 2

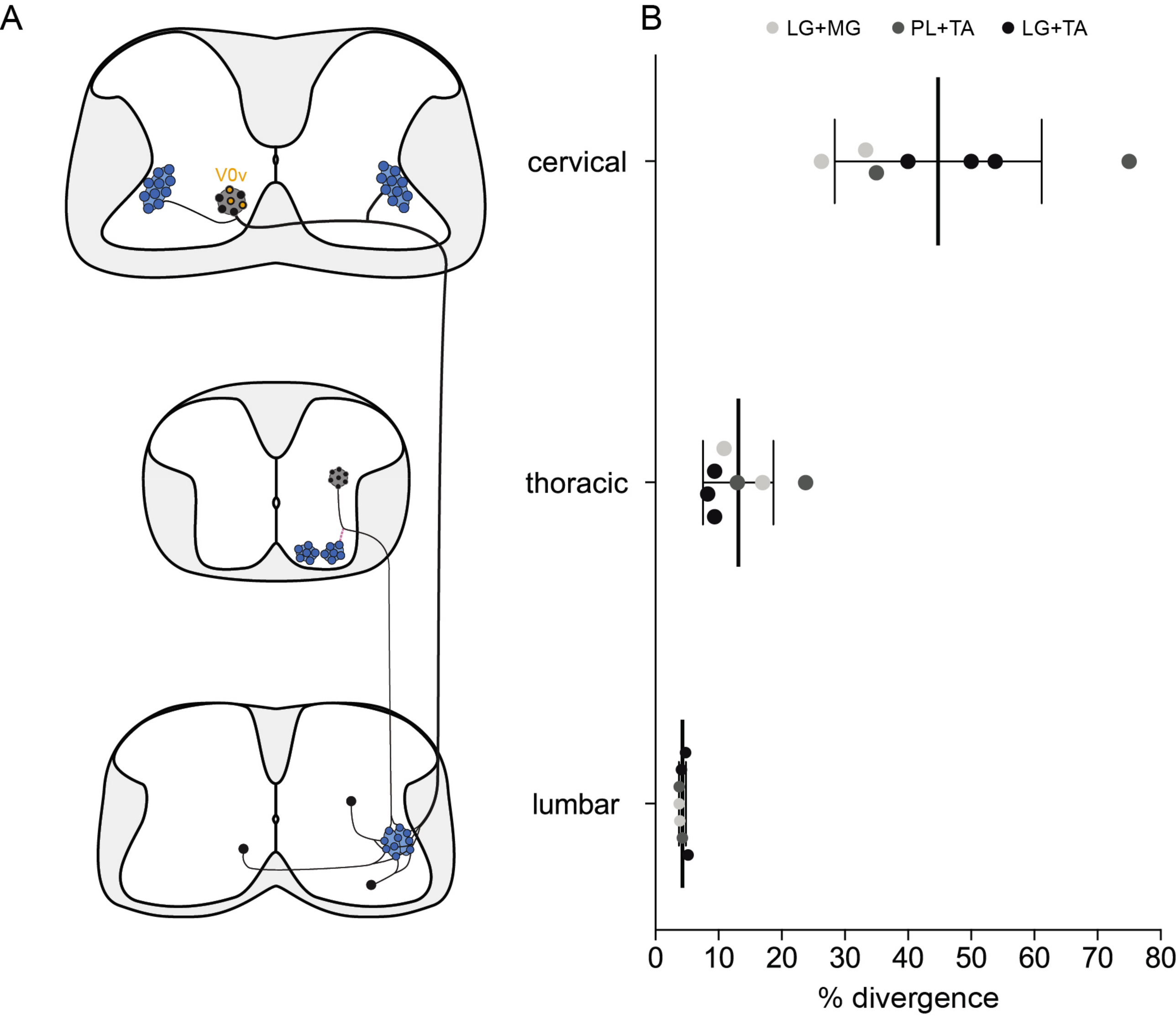
A
V0v
B
LG+MG
PL+TA
LG+TA
cervical
thoracic
lumbar
0
10
20
30
40
50
60
70
80
% divergence

Figure 7

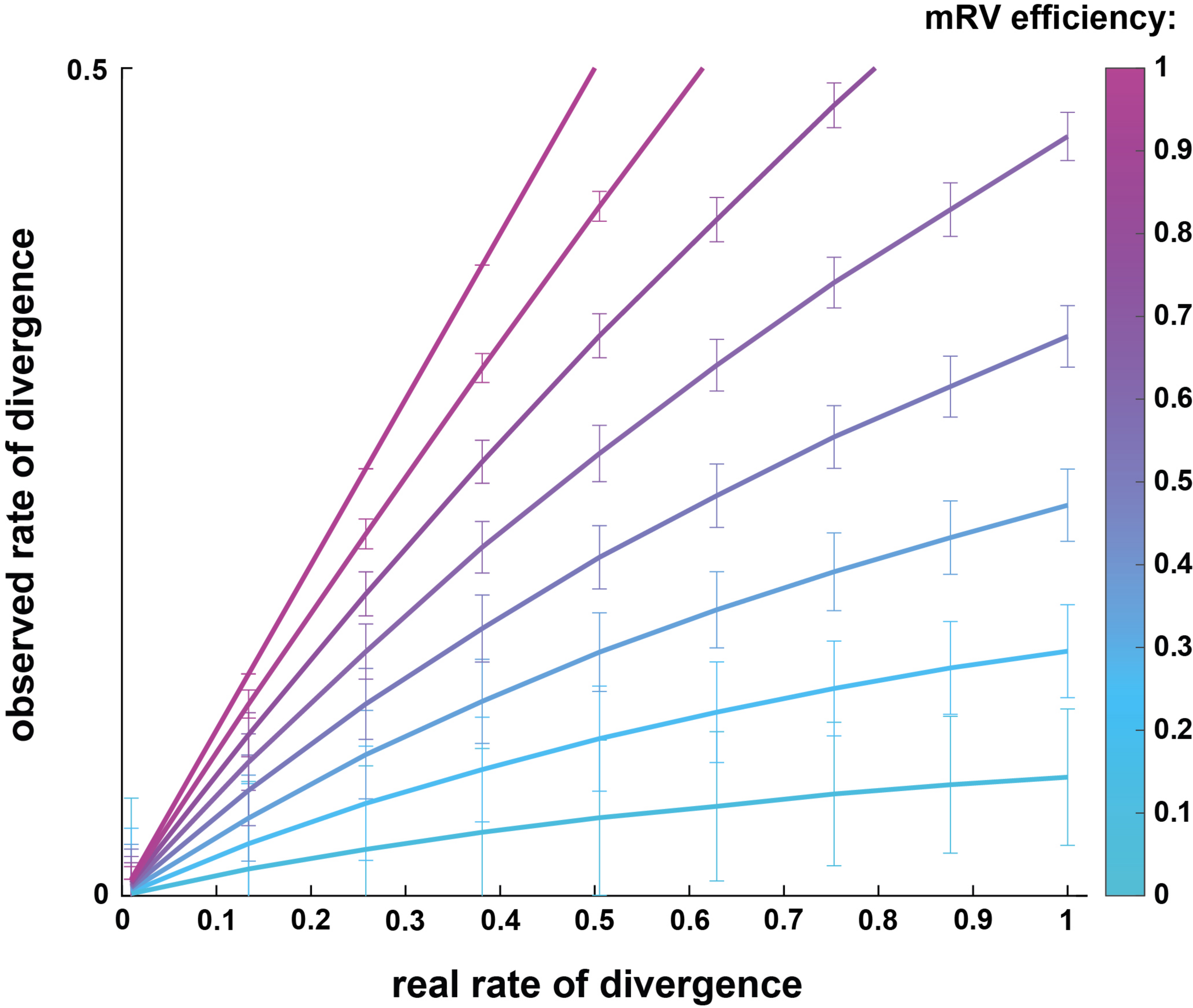
mRV efficiency:
1
0.9
0.8
0.7
0.6
0.5
0.4
0.3
0.2
0.1
0
observed rate of divergence
0.5
0
0
0.1
0.2
0.3
0.4
0.5
0.6
0.7
0.8
0.9
1
real rate of divergence

Figure 8